EPFL

FATIGUE EXAMINATION OF REINFORCED-CONCRETE BRIDGE SLABS USING ACOUSTIC EMISSION AND STRAIN MONITORING DATA

Présentée le 6 mai 2021

Faculté de l'environnement naturel, architectural et construit
Laboratoire de maintenance, construction et sécurité des ouvrages
Programme doctoral en génie civil et environnement

pour l'obtention du grade de Docteur ès Sciences

par

Imane BAYANE

Acceptée sur proposition du jury

Dr M. Fernández Ruiz, président du jury
Prof. E. Brühwiler, directeur de thèse
Dr E. Niederleithinger, rapporteur
Dr A. Kalogeropoulos, rapporteur
Prof. I. F. C. Smith, rapporteur

École
polytechnique
fédérale
de Lausanne

2021

"Nothing in life is to be feared; it is only to be understood."

"Dans la vie, rien n'est à craindre, tout est à comprendre."

Marie Curie (1895 – 1906), taken from *institut-curie*.

Foreward

In February 2017, Imane Bayane joined my research group as a doctoral student (ESR) of the ITN (Innovative Training Network) Project "Infrastar" (Marie Skłodowska-Curie grant agreement No 676139), a project within the European Union's Horizon 2020 research and innovation program.

Examination of bridges under service loadings is a key issue to understand their condition for sustainable and economical use. The objective of the present doctoral research was to develop knowledge and methods to characterise fatigue-related damage in bridge-deck slabs using nondestructive testing methods. The influence of low fatigue stress on reinforced concrete behaviour was studied at a microscale structural level to quantify existing damage and increase of fatigue damage in concrete. An extensive long-term monitoring campaign was carried out on a road bridge in service for 60 years, using several nondestructive testing methods like acoustic emission and strain measurements, to understand the fatigue behaviour of the reinforced-concrete slab under operational loading. The effectiveness of different nondestructive methods and their combination was evaluated. Imane Bayane succeeded in deducing from her data new findings and understanding of the fatigue damaging process in concrete under low stresses.

With her doctoral thesis, Imane Bayane provides the proof of her capabilities to conduct a scientific study and to solve complex scientific questions by applying scientific methods. Overall, her thesis is an excellent contribution as it delivers novel scientific findings useful for the implementation in structural engineering. The high value of the conducted research work is also evident from Imane Bayane's publications record.

Imane Bayane has shown passion for research and willingness to cooperation. Importantly, her collaboration with other doctoral students (ESRs) from foreign universities involved in the EU ITN-"Infrastar" research project through secondments, lead to true synergy, demonstrating the importance of exchanges among researchers and their institutions.

In the name of the whole MCS Team, I thank her for her constant and thorough investment to the thesis topic as well as for her professional skills and personal qualities.

Lausanne, December 2020   Professor Eugen Brühwiler

Acknowledgements

Nearly a quarter of century has passed, me being in different schools, a quarter of fun, perseverance and luck. Fun because learning new things, facing problems and creating solutions have been always related to excitement. Perseverance, because from a very young age I have categorically refused to be dictated the path to take. Luck because I have been surrounded by people who have helped me to become a better version of myself. Those people to whom I am very grateful today.

I would like to express my sincere gratitude to my supervisor Professor Eugen Brühwiler for giving me the opportunity to conduct my research at EPFL in the best work conditions. Thank you for your positive spirit, continuous support and for sharing your passion and introducing me to sustainable and responsible engineering practices.

Thanks are extended to the jury members: Professor Ian F. C. Smith, Dr. Ernst Niederleithinger, and Dr. Alexis Kalogeropoulos for the fruitful discussion and the valuable suggestions for bringing out the best in my doctoral thesis. I would also like to thank Dr. Miguel Fernández Ruiz for chairing smoothly and effectively my oral exam.

Special thanks to Dr. Emmanuel Denarié for his constructive discussions, valuable advices and his great support to my research project, especially during the preparation of candidacy exam and the choice and purchase of the acoustic emission system.

Many thanks are reserved to Florence Grandjean for her precious support, her continuous assistance and her priceless help with administrative issues, especially for my travels and secondments.

I would like to thank Gilles Guignet for his valuable assistance and contribution to implement and calibrate the monitoring systems on-site. Thanks are extended to Gérald Rouge who gave me a precious help during the implementation of the acoustic emission system. Many thanks are reserved to Territorial Roads and Bridges Department of Cantonal Roads Office of Neuchâtel particularly Roger Spichiger and Pascal Richina for their precious support within the monitoring of the case study.

Sincere thanks to my colleagues for the beautiful moments we have shared and valuable discussions we had: Jian Zhan, Dr. Numa Joy Bertola., Dr. Bartlomiej Sawicki, Philippe Schiltz, and Dr. Amir Hajiesmaeili. Special thanks to my colleagues Xiujiang Shen 'Gianni', for integrating me to MCS and for our international dinners, and Mohamed Abdul Hafiz for the rich exchanges and the valuable help with English writing. Many thanks to Dr. Sai Ganesh Sarvotham Pai for the fruitful discussions and the precious support.

Lausanne, December 2020   Imane Bayane

Abstract

The examination of bridges under service loading is key for understanding their condition and thus for their sustainable and efficient use. The need to extend the service duration of existing bridges is increasing, and therefore, efficient tools for examining and maintaining them are required. Monitoring of structures is recognised as an efficient method for investigating structural behaviour and evaluating structural performance. However, there is a lack of methods for choosing suitable sensors and performing monitoring on-site. The main challenges associated with monitoring include environmental conditions, complex loading, big data storage, and measurement calibration. Thus far, no research has developed and implemented a complete strain-acoustic-emission monitoring method, from instrumentation to data interpretation, to evaluate long-term changes in the internal state of reinforced-concrete road bridges under operational conditions.

The general objective of this thesis is to characterise fatigue-related damage in the reinforced concrete of bridge-deck slabs using nondestructive methods. The influence of low fatigue stress on reinforced-concrete behaviour was studied at a microscale structural level, and this research was then used to define two indices that quantify existing damage and fatigue-damage increase over time.

An extensive long-term monitoring campaign was conducted on a bridge in service to understand the fatigue behaviour of reinforced-concrete slabs under operational loadings and to evaluate the effectiveness of different nondestructive methods. For the first monitoring method, strain measurements were performed on steel reinforcement bars using strain gauges for which a load test was conducted to determine the structural response and to calibrate structural analysis models. For the second monitoring method, acoustic emission was utilised to study internal changes in the concrete's volume. The collected data were subsequently used to identify potential fatigue-related damage to reinforced concrete under service loading by means of new data-interpretation methods. An inverse method was developed to estimate the load and the position of vehicles from load-test results. Furthermore, measurements were utilised to define information that assists the development of structural analysis models that evaluate the fatigue behaviour of noninstrumented parts. Finally, acoustic emission data were interpreted, and the detected events were localised in three dimensions to visualise and characterise microcracks in concrete volume.

The instrumentation, calibration, and synchronisation of the used nondestructive measurements produced recommendations for the examination of reinforced-concrete bridge-deck slabs. The methods provide a solid understanding of how to quantify the influence of traffic loading and environmental changes on structural behaviour, such as fatigue behaviour, and structural characteristics such as the connection between bridge components. The results derived from the monitoring data indicate that the instrumented bridge is safe with respect to the fatigue limit despite the potential difference between the present and original design conditions.

The developed inverse method identifies the probabilistic distribution of the position and the load of vehicles crossing the instrumented slab. The results of this method define the link between the fatigue-damage distribution and the position and the load of vehicles, and clearly reveal the sensitivity of fatigue damage to different sources of uncertainties associated with the compressive strength of concrete, the level of stresses, and the magnitude of annual traffic.

Combining information from monitoring data and structural analysis models allows for accurate data interpretation and accurate model development. The results reveal that the identification of structural parameters and the prediction of fatigue endurance of the noninstrumented structural elements can be performed accurately.

Integrating acoustic emission and strain measurement results is a comprehensive method for analysing the fatigue of reinforced-concrete members by which microcracks in the concrete volume can be localised and visualised under operational loading. The stationary movement of existing microcracks and low microcrack growth govern the concrete's behaviour under low fatigue stresses. Reinforced concrete was found to be in the stage of new-microcrack nucleation and stable microcrack growth with respect to the fatigue process.

Keywords: Bridge, reinforced concrete, fatigue, damage, monitoring, acoustic emission, strain measurement

Résumé

L'évaluation des ponts dans leurs conditions de service est une question clé pour comprendre leur état en vue d'une utilisation durable et économique. La nécessité d'allonger la durée de service des ponts s'accroît et, par conséquent, des outils efficaces pour leur examen et leur entretien sont nécessaires. La surveillance des infrastructures est reconnue comme une méthode efficace pour étudier leur comportement et évaluer leur performance. Cependant, il y a un manque de méthodes pour choisir les capteurs appropriés et effectuer la surveillance sur place. Les principaux défis associés à la surveillance sont les différentes conditions environnementales, les charges complexes, le stockage de données volumineuses, l'étalonnage des mesures et le manque de référence. Jusqu'à présent, aucune recherche n'a été effectuée pour développer et mettre en œuvre une méthode complète de surveillance basée sur des mesures de déformations et d'émissions acoustiques, qui part de l'instrumentation à l'interprétation des données pour évaluer les changements de l'état interne des ponts routiers en béton armé à long terme.

L'objectif général de cette thèse est de caractériser les endommagements liés à la fatigue des dalles de ponts en béton armé par le biais de méthodes non destructives. L'influence des faibles contraintes cycliques sur le comportement du béton armé est par ailleurs étudiée au niveau de la structure à l'échelle microscopique, et est utilisée pour définir deux indices permettant de quantifier les endommagements existants et évaluer l'augmentation des endommagements dus à la fatigue.

Une vaste campagne de surveillance à long terme est menée sur un pont en service pour comprendre le comportement à la fatigue des dalles en béton armé sous des charges opérationnelles, tout en considérant l'efficacité de différentes méthodes non destructives. Des mesures de déformation sont effectuées sur les barres d'armature à l'aide des jauges de contrainte comme première méthode de surveillance. Un essai de charge est réalisé par la suite pour déterminer la réponse structurelle et calibrer des modèles des éléments finis. La seconde méthode de surveillance est la mesure d'émissions acoustiques, utilisée pour étudier les changements internes du béton. Finalement, des essais nondestructifs, notamment des essais de rebondissement, des mesures de déflexion et des mesures de la vitesse du son sont effectués pour faciliter l'évaluation des caractéristiques des matériaux et des éléments structuraux. Les données recueillies sont utilisées pour identifier l'endommagement du béton armé dû à la fatigue sous des charges de service au moyen de nouvelles méthodes d'interprétation. Une méthode inverse est développée en premier pour calculer la charge et la position des véhicules à partir des mesures de déformations et des résultats de l'essai de charge. Les données de mesures sont utilisées par la suite pour développer des modèles des éléments finis et évaluer le comportement à la fatigue des éléments non instrumentés. Enfin, les données des émissions acoustiques sont interprétées et localisées en trois dimensions pour visualiser et caractériser les microfissures du béton.

Des recommandations solides pour l'évaluation des dalles de tabliers de ponts en béton armé sont tirées de l'instrumentation, l'étalonnage et la synchronisation des méthodes non destructives utilisées. En particulier pour quantifier l'influence de la charge du trafic et des changements environnementaux sur le comportement structurel, comme le comportement à la fatigue, et les caractéristiques structurelles, comme la connexion entre les composants du pont. Les résultats des données de surveillance indiquent que le pont instrumenté ne présente aucun problème à l'état limite de fatigue, malgré la variabilité potentielle entre les conditions de conception actuelles et originales

Le développement de la méthode inverse permet d'identifier la distribution de la position et de la charge des véhicules traversant la dalle instrumentée. Les résultats indiquent que la distribution des endommagements dus à la fatigue pour les armatures et le béton est fonction de la position et de la charge des véhicules, et révèlent clairement leur sensibilité aux différentes sources d'incertitudes associées à la résistance à la compression du béton, au facteur d'intensité des contraintes et à la fréquence du trafic annuel.

La combinaison des informations provenant des données de surveillance et des modèles des éléments finis permet d'élaborer des modèles rigoureux pour interpréter les données précisément. Les résultats révèlent que l'identification des paramètres structurels et la prédiction de l'endurance à la fatigue des éléments structuraux non instrumentés peuvent être réalisées avec précision.

L'intégration des mesures d'émissions acoustiques et de déformations constitue un outil complet pour l'analyse de la fatigue des éléments en béton armé, grâce à laquelle les microfissures du béton peuvent être localisées et visualisées sous charges opérationnelles. Le comportement du béton sous de faibles contraintes de fatigue est régie par le mouvement stationnaire des microfissures existantes et la faible croissance des microfissures. Le béton armé se trouve éventuellement au stade de la nucléation de nouvelles microfissures et de la croissance stable des microfissures par rapport au processus de fatigue.

Mots-clés: Pont, béton armé, fatigue, endommagement, surveillance, émission acoustique, mesure de déformations

Zusammenfassung

Die Untersuchung von Brücken unter Betriebslasten ist ein Schlüsselthema, um ihren Zustand im Hinblick auf eine nachhaltige und wirtschaftliche Nutzung zu verstehen. Die Notwendigkeit, die Nutzungsdauer bestehender Brücken zu verlängern, nimmt zu. Daher werden effiziente Methoden für ihre Untersuchung und Instandhaltung benötigt. Die Überwachung von Bauwerken mit Hilfe eines Monitorings ist als effiziente Methode zur Untersuchung des Bauwerksverhaltens anerkannt. Es mangelt jedoch an Methoden zur Auswahl geeigneter Sensoren und zur Durchführung der Überwachung vor Ort. Zu den größten Herausforderungen bei der Überwachung gehören die unterschiedlichen Umgebungsbedingungen, die komplexe Belastung, die große Datenspeicherung und die Kalibrierung der Messungen. Bisher wurde keine systematische Forschung betrieben, um eine Überwachungsmethode auf der Basis von Schallemissions- und Dehnungsmessungen zu entwickeln und zu implementieren, von der Instrumentierung bis zur Dateninterpretation, um langfristige Veränderungen des inneren Zustands des Stahlbetons von Straßenbrücken unter Betriebsbedingungen zu bewerten.

Das allgemeine Ziel der Arbeit ist es, eine ermüdungsbedingte Schädigung im Stahlbeton von Brückenfahrbahnplatten mit zerstörungsfreien Methoden zu beschreiben. Der Einfluss einer geringen Ermüdungsbeanspruchung auf das Verhalten von Stahlbeton wurde auf der Mikrostrukturebene untersucht, woraufhin zwei Indizes zur Quantifizierung vorhandener Schäden und der zeitlichen Zunahme von Ermüdungsschäden definiert wurden.

Dementsprechend wurde eine umfangreiche Langzeitüberwachungskampagne durchgeführt, um das Ermüdungsverhalten von Stahlbetonplatten unter Betriebsbelastungen zu verstehen und die Wirksamkeit verschiedener zerstörungsfreier Methoden zu bewerten. Bei der ersten Überwachungsmethode wurden Dehnungsmessungen an Betonstahlstäben mit Dehnungsmessstreifen durchgeführt, für die ein Belastungstest zur Bestimmung der Tragwerksantwort und zur Kalibrierung von Modellen der Tragwerksanalyse durchgeführt wurde. Bei der zweiten Überwachungsmethode wurde die Schallemission genutzt, um interne Veränderungen im Betonvolumen zu untersuchen. Die gesammelten Daten wurden anschließend verwendet, um potenzielle ermüdungsbedingte Schäden von Stahlbeton unter Betriebsbelastung mit Hilfe neuer Methoden der Dateninterpretation zu identifizieren. Es wurde eine inverse Methode entwickelt, um die Belastung und die Position der Fahrzeuge aus den Ergebnissen der Belastungstests zu ermitteln. Zudem wurden die Messungen genutzt, um Informationen zu definieren, welche die Entwicklung von Tragwerksmodellen zur Bewertung des Ermüdungsverhaltens von nicht instrumentierten Bauteilen unterstützen. Schließlich wurden die Schallemissionsdaten interpretiert und die aufgenommenen Ereignisse in drei Dimensionen lokalisiert, um Mikrorisse im Betonvolumen zu visualisieren und zu charakterisieren.

Die Instrumentierung, Kalibrierung und Synchronisation der verwendeten zerstörungsfreien Messungen stellen Empfehlungen für die Untersuchung von Brückenfahrbahnplatten aus Stahlbeton dar. Die Methoden liefern ein grundlegendes Verständnis für die Quantifizierung des Einflusses von Verkehrsbelastungen und Umweltveränderungen auf das strukturelle Verhalten, wie z.B. das Ermüdungsverhalten und Tragwerkseigenschaften wie z.B. die Verbindung zwischen Brückenkomponenten. Die Ergebnisse der Messdaten deuten darauf hin, dass die instrumentierte Brücke im Hinblick auf die Ermüdung sicher ist, trotz der potenziellen Variabilität zwischen den aktuellen und den ursprünglichen Bauwerksbedingungen.

Die entwickelte inverse Methode identifiziert die probabilistische Verteilung der Position und der Belastung der Fahrzeuge, welche die instrumentierte Platte überqueren. Die Ergebnisse zeigen, dass die Verteilung der Ermüdungsschädigung in der Stahlbewehrung und im Beton eine Funktion der Position und der Last der Fahrzeuge ist, und sie zeigen deutlich die Empfindlichkeit der Ermüdungsschädigung gegenüber verschiedenen Quellen von Unsicherheiten, die mit der Druckfestigkeit des Betons, der Höhe der Spannungen und der Größe des jährlichen Verkehrs verbunden sind.

Die Kombination von Informationen aus Überwachungsdaten und Modellen der Tragwerksanalyse ermöglicht eine genaue Dateninterpretation und eine genaue Modellentwicklung. Die Ergebnisse zeigen, dass die Identifizierung von Strukturparametern und die Vorhersage der Ermüdungsfestigkeit der nicht instrumentierten Strukturelemente genau durchgeführt werden können.

Die Integration von Schallemissions- und Dehnungsmessungen stellt ein umfassendes Werkzeug für die Ermüdungsanalyse von Stahlbetonbauteilen dar, mit dem Mikrorisse im Betonvolumen unter Betriebsbelastung lokalisiert und visualisiert werden können. Die stationäre Bewegung vorhandener Mikrorisse und ein geringes Mikrorisswachstum bestimmen das Betonverhalten unter geringen Ermüdungsbeanspruchungen. Der Stahlbeton befindet sich schließlich im Stadium der Keimbildung neuer Mikrorisse und des stabilen Mikrorisswachstums im Hinblick auf den Ermüdungsprozess.

Schlüsselwörter: Brücke, Stahlbeton, Ermüdung, Schädigung, Überwachung, Schallemission, Dehnungsmessung.

مقتطف

يُعدُّ تقييمُ حالة الجسور تحت ظروف الخدمة أمرا في غاية الأهمية لفهم التغيرات التي تطرأ عليها، ولاتِّخاذِ التّدابير الفعّالةِ الفورية لصيانتها، ولإيقافِ الإرهاقِ الذي يطالها جرّاء الحمولات المختلِفة، بغرض إطالة مدّة استعمالها. إن مراقبةَ الجسور تُعتَبَر منَ الأساليب المعترف لها بفعّاليتها في اتّخاذ قرارات وإصدار أحكامٍ صائبةٍ بشأن مدى صلاحيتها، وتحديد نوع وحجم الصيانات المناسبة لها. مراقبة كهذه، يجب أن تَتِّم بأدواتٍ فعّالةٍ، دقيقةٍ وجِدِّ متطورة. إلّا أن هناك نقصا معرفيّا ملحوظا في كيفيّة اختيار هذه الأدوات من مُستشعِراتٍ إلِكترونيّة مناسبة لمراقبةٍ مَوضِعيّة دقيقة وطويلة الأمد. يعود هذا النّقص إلى التّحديات التي يجب أخذها بعين الاعتبار في أي تتبّع من تباين الظّروف البيئية، الحمولاتِ المعقّدة للعربات العابرة للجسر، صعوبةِ تخزين الكمّ الهائل من البيانات، معايرةِ القياسات، وغيابِ المرجعيات. إلى حدِّ الآن لم يجْرُ أيُّ بحثٍ على تطوير طريقة التّتبّع والمراقبة الشّاملة، وذلك اعتمادا على قياس التشوّهات وقياس انبعاث الإشارات الصّوتية، انطلاقا من اختيار الأدوات، فتخزين البيانات، وصولا إلى قراءتها وتأويلها بشكل دقيق لتقييم الحالة الدّاخليّة للجسور.

يُعد الهدفُ الأساسي لهذه الاطروحة، تمييزَ وتكميمَ الأضرار التي تلحق بالجسور المُشَيَّدَةِ من الخرسانة المسلّحة من شدّة الإرهاق، باعتماد طرقٍ ليس فيها كسرٌ ولا تخريب. تَمَّت من أجل ذلك دراسة الآثار المتتابعة للحمولات على جسرٍ مِنَ الخرسانة المسلّحة على المستوى الميكروسكوبي، ممّا مَكَّن من صياغة مؤشّرين للتّحديد الكَمّيّ للأضرار، ولقياس مدى تطوُّرها جرّاء الإرهاق الذي يلحق بالخرسانة المسلحَّة مع مرور الوقت.

أُجرِيَت حملة واسعة للمراقبة طويلة المدى بأساليبَ غير مخرّبة على الجسر تحت الخدمة، كمحاولة أولى لفهم استجابة الخرسانة والألواح الخرسانية للحمولات الإجرائيّة جرّاء الإرهاق الذي يطالها. بدايةً أُخِذت قياساتٌ للتّشوُّهات على الألواح الخرسانيّة. ثُم تَمَّ التأثير على الجسر بعربةٍ ذاتِ حمولة محدَّدة وسُرُعات عبور مختلِفة وتموقعات مختلِفة لبيان مدى الاستجابة البنيويّة للجسر، ولمعايرة نماذج العناصر المنتهية. بعدها، تَمَّ التركيزُ على قياس الإنبعاثات الصّوتية لدراسة التّغيّرات الدّاخِليّة لبنية الخرسانة. أخيرا، أجريت اختباراتٌ غير مخرّبةٍ تتمحور حول اختبار الإرتداد، واختبار قياس الإنحراف، واختبار قياس سرعة الصّوت، بهدف تيسير تقويم خصائص مواد وعناصر بنية الجسر. استُعملت طُرقٌ حديثةٌ لتأويل المعطيات المُحصَّل عليها من الدراسة، ولبيان نوع وشِدّة الأضرار التي لحِقت بالخَرَسانة جرّاء الإرهاق بِفعل حمولات متباينة في الكمّ وفي التّوزيع وفي التّموقع. تَمَّ تطوير طريقةٍ عكسيّة لحساب كمّيات حمولات العربات العابرة وتموقعها على الجسر من خلال قياس الانفعالاتِ المحصَّل عليها وتمَّ تفسير المعطيات الصوتية وتمثيلها بأبعاد ثلاثيةٍ لتكميم ورؤية التشققات الميكروسكوبية في الخَرَسانة.

مَكَّنت الأدوات المعتمدةُ، ومعايرةُ القياسات وتزامنِ الطُّرُق من التّوصّل الى استنتاجات وتوصيات صلبةٍ بشأن تَقييم الخرسانة والألواح الخرسانية المشكِّلة لهيكل الجسر. خصوصا للتّحديد الكَمّي لتأثير حمولات العربات وتأثير الظُّروف البيئيَّة وعلاقتهما بالإرهاق الذي يطال تماسك مكونات الجسر. تُشير القياسات المُحصَّل عليها وخلاصات دراستها وتأويلها بالنسبة للجسر الذي تمت مراقبته، إلى أنه ليس هناك حدٌّ في الإرهاق الذي طاله يوجب إيقاف استعماله، بالرُّغم من التّباين الواضح بين ظروفِه الحالية وظروف تصوُّره الأصليَّة.

مَكَّنت الطريقة المعكوسة من تحديد توزيع تموقع العربات وحمولاتها على سطح الجسر، ومن خلال نتائجها تَمَّ التّوصل الى علاقة بين الأضرار النّاتجة عن إرهاق الخرسانة والألواح الخرسانية وتموقع وحمولات عربات المرور. أبانتِ النّتائج بكل وضوح عن حساسيّة الأضرار لمختلف الإرتيابات المرتبطة بمقاومة الخرسانة للإنضغاط، ولشدّة المؤثِّرات، وللتّدفُّق السنوي للعربات العابرة للجسر.

مَكَّنت عمليات تركيب البيانات المُستقاةِ من المراقبة ومن نماذج العناصر النهائيّة من صياغة نماذجَ دقيقةٍ لتأويل دقيق لإرهاق الجسور الخرسانية. وقد أبانت النّتائج على أنَّ تحديد العناصر النّهائية، وتوقُّع تحمُّل إرهاقِ العناصر غير المزوَّدة بأدوات الرّصد ممكِنة وقابلة للتّحقُّق بكثير من الدِّقة.

يُشكِّل إدماج قياسات الإنبعاثات الصوتية وقياسات التّشوهات أداةً تامَّة لتحليل إرهاق عناصر الخرسانة. إذ من خلالها يُمكن تحديد ورؤيةُ التّشققات النّاتجة عن حمولات إجرائية وتتبُّع الإرهاق الضعيف الذي يَطال مكوِّنات الخرسانة الذي يتميزبالحركة البطيئة للتشققات المجهرية. تصبح الكتلة الخرسانية بالتالي حاضنة لسلسلة من التشققات المجهرية ولتزايد منتظم لها بالنسبة لنَسَق الإرهاق الذي يطالها
.

الكلمات المفاتيح: جسر، خرسانة مسلحة، إرهاق، ضرر، مراقبة، انبعاثات صوتية، قياس التشوهات.

Contents

List of Figures

List of Tables

Nomenclature

Abbreviations

3D	Three Dimensional
ABSenergy	Absolute Energy
AE	Acoustic Emission
AF	Average Frequency
Amp.	Amplitude
CMS	Candidate Model Set
EDMF	Error Domain Model Falsification
FE	Finite Element
FEDRO	Federal Roads Office
FEM	Finite Element Model
FIB	International Federation for Structural Concrete
FTP	File Transfer Protocol
HDT	Hit Definition Time
HLT	Hit Lockout Time
Ib	Improved b-value
IMS	Initial Model Set
Long.	Longitudinal
LVDT	Linear Variable Differential Transformer
Max	Maximum
Min	Minimum
NDT	Nondestructive testing
Pcount	Counts to Peak

PDT   Peak Definition Time

POT   Peak Over Threshold

RC   Reinforced Concrete

RM   Residual Minimisation

UT   Ultrasonic Testing

WIM   Weight In Motion

Greek symbols

α Dilatation coefficient in [°C^{-1}]

Δ Difference between final and initial states

ε Strain [-]

ε^* Error

θ_i Model class [-]

$\hat{\theta}$ Model parameter [-]

μ Mean value

ρ Density [kg/m^3]

σ Stress in [N/m²]

υ Poisson ratio [-]

ϕ Reliability [-]

Latin symbols

A_{dB} Amplitude [dB]

E Young modulus [N/m²] or [Pa]

$f_{ck,fat}$ Fatigue reference compressive strength [N/m²] or [Pa]

$f_{U_c}(.)$ Probabilistic distribution function

$g_i(.)$ Model response function

g_{ki}	Model predictions
K	Stiffness [N/m]
L	Load [N]
Q_i	True response of a system
S_c	Compressive stress level [-]
t	Time [s]
T	Temperature [°C]
U_c	Uncertainty
v	Velocity [m/s]
V	Signal voltage [V]
x	Position [m]
y	Measurement
$\hat{y}_i$	Measurement at a location i

Software

AEwin for Sensor Highway III

Ansys 18.2

APDL 18.2

AutoCAD 2019

Catman AP V5.3.1

Matlab 2019b

MS Office 2016

Noesis 9.0

Chapter 1 Introduction

1.1 Motivation and Scope

Structural engineers are faced today with new requirements regarding the examination of existing structures, and allocated budgets for these examinations are significantly growing. In Europe, for example, the allocated budget for maintenance represents 50% of the budget devoted to the development of infrastructures [1]. However, structural engineers still rely on traditional-old-fashioned methods such as visual inspection to assess structures requiring maintenance, rehabilitation, or even replacement. There is a necessity to develop and implement knowledge and recommendations regarding the examination of existing structures, particularly ones subject to fatigue loading.

Bridges are subject to fatigue due to cyclic loadings from traffic and environmental factors such as temperature variations. However, in the United States and Europe, more than 75% of the existing reinforced-concrete (RC) bridges were constructed before the introduction of fatigue design rules in the design codes [2], [3]. Fatigue safety assessments of existing bridges are therefore more challenging than designing new ones. The assessment of existing structures using the methods and models established to design new structures has been found to be too conservative, and has led to classifying structures as structurally deficient when they are in good condition [4], [5].

Moreover, bridge instrumentation and monitoring are still considered expensive compared to the knowledge gained for which data is often collected without further processing. The most frequent method for bridge inspection relies on weight-in-motion (WIM) and deflection measurements. They are used to assess the development of traffic and structural analysis models to evaluate the fatigue behaviour of structures, but they do not consider present structural characteristics and performance. Uncertainties regarding structural identification increase and lead to potentially unreliable results.

To use existing bridges for a long service duration, novel methods are required to address their fatigue behaviour under low fatigue stresses and to quantify potential fatigue damage. Within this context, new methodologies are being developed for the fatigue examination of existing RC bridges. The implementation of various nondestructive methods with measurement calibration, data interpretation, damage quantification and visualisation are addressed in this thesis. The methodologies are demonstrated using a case study, where long-term monitoring is performed to tackle possible effects on fatigue behaviour under operational loading and environmental conditions. Figure 1.1 illustrates the nondestructive methods used in this work.
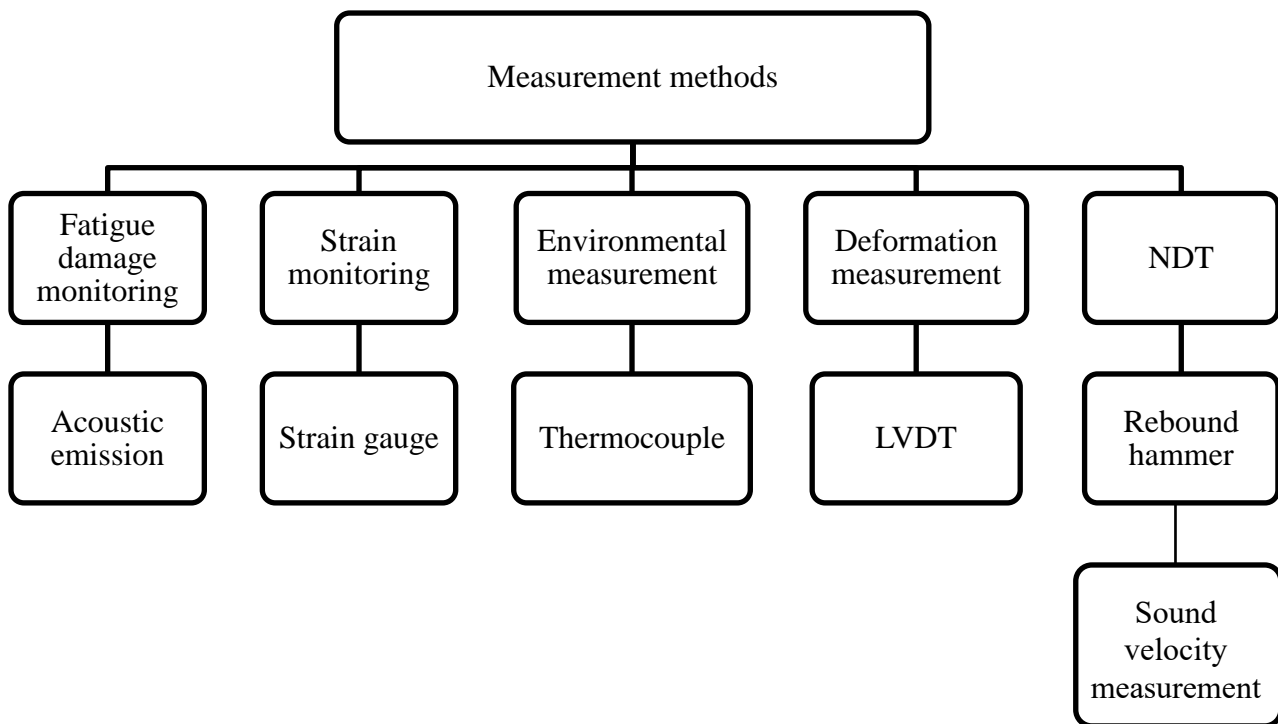
Figure 1.1. The used nondestructive measurement methods for bridge inspection and monitoring.

1.2   Research Question

The present research aims to address the fatigue behaviour of RC in structural elements subjected to low fatigue stresses at an early stage. Bridge-deck slabs are potentially one of the most loaded structural elements subjected to cyclic low fatigue stresses. Many studies have been conducted to understand the fatigue failure mechanism of RC in the last century. However, there are still knowledge gaps concerning the fatigue behaviour of RC slabs under operational loading. These gaps are due to the complex behaviour of the nonhomogenous material as well as the complex characteristics of operational loading. Therefore, the primary goal of this dissertation is to identify and quantify, by means of nondestructive measurement methods, the fatigue damage of RC slabs under traffic and environmental loadings at an early stage.

The issues are addressed using a long-term monitoring campaign of an RC slab of a viaduct currently in service. Strain gauges were used to instrument reinforcement bars, and acoustic emission (AE) measurements were used to examine the fatigue behaviour of concrete. Various data-interpretation methods were performed, such as inverse analysis, probabilistic analysis, model-based data interpretation, and three-dimensional location of AE events to evaluate the relevant data for fatigue behaviour and to predict fatigue damage under operational loading and under conditions different from those monitored and for nonaccessible parts.

The overall novelty of this thesis is that it develops a global approach for the fatigue examination of RC bridge-deck slabs by means of long-term monitoring and new data-interpretation methods. The approach can be used to preserve structures suspected of detrimental fatigue behaviour from unnecessary interventions and to avoid classifying structures in good condition as structurally deficient. The study also aims to evaluate the effects of traffic distribution and temperature variation and to clarify the extent of existing fatigue damage and how it increases under low fatigue stresses.

1.3 Objectives

The specific objectives of this thesis are as follows:

1. Develop methods for interpreting measurements to evaluate the fatigue safety of reinforced-concrete slabs under low fatigue stresses.
2. Perform fatigue evaluation of locations in structures that cannot be monitored.
3. Examine concrete microcracking under long-term traffic conditions and temperature variations.
4. Evaluate the relevant monitoring data to understand the fatigue behaviour of structural elements under operational loadings.
5. Propose recommendations for conducting on-site measurements and for ensuring long-term monitoring of bridges in service, with the aim of evaluating fatigue behaviour and increases in fatigue damage over time.

1.4   Structure of the Thesis

The thesis comprises six chapters. The first chapter introduces the research topic. The four main chapters, Chapters 2 through 5, were written individually and submitted for publication in international peer-reviewed journals. The last chapter, Chapter 6, comprises conclusions and recommendations for further research. An overview of the structure of the thesis is shown in Table 1.1.

Chapter 1 introduces the research topic and describes the motivation, the objectives of the thesis, and the research question.

Chapter 2 (Paper I) provides an inverse method to estimate the probabilistic distributions of the load and the position of vehicles from recorded strain, which are used to predict the distribution of fatigue damage of steel reinforcement and concrete as a function of traffic and environment conditions [6].

Chapter 3 (Paper II) presents a monitoring approach for evaluating fatigue of RC slabs of bridges in service, in which AE is connected to strain and temperature measurements to introduce a new approach to data recording and interpretation for fatigue examination [7].

Chapter 4 (Paper III) highlights the use of various measurements and error-domain model falsification to develop an accurate set of models that allows for the fatigue behaviour evaluation of noninstrumented elements with respect to uncertainties related to monitoring and modelling.

Chapter 5 (Paper IV) introduces two indices to estimate existing fatigue damage and damage increase over time based on three-dimensional location of AE events and the visualisation of microcracks in concrete under traffic and temperature variation using acoustic emission measurements.

Chapter 6 provides the main conclusions of the thesis with an outlook and scope for future research.

Table 1.1. Structure of the thesis

Chapter 1: Introduction

Chapter	Paper	Research question	Methods	Data
2	I	What are the most relevant data for the fatigue evaluation of RC bridge-deck slabs?	• Inverse method • Structural analysis models	• One year of continuous high-frequency strain monitoring • Load test • WIM • Temperature monitoring
3	II	How can the integration of AE and strain measurements help evaluate the fatigue behaviour of RC bridge-deck slabs?	• *b*-value analysis • Parametric study • Statistical analysis • Crack mode classification	• One year of strain and AE monitoring • Pencil-lead break testing • Temperature monitoring
4	III	What impact does the use of the model-based interpretation of measurements have on the fatigue safety evaluation of RC bridge-deck slabs?	• Data clustering • Improved *b*-value analysis • EDMF • Residual minimisation • Structural analysis models	• One year of AE monitoring • Rebound hammer • Sound-velocity measurement • Load test • Deflection measurements • Strain measurements
5	IV	What is the fatigue behaviour of concrete under low fatigue stresses for RC bridge-deck slabs?	• Three-dimensional location of AE sources • AE energy-based analysis • AE frequency-based analysis	• Three years of continuous high-frequency strain monitoring • 18 months of AE monitoring

Chapter 6: Conclusions and further work

Chapter 2 Quantification of Traffic and Temperature Effects on the Fatigue Safety of a Reinforced-Concrete Bridge Deck based on Monitoring Data

Paper details

Chapter 2 contains a post-print version of the paper "I. Bayane, A. Mankar, E. Brühwiler, J.D. Sørensen (2019). Quantification of traffic and temperature effects on the fatigue safety of a reinforced-concrete bridge deck based on monitoring data" published in October 2019 in the Journal "Engineering Structures". Minor modifications are introduced in the text for adapting the paper to the thesis format.

Author contributions

The author of this thesis conducted the research and wrote most of the paper. Mr. A. Mankar provided guidance when developing the inverse method and the numerical model adding to the discussions offered. Professors E. Brühwiler and J.D. Sørensen contributed by proofreading the paper and by providing overall supervision.

Overview

This paper presents the development and validation of an inverse method able to provide the load and the position of the vehicles crossing an RC-bridge-deck slab using load test results and measurements from two strain gauges in the longitudinal direction and two strain gauges in the transverse direction. Results were implemented in numerical models to calculate fatigue damage distribution as a function of the load and the position of vehicles and temperature variations. Finally, relevant parameters for fatigue damage estimation were evaluated for concrete and steel reinforcement for different traffic scenarios.

Link to other chapters

This chapter provides an interpolation of load test results to estimate the distribution of the load and the position of the vehicles from strain measurements. It is linked with all the remaining chapters of the thesis. First, in Chapter 3 the results of the inverse method were used to interpret the source of AE activity. In Chapter 4, extrapolation of load test results were used along with an improved numerical model to evaluate accurately fatigue behaviour of noninstrumented parts, and finally, in Chapter 5, the results of the inverse method were used to understand the microcracking activity of concrete under low fatigue stresses.

Paper I

Quantification of Traffic and Temperature Effects on the Fatigue Safety of a Reinforced-Concrete Bridge Deck based on Monitoring Data

Abstract

Only a few rules and recommendations are available for the assessment of existing reinforced-concrete bridges, and engineers meanwhile apply design codes for new bridges in the evaluation of the fatigue safety of existing bridges, leading to unrealistic approaches and conclusions. Design codes for new structures are often based on worst-case scenarios, and they are not made to assess existing structures with specific loadings and material properties. Direct monitoring provides an important source of information about the actual structural loading and response. This article presents an integral approach for identifying the fatigue damage of a reinforced-concrete deck as a function of the relevant conditions for fatigue using monitoring data. This approach comprises a long-term monitoring system to measure strain and temperature in the most loaded parts, an inverse method using monitoring data to reconstruct traffic conditions from the structural response, and a simulation of traffic loading and its effects using a compiler and a finite element model to estimate fatigue damage. The presented approach can be used as a base for how to monitor and analyse recorded data to evaluate the fatigue safety of existing reinforced-concrete slabs in road bridges.

Keywords: Fatigue, reinforced concrete, existing road bridge, traffic, temperature, inverse method, monitoring.

2.1   Introduction

Reinforced concrete (RC) is a composite material in which concrete is designed to resist compression stresses and steel reinforcement is designed mainly to resist tensile stresses. Investigating the fatigue of RC elements requires the examination of both materials, concrete and steel.

Steel's fatigue phenomenon has been known as a possible cause of structural failure since the 19th century. Fatigue design rules were introduced particularly following the findings of Wöhler (1867) [8], who recognised that repeated loading far below the ultimate static resistance of a structural element could induce failure [9]. Knowledge about fatigue in metals and other materials has evolved since then.

A century later, fatigue design rules for concrete and RC were introduced in Concrete VB (1974), FIP (1975), TNO-IBBC procedures (1974), DNV rules (1977), NPD regulations (1985), the draft Rules of Concrete Bridges (1988)[10], and SIA (1989)[11].

Most of today's RC bridges were constructed before introducing these rules, and fatigue was not considered in their design as a possible failure cause. In Europe, around 75% of RC bridges were constructed before 1988, and in Switzerland, most were constructed before 1976 [12]. Therefore, there is a need to develop methodologies and approaches to investigate the fatigue safety of existing RC bridges.

The State of the Art Report 188 [13] reported 17 cases of RC structural elements mainly bridge decks from around the world (Japan, Sweden, the Netherlands, Germany, the United Kingdom, and the United States), where fatigue was the main factor contributing to the deterioration of the structural elements.

For road bridges, RC decks are the part most vulnerable to fatigue due to the pronounced effect of axle loads [14]–[18]. Different experiments and simulations were conducted on RC slabs under moving loads to investigate the fatigue failure mode [19]–[24]. Fatigue-life predictions of RC decks were found challenging to make because they are affected by various sources of uncertainties, including material properties, vehicle loads, structural responses, and environmental conditions. Therefore, one effective way to cover all these uncertainties is the direct monitoring of structures. Structural analysis implementing load models from standards is not a reliable approach for examining existing RC decks. The load models of the standards are conservative since they do not rely on actual loading and actual structural conditions. In contrast, monitoring provides explicit information about the structural response and thus reduces most uncertainties of parameters related to fatigue safety investigation.

This paper presents a probabilistic methodology for investigating the fatigue safety of existing RC slabs that is based on data obtained from monitoring. The originality of this work includes the following:

- The development of an inverse method to identify the position and load of traffic from long-term monitoring data.
- The quantification of the effect of vehicle position and load and temperature variations on the fatigue damage of an RC bridge-deck slab.

- The combination of monitoring data, numerical simulations, and probabilistic assessments to define a procedure for fatigue safety examination.

The methodology can be used as a base for how to monitor existing RC decks and how to process data to evaluate their fatigue safety. It will be illustrated using the case of an existing bridge, the Crêt de l'Anneau viaduct in Switzerland.

2.2 Monitoring

2.2.1 Description of the Monitored Structure

The Crêt de l'Anneau viaduct is built in 1957 and is located in Switzerland on cantonal road 10, which is 20 km away from the French border (Figure 2.1). It is a composite steel-concrete structure with seven typical spans of 25.6 m and one 15.8 m approach span, giving it a total length of 195 m. The viaduct is composed of an RC slab fixed on two 1.3-m-high steel-box-girder beams of variable thickness ranging in the transverse direction from 24 cm near the supports to 17 cm at the midspan. The spans are linked to each other by hinges and supported by the piers located 5 m away from each hinge (Figure 2.2).
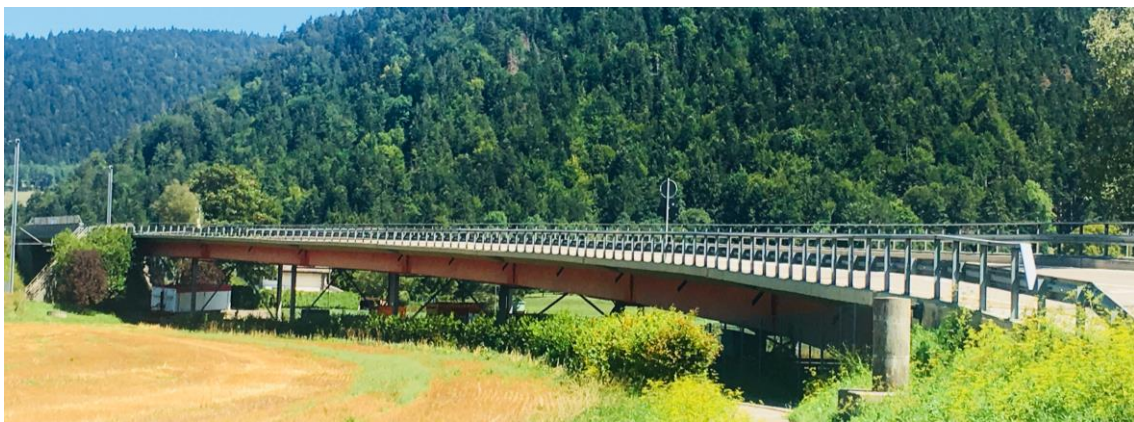
Figure 2.1. View of the investigated steel-concrete composite viaduct.

The RC slab was cast with concrete containing 350 kg of cement per m^3; its cube strength was equal to 45 N/mm² at 28 days. The deck slab has orthogonal grid reinforcements in both tensile and compression zones with diameters of 10 mm, 14 mm, and 18 mm. A single layer of reinforcement consisting of 25 Ø10 @200 in the longitudinal direction and 5 Ø10 @240 in the transverse direction on the compression side was provided. On the tensile side, a single layer of reinforcement consisting of 5 Ø14 @l/3 and 20 Ø14 @6/m in the longitudinal direction and 10 Ø14 @106.66 and 2 Ø 18 @l/3 in the transverse direction was provided. A compression-tensile strength of 300 N/mm² was assumed for rebars and 235 N/mm² was assumed for the steel girder.

2.2.2 Description of the Monitoring System

The monitoring system used to investigate the fatigue safety of the RC slab is composed of strain gauges and thermocouples. It is cost-effective and easy to install, use, and maintain. It is available for any engineering company.

The monitoring system implements recent technologies in data storage and high frequency acquisition to perform continuous real-time monitoring of the structural response resulting from action effects, mainly traffic loading and temperature effects. It is used for occasional inspections as well as for long-term monitoring. The bridge structure was instrumented in June 2016 with the monitoring system to measure strain and temperature histories at two main spans, Spans 2 and 4 (Figure 2.2).
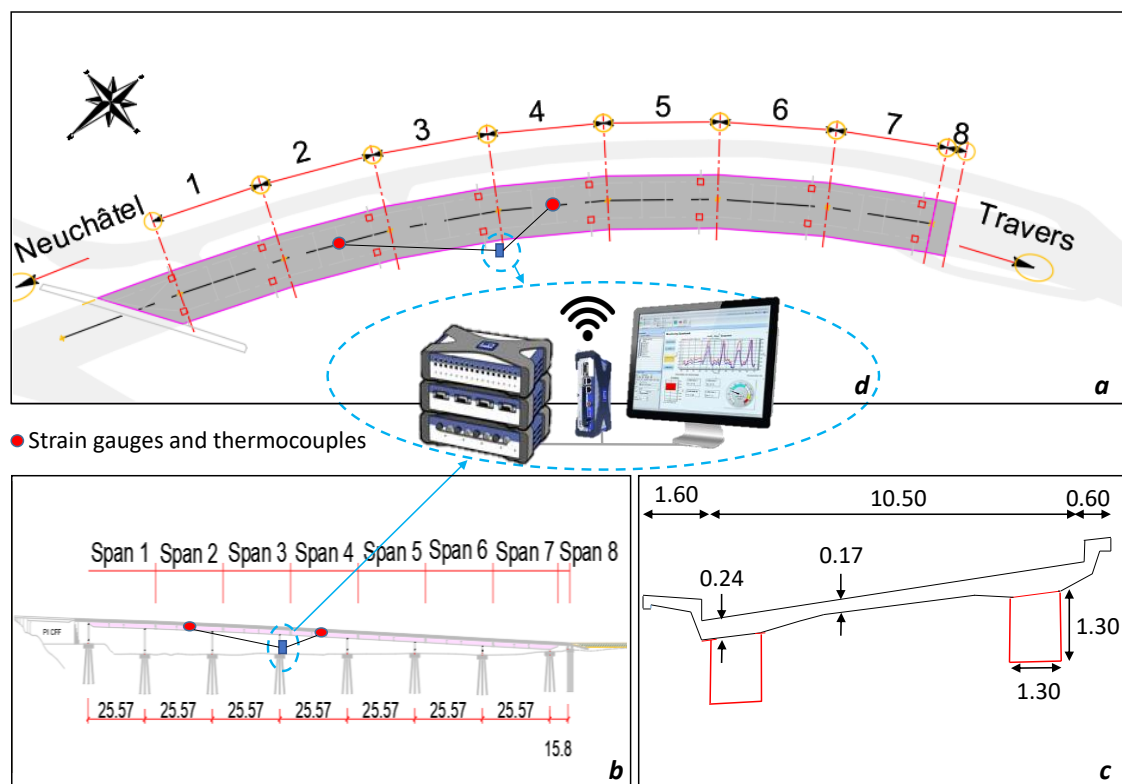
Figure 2.2. Drawing of the viaduct (a) plan view; (b) elevation side; (c) typical cross-section; (d) data acquisition and storage unit; dimensions in [m].

Transverse strains were measured by means of two strain gauges installed on the transverse rebars at the midspan of Slabs 2 and 4 (Figure 2.2). Longitudinal strains were measured by two strain gauges installed on the longitudinal rebars at the midspan of the same Slabs 2 and 4 and via one strain gauge installed on the steel girder beam at the midspan of Slab 4. To monitor temperature variation, three thermocouples were installed, with one in the concrete of the slab, one on the steel girder, and one in the air (Figure 2.3).
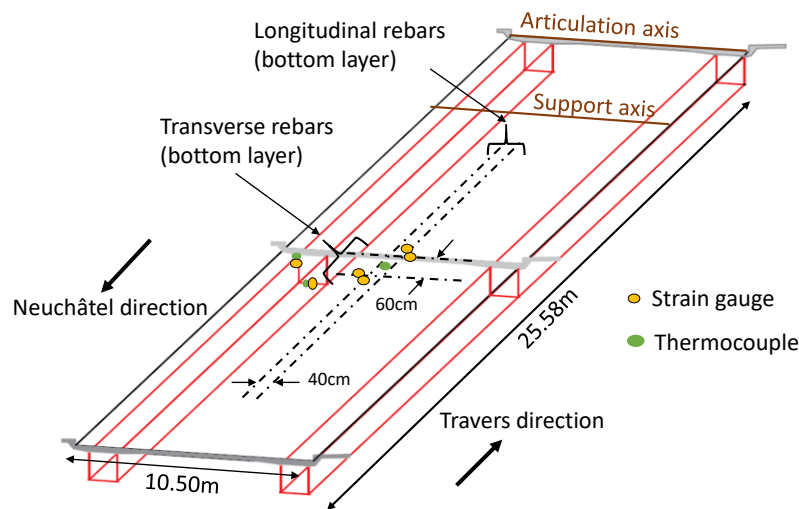
Figure 2.3. Location of the sensors in Span 4.

The monitoring system has been operating since June 2016. During the first year of monitoring, 44 GB of data were collected and analysed. The data were recorded continuously with sampling frequencies of 50 and 100 Hz for strain, and frequencies 2 and 1 Hz for temperature. The different sampling frequencies were used to evaluate the effect of frequency on capturing vehicle passages and temperature variation and to reduce the amount of collected data. Every 24 hours a binary file was created and stored in the server. It was converted afterwards to a MATLAB file to process the data.

2.2.3   Description of the Load Test

A load test was conducted after the instrumentation of the structure using a five-axle truck with the maximum legal load of 400 kN. Linear variable differential transformer (LVDT) sensors were installed on the instrumented slabs to evaluate the deflection of the cross-section. Four truck passages per direction were performed. The truck speed were 80, 40, 35, and 10 km/h. The five axles of the truck were separately weighed, and their effects on the viaduct were identified.

Transverse rebars were under tensile stresses during the passage of the truck. In the longitudinal direction, the girder and the longitudinal rebars showed the expected stress reversal (i.e., both tensile and compressive stresses due to vehicle passage; Figure 2.4). The five peaks in the longitudinal response represent the passage of the five axles of the truck. The measured strains were mainly influenced by the truck position and by the slab slenderness that accentuates local strains under the wheels. Identical structural responses were obtained from passages that follow the same trajectory.
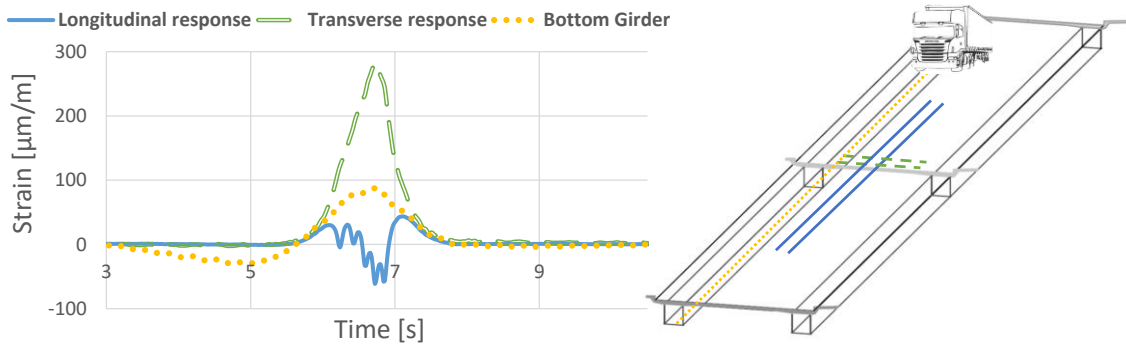
Figure 2.4. Strain variations due to a moving load (35km/h).

The axle configuration of the load-test truck has no influence on the response of the transverse reinforcement and the steel girder, which means that the effect of vehicles can be directly related to their total load when analysing the structural response of the cross-section. The results of the load test serve as a base for performing an inverse method to identify traffic features from the recorded strain.

2.3 Relevant Fatigue Actions

2.3.1 Traffic

2.3.1.1 Approach

An inverse method was developed to identify traffic features from the recorded strain. The method is called inverse because the loads and the positions of the vehicles crossing the viaduct are estimated from the recorded strain. The results of the load test were used to correlate the strain with the positions and the loads of the vehicles. Weight in motion (WIM) data collected from the same road about 1 km away from the viaduct were used to confirm the results of the inverse method and to evaluate traffic loads in the past and future [25], [26]. The long-term statistical distributions of the load and position of all the vehicles crossing the bridge-structure were then established for an assumed service duration of 120 years.

2.3.1.2 Identification of Vehicles

A peak-over-threshold (POT) approach was applied to the recorded strain to identify all light vehicles and heavy trucks crossing the bridge. Minimum peaks chosen to be included in the dataset were to be above the measurement error, determined from the observation of strain signals, which was 1µm/m, and the minimum time between each peak was set to 3 s such that only one peak was identified per

vehicle (Figure 2.5). The threshold of 1 µm/m eliminates motorbikes and very light cars that are not relevant for structural safety.
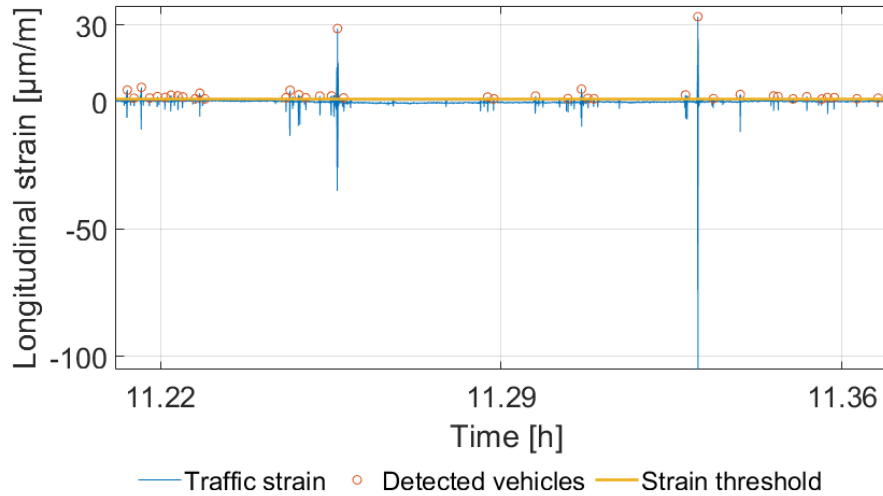
Figure 2.5. Peak over threshold (POT) for vehicle identification.

This method was applied to strain measurements of the instrumented longitudinal and transverse rebars. A comparison between the identified peaks in each case showed that the longitudinal response represented the vehicles better when compared with WIM data. The identification of the vehicles was thus performed based on the longitudinal response.

2.3.1.3   Identification of Vehicle Position

The roadway width of the viaduct has two lanes, one for the *Neuchâtel* direction and one for the *Travers* direction. To quantify the position of the vehicles, the coordinates of their gravity centre over the width of the roadway were defined as being 0 m for the end of the lane in the *Neuchâtel* direction, 5.25 m in the centre of the road, and 10.5 m for the end of the lane in the *Travers* direction, as shown in Figure 2.6.
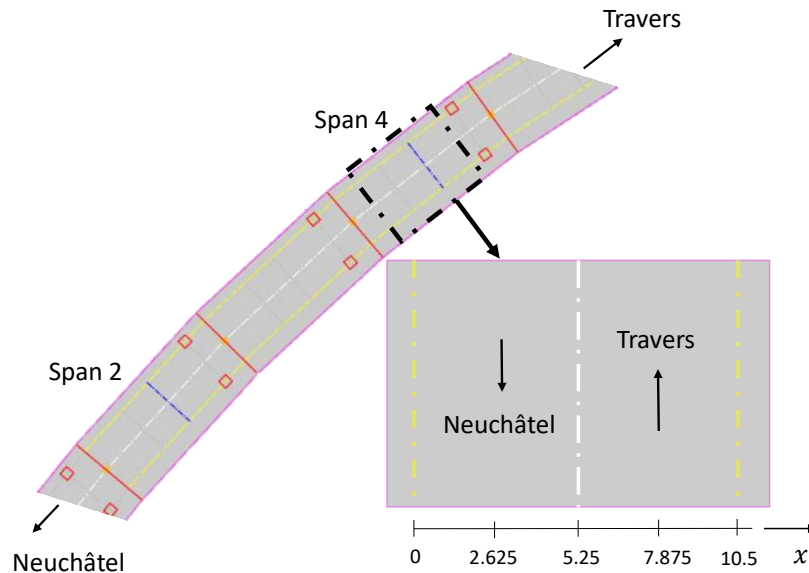
Figure 2.6. Vehicle positions in [m] over the roadway width.

During the load test, the truck passed over the viaduct at five positions with respect to the roadway's width. Strains in the rebars (transverse and longitudinal) and the girder versus the five positions of the truck were analysed to determine an explicit correlation between recorded strains and vehicle positions.

It was found that strain in the transverse rebars was the most sensitive to the position of the vehicles. To quantify this sensitivity, different combinations between transverse strains versus the positions of the test-truck were analysed and compared to the measured data. The ratio r of strains $\varepsilon_{transverse\ rebar\ 1}$ and $\varepsilon_{transverse\ rebar\ 2}$ in the two-instrumented transverse rebars was the parameter directly related to the position, giving similar values for passages with the same position (see Equation (2.1)). This ratio is approximately 1:1 when the vehicle is located at the centre of the roadway.

$$r = \frac{\varepsilon_{transverse\ rebar\ 1}}{\varepsilon_{transverse\ rebar\ 2}} \tag{2.1}$$

The ratio r as a function of the vehicle position was fitted with a third-degree polynomial equation:

$$r = ax^3 + bx^2 + cx + d \tag{2.2}$$

where x is the position of the vehicle, and a, b, c, and, d are the polynomial coefficients, defined from the load-test data. Figure 2.7 illustrates the fit of this ratio against the position of the 400 kN test-truck used to calculate the positions of the detected vehicles.
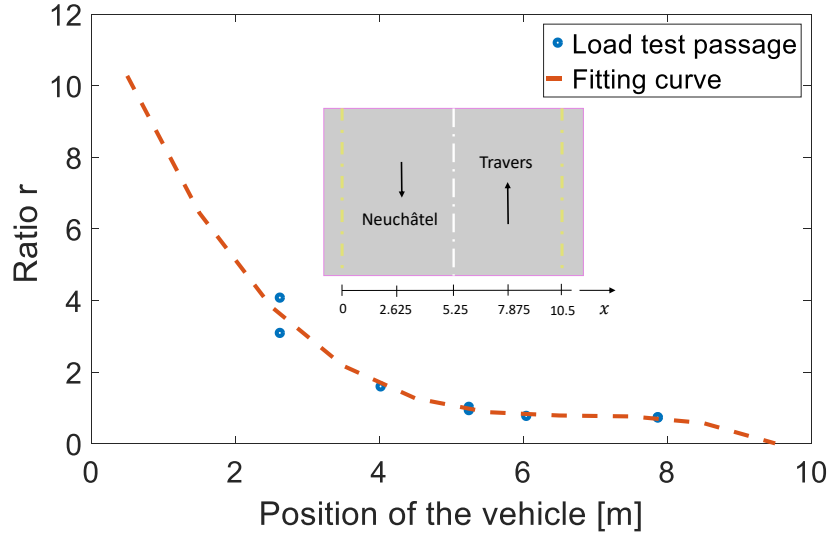
Figure 2.7. Fitting curve to calculate the position of the vehicles across the roadway width.

To obtain the long-term statistical distribution of truck positions, the vehicles were first identified using the POT approach applied to the longitudinal recorded strains. The corresponding peaks of strains in the two-instrumented transverse rebars were identified, and the ratio r between the peaks was calculated. The real solution of the polynomial $ax^3 + bx^2 + cx + d - r = 0$ corresponds to the position.

The roadway width of the viaduct is 10.5 m, and the wheels of the vehicles can have extreme positions such as 0 m and 10.5 m. The maximum width of the vehicles was assumed 2 m (Section. 2.3.1.6) and then, in this case, the centre of gravity of the vehicles cannot be less than 1.2 m and cannot be more than 9.3 m. When the calculated position was not in the defined interval, the centre of gravity was directly set at 1.2 m or 9.3 m for vehicles travelling in the *Neuchâtel* and *Travers* directions, respectively. The possible positions were then defined in the interval [1.2 m, 9.3 m].

Figure 2.8 presents the normalised long-term distribution of vehicle positions over the roadway width. An increment of 0.1 m was used to define this discrete distribution for the possible positions in the interval [1.2 m, 9.3 m]. Therefore, 82 positions were defined along with their normalised probability of occurrence.
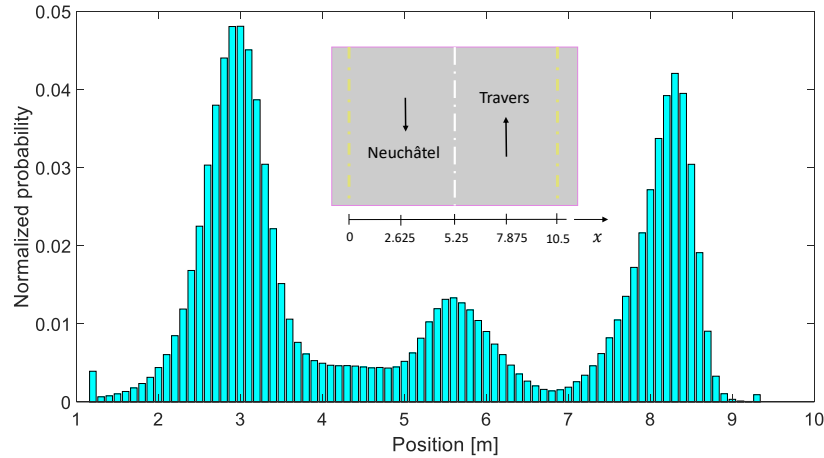
Figure 2.8. Normalised annual distribution of vehicle positions.

There are three clear peaks for vehicle positions. The peak in the middle represents the vehicles crossing the road from the centre, which can be due to the important slab-slope of 7% and the bend in the road creating a centrifugal force toward the centre for the light vehicles moving in the *Travers* direction. Moreover, the vehicles simultaneously crossing the instrumented slab from different directions can create a ratio r near to unity; accordingly, they were also counted in the middle peak.

The two other peaks represent the vehicles crossing the viaduct from the middle of the lane in the *Neuchâtel* and *Travers* directions respectively.

The algorithm well predicts the positions of the vehicles since their number in each direction corresponds to the number of vehicles provided by the WIM data (Section 2.3.1.5). The vehicles that are not in the interval [1.2 m, 9.3 m] were infrequent.

2.3.1.4   Identification of Vehicle Load

The loads were calculated after identifying the vehicles and their positions. It is assumed that the load and the corresponding strain follow a linear relationship for a specific position.

This assumption of linearity is supported by the results of the load test, where the deflection and the strain values under the 400 kN test-truck (load limit) regained their initial values after each passage. Moreover, identical structural responses were obtained from passages following the same trajectory. The data of the load test contain one set of positions for the same load (400 kN), and they were used to estimate vehicle loads knowing their positions.

The distribution of strain over the roadway width was modelled by a third polynomial fitting of load-test results:

$$\varepsilon\ (L = 400\ kN\ and\ x = i) =\ ai^3 + bi^2 + ci + d \tag{2.3}$$

where ε is the strain due to the passage of vehicle with load $L = 400\ kN$ and position $x = i$, $i \in [1.2\ m, 9.3\ m]$.

The response of the girder was found to be the most sensitive to truck positions after the response of transverse rebars. Therefore, they were used to calculate the load distribution for the 400 kN truck and the identified vehicles according to Equation (2.4).

$$L\ (x = i) = 400\ kN\ \frac{\varepsilon(x=i)}{\varepsilon\ (L=400\ kN\ and\ x=i)}$$

(2.4)

where $\varepsilon(x = i)$ is the recorded strain at position $x = i$.

Equation (2.4) was applied to the recorded strain in the transverse rebars and the girder, and for each vehicle, three loads L were calculated to find the best estimate. Different combinations of the calculated loads were then compared to the WIM data to identify the actual load. Subsequently, the loads of the vehicles travelling in the *Neuchâtel* direction were set equal to the mean of the calculated loads using the strain measured in the girder and the transverse rebar at the midspan (see Equation (2.5)). For the *Travers* direction, the loads were directly calculated from the strain measured in the transverse rebar at the midspan (see Equation (2.6)).

$$L\ (x = i)_{Neuchâtel} = 400kN\frac{1}{2}\left(\frac{\varepsilon_{transverse\ rebar}\ (x=i)}{\varepsilon_{transverse\ rebar}\ (L=400kN\ and\ x=i)} + \frac{\varepsilon_{girder}(x=i)}{\varepsilon_{girder}\ (L=400kN\ and\ x=i)}\right)$$

(2.5)

$$L\ (x = i)\ _{Travers} = 400kN\left(\frac{\varepsilon_{transverse\ rebar}\ (x=i)}{\varepsilon_{transverse\ rebar}\ (L=400kN\ and\ x=i)}\right)$$

(2.6)

Equations (2.5) and (2.6) were applied to analyse one year of measurements and establish the normalised annual distribution of vehicle loads. An increment of 10 kN was used to represent this discrete distribution, and overall, 64 load categories were identified with their normalised probability of occurrence (see Figure 2.9).
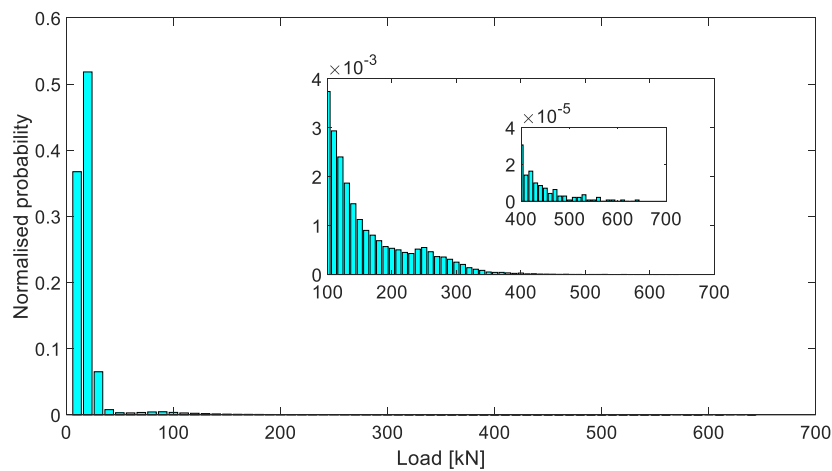
Figure 2.9. Normalised annual distribution of vehicle load.

The developed algorithm is efficient in identifying the composition of traffic based on the measured structural response. The resulting traffic distribution reveals that more than 96% of all detected vehicles were cars or small trucks, and 4% were heavy trucks (with a load more than 35 kN). Overloaded trucks exceeding the limit of 400 kN were identified with their position, their velocity, and the time they crossed the viaduct. One hundred ten trucks did not respect the 400 kN legal limit over the first year of monitoring, with the heaviest recorded load being 640 kN. The heavy trucks represent 8.10^{-5} of all detected vehicles. They were frequent during October 2016 for the *Neuchâtel* direction and during June-July 2017 for the *Travers* direction and almost absent during December and January. They were crossing the viaduct mostly from the centre of each lane.

The efficiency of the inverse method depends on the location of strain gauges and their number. It is important to design the position of the gauges over the longitudinal and cross-sections and to choose their numbers. The sensors should provide, firstly, the strain in the most loaded parts to verify the structural safety (with respect to fatigue at the midspan for the present study). Secondly, four aligned and separated strain gauges for the cross-section are necessary to detect the position of the vehicles in each lane, assuming that the road bridge has two directions. Finally, two separated strain gauges in the longitudinal section are needed to detect the vehicles and calculate their velocity.

2.3.1.5 *Validation and Calibration Using WIM Data*

The WIM data collected from the local territorial development department [26] were used to validate and calibrate the results of the inverse method (Table 2.1 and Table 2.2).
The WIM system was installed 1 km away from the viaduct, during the last week of September 2017 (from Monday 25 September to Sunday 1 October). It provided one week of continuous measurement of light and heavy traffic, which provides a solid database for verifying and calibrating the results of the inverse method.

The results of the inverse method were calibrated by introducing a calibration factor, which was equal to the ratio of the results of the inverse method and the WIM data. The weekly number of vehicles for each direction was used to calculate this factor, and accordingly, the number of daily vehicles was calibrated (Table 2.1 and Table 2.2). An error estimate was calculated according to Equation (2.7) as the ratio of the difference between the WIM data and the calibrated results of the inverse method and the WIM data.

$$Error = \frac{WIM\ data - Inverse\ method\ after\ calibration}{WIM\ data} \tag{2.7}$$

Table 2.1. Detected light vehicles according to the WIM data and the inverse method.

Light vehicles								
	WIM data		Inverse method				Error	
			Before calibration		After calibration		After calibration	
Direction	*Travers*	*Neuchâtel*	*Travers*	*Neuchâtel*	*Travers*	*Neuchâtel*	*Travers*	*Neuchâtel*
Monday	4'124	4'217	2'418	2'439	4'256	4'293	-3%	-2%
Tuesday	4'322	4'384	2'403	2'531	4'229	4'455	2%	-2%
Wednesday	4'408	4'436	2'508	2'546	4'414	4'481	0%	-1%
Thursday	4'544	4'644	2'538	2'591	4'467	4'560	2%	2%
Friday	4'678	4'826	2'618	2'684	4'608	4'724	1%	2%
Saturday	3'363	3'477	2'113	2'250	3'233	3'443	4%	1%
Sunday	2'574	2'597	1'744	1'753	2'668	2'682	-4%	-3%
Total	28'013	28'581	16'342	16'794	27'875	28'638	0%	0%

Table 2.2. Detected heavy trucks according to the WIM data and the inverse method.

Heavy trucks								
	WIM data		Inverse method				Error	
			Before calibration		After calibration		After calibration	
Direction	*Travers*	*Neuchâtel*	*Travers*	*Neuchâtel*	*Travers*	*Neuchâtel*	*Travers*	*Neuchâtel*
Monday	126	119	122	191	122	125	3%	-5%
Tuesday	128	135	164	191	164	148	-28%	-10%
Wednesday	134	130	143	183	143	134	-7%	-3%
Thursday	138	138	141	185	141	137	-2%	1%
Friday	148	132	156	196	156	127	-5%	4%
Saturday	51	46	44	66	44	36	14%	22%
Sunday	29	26	13	23	13	7	55%	73%
Total	754	726	783	1'035	783	714	-4%	2%

Light vehicles such as cars weighing less than 35 kN and motorcycles identified by the established algorithm do not match with WIM data because most of these vehicles have strain peaks in the domain of error of measurements (i.e., 1 µm/m). This number can easily be matched by changing the threshold of the POT approach or simply by introducing the missing vehicles. These underestimated vehicles can be neglected compared to other vehicles for the following case study. This assumption is justified in the results section (Section. 2.5).

The error in the estimation of the heavy trucks during the weekend is large. This error is due to their small number, which leads to an increase in the ratio used to calculate the error. However, by comparing the detected number of trucks directly, the difference between the WIM data and the inverse method is not important. Moreover, verifying the load of these trucks showed that they are near the 35 kN used to separate heavy trucks from light vehicles. Therefore, the error of detection could also be due to the WIM system during the classification.

The loads and the positions of the vehicles were evaluated by comparing the calculated and the measured numbers of heavy trucks for each direction. It was found that the inverse method provides the correct number of heavy trucks in the *Neuchâtel* direction and overestimates the number in the *Travers* direction. This result is mainly due to the use of only one strain gauge response to calculate vehicle loads in the *Travers* direction. In fact, a more reliable prediction can be achieved in the future by installing a strain gauge in the noninstrumented girder to obtain the transverse response of two aligned strain gauges for each direction. This overestimation was corrected by introducing a factor reducing the difference between the data of the model and the WIM data. The calculated and the measured daily number of heavy trucks in the *Travers* direction were evaluated, and the daily average of overestimation was found to be 42%. Therefore, the calculated number of heavy trucks ($N°$ (heavy traffic)) was reduced by introducing a factor of 0.7 (= 1/1.42; see Equation (2.8)).

$$N° \ (heavy \ traffic)_{corrected} = \ 0.7 \ N° \ (heavy \ traffic)_{calculated} \tag{2.8}$$

After calibrating the results using one week of local continuous WIM data, the robustness of the model was evaluated using continuous monthly WIM data and some daily data recorded during the same period of monitoring (07/2016 – 07/2017). The data were collected from the Federal Roads Office (FEDRO) in Switzerland [25], where the WIM system was installed on the same road a few kilometres away from the viaduct. To use the provided data, a coefficient of 1.47 was applied to reduce the difference between the FEDRO WIM data and the local WIM corresponding to the traffic crossing the viaduct according to Equation (2.9).

$$\frac{N°(traffic)_{local \ WIM}}{N°(traffic)_{FEDRO}} = 1.47 \tag{2.9}$$

The results of the inverse method were compared with the FEDRO WIM data. The calculated and the measured monthly averages of light vehicles and heavy trucks and the daily averages of the most loaded days were similar. The calibrated model is efficient in predicting the load and the position of the vehicles.

2.3.1.6 *Traffic Growth*

Local WIM data [26] and FEDRO data [25] were used to define traffic growth. The data showed how the annual traffic since 2002 for the same cantonal road X10 evolved. Figure 2.10 includes the ratio

of traffic evolution for the collected data, with a linear fitting curve defining the annual ratio of traffic growth.
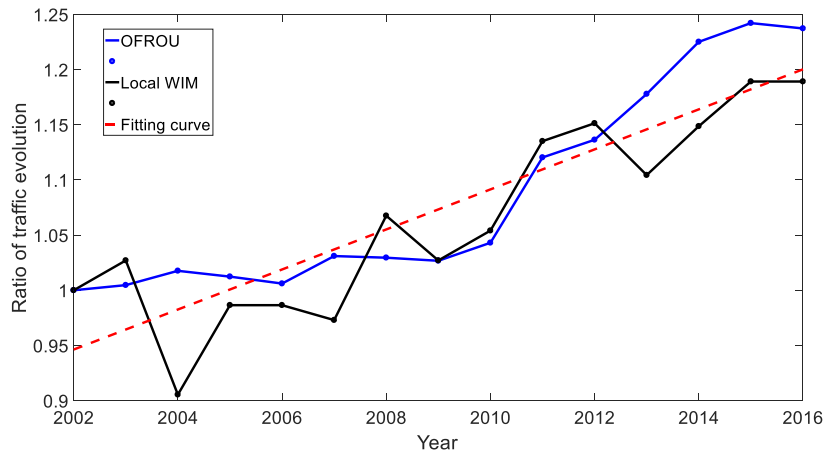
Figure 2.10. Ratio of traffic growth from 2002 to 2016.

Traffic evolution between 2002 and 2016 was defined according to the ratio of the annual increase in traffic, which is equal to 1.8%. Since no information was available about the traffic in the past and the evolution of traffic in the future, the percentage 1.8% was used to define four traffic scenarios for 120 years of service, from 1957 to 2077 (Figure 2.11).

Scenario 1: constant traffic before 2002 and after 2017 and a linear increase between 2001 and 2017.

Scenario 2: a linear increase in traffic before 2017 and constant traffic after 2017.

Scenario 3: constant traffic before 2002 and a linear increase in traffic after 2002.

Scenario 4: linearly increasing traffic.
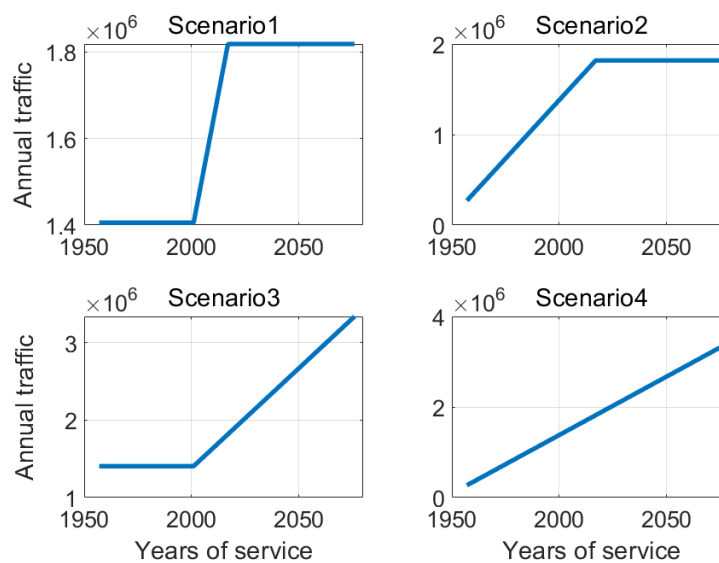
Figure 2.11. Scenarios of traffic growth.

The four scenarios of traffic evolution were used to define the annual statistical distribution of traffic based on the results of the inverse method. The normalised probability of the long-term distribution of vehicle positions and loads was assumed constant while changing the annual number of vehicles according to traffic-growth scenarios.

2.3.1.7 The Contact Surface of Vehicles

Axle dimensions and contact surfaces were assumed to be similar because the local effect of axle dimension was small when simulating the stresses in the finite element model (FEM), and the applied loads were correctly diffused in the slab (Section 2.4). Moreover, the contact surface was modelled only by two or five axles, since there was not a large difference between the simulated stresses using two, three, four or five axles (Section 2.4.2). The vehicles of traffic flow were classified into three categories according to their load to define their surface of contact, and these were used to apply loads in the FEM.

The first category represents the light vehicles weighing less than 35 kN (cars and small trucks); it was modelled using two equally loaded axles. Heavy trucks weighing more than 35 kN were divided into categories, two and three. The second category of vehicles with the load range [35, 100] kN was modelled by two differently loaded axles. The third category is for the vehicles heavier than 100 kN, and was modelled using five axles loaded according to the truck model provided by FEDRO [27]. The load legal limit of a single axle is 100 kN; therefore, this load was defined as the transition from two to five axles. The details of each category are summarised in Table 2.3.

Table 2.3. Contact surface of the classified vehicles.

Category		Axles	Contact surface	Axle load distribution	Load category
Light vehicles	1	2	0.4*0.4m	Equally distributed	[0,35] kN
Heavy trucks	2	2	0.4*0.4m	30% and 70%	[35,100] kN
	3	5	0.4*0.4m	15%, 15%, 20%, 25%, and 25%	[100,700] kN

The spacing of the axles was also taken from the updated traffic load for concrete deck slabs of existing bridges provided by FEDRO, as shown in Figure 2.12 [27].
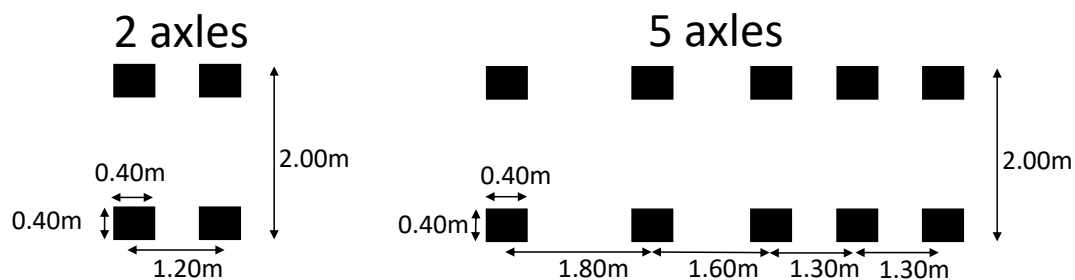
Figure 2.12. Spacing of the axles.

The location of the centre of gravity of each category was calculated. This location corresponds to the position provided by the inverse method and was used with the defined loads to distribute and load the contact surfaces for each identified vehicle.

2.3.2 Temperature

2.3.2.1 Introduction

The thermal effect on concrete bridges has been widely studied in the literature. The literature shows that temperature significantly affects the evolution of damage for concrete elements [15], [28]–[31]. Many studies have tried to model this effect, particularly [32]–[34], [29]. However, these models were generally subject to many uncertainties, especially when applied to existing bridges, where the state of concrete is not well known. Moreover, the thermal gradient is dependent on local conditions. Design codes, for example, provide different requirements for each country [31].

Thermal response is actually specific to each bridge and only precise monitoring of temperature and its effect with an explicit analysis of the measured parameters can reduce uncertainties and provide clear information about structural response due to thermal variations. For this aim, a detailed study of monitoring data was conducted to define the distribution of temperature and thermal strains in the RC slab.

2.3.2.2 Temperature Cycles

Temperature variation is a combination of two cycles, the daily and seasonal cycles. As such, the effect of temperature is a function of two parameters, the period of the day and the period of the year. To separate these cycles and their effects, a moving average was used in the present case. The daily effect is directly presented with 24 hours of measurements for a moving average with a subset of generally 10 minutes. The seasonal effect was deduced by the moving average with a subset of 30 days. This processing is outlined in Figure 2.13, where the combined, annual, and daily cycles of concrete temperature are presented for the Crêt de l'Anneau viaduct.
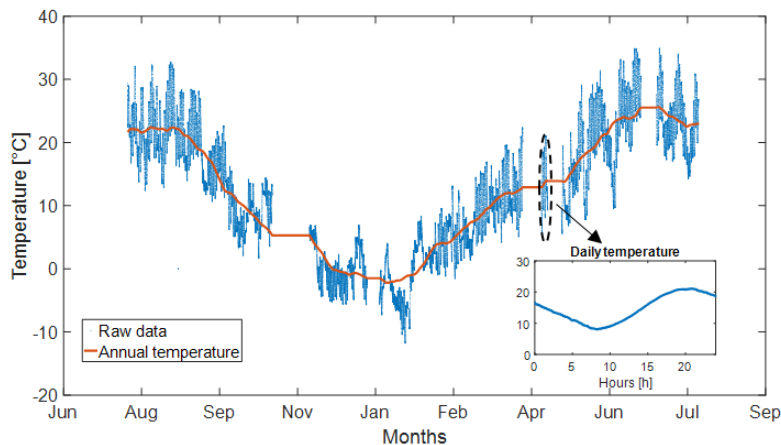
Figure 2.13. Annual and daily cycles of concrete temperature.

2.3.2.3 Temperature Effect

Temperature variations can have two direct effects (i.e., thermal diffusivity and thermal expansion). Thermal diffusivity is the transfer of thermal energy from the warm side to the cold side of the structural element, producing a gradient of temperature that creates a gradient of thermal strain due to thermal expansion. Thermal expansion is manifested by the contraction and expansion of materials and is characterised physically by the dilatation coefficient α (see Equation (2.10)).

$$\Delta\varepsilon = \alpha\,\Delta T$$

$$(2.10)$$

where $\Delta\varepsilon$ is the thermal strain variation, α is the dilatation coefficient [°C^{-1}], and ΔT is the temperature variation [°C]. For concrete and steel, the dilatation coefficient is equal to 10^{-5} °C^{-1}.

During monitoring, the configuration of strain gauges was adapted to compensate for the thermal expansion of materials and to measure the thermal expansion of structural elements. Stresses due to temperature are in fact produced when thermal expansion or contraction is restrained in structural elements [33].

This effect is remarkable because of its low frequency compared to traffic. Subsequently, the recorded time-series of strain measurements were filtered according to their frequency. The short-term fluctuations due to traffic action effects and the long-term fluctuations due to temperature effects were separated using a moving average that creates a serie of averages for each subset of 10 minutes. Three resultant signals are presented in Figure 2.14.

Raw data   = recorded strain

Thermal strain   = moving average of raw data each 10 minutes

Traffic strain   = raw data – moving average
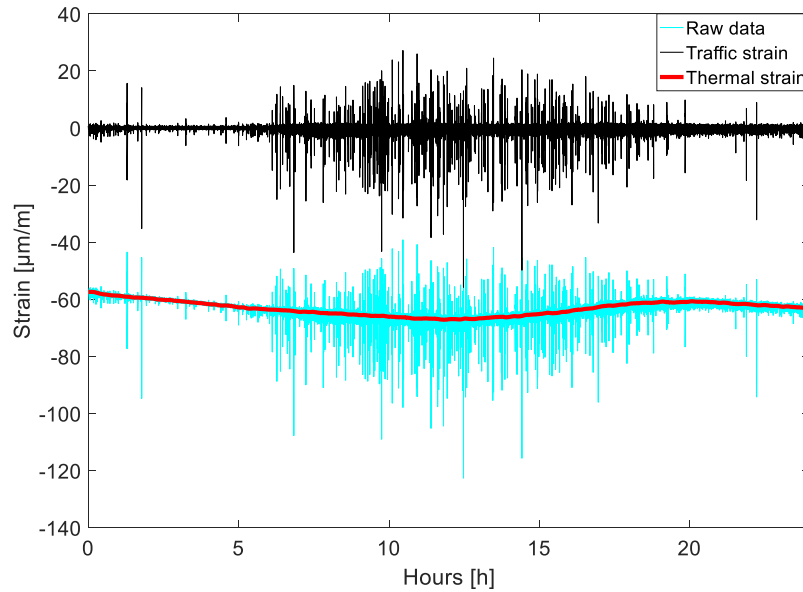
Figure 2.14. Daily raw data, thermal strain, and traffic strain.

The subset of 10 minutes was chosen via a sensitivity analysis of the structural response. The parameter was modified until a signal with all the targeted features for traffic strain and thermal strain was obtained. Thereby, thermal strains are properly extracted from the recorded data and can be used to evaluate the effect of temperature on fatigue. The probability of occurrence of the recorded temperature and thermal strain within one year of monitoring was normalised, and the annual statistical distributions of temperature and its effect are presented in Figure 2.15 for the transverse reinforcement at the midspan of Slab 4. An increment of 2 μm/m was used to define this discrete distribution for the possible thermal strain of concrete such that 51 strains were defined with their normalised probability of occurrence. The statistical distribution of temperature and its effect are used to define the mean stress relevant for fatigue reliability investigations for concrete.
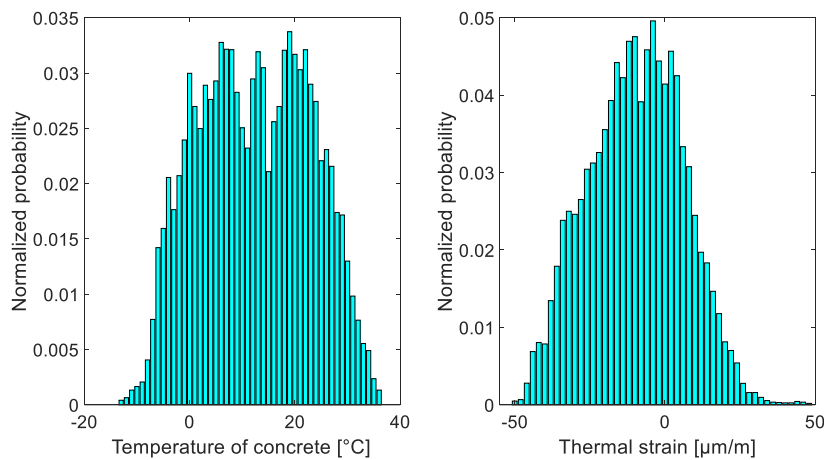
Figure 2.15. Normalised annual probability of concrete temperature and thermal strain.

2.4 Numerical Simulations

2.4.1 Finite Element Model

2.4.1.1 *Approach*

A two-dimensional FEM was developed using the commercial program ANSYS R18.2 for one span of the viaduct, to define the statistical distribution of stresses in the slab due to traffic loading.

Numerical models of large civil engineering structures are disposed to uncertain system parameters, which affect the ability of such models to accurately predict structural responses [35]. It is therefore necessary to develop a detailed FEM when analysing the structural response to a specific loading. For this aim, the model was calibrated with monitoring data to reduce the difference between the finite element results and the real-time structural response obtained by monitoring.

2.4.1.2 *Description of the Finite Element Model*

Structural analysis of only one span was performed since the seven spans are identical. The concrete and steel were modelled using their initial mechanical properties. To account for the evolution of material properties during the 60 years of service, the model was calibrated by comparing the simulated strains with the results of the load test. The simulations were performed in the elastic domain.

The element Shell 181 in the ANSYS software was used to model the concrete slab and steel girder. For the slab, an elastic modulus of 35'000 N/mm², a Poisson ratio of 0.2, a density of 25 kN/m³, a compressive strength of 35 N/mm² and a tensile ultimate strength of 3 N/mm² were used.

For the steel girder, an elastic modulus of 210'000 N/mm², a Poisson ratio of 0.3 and a compression-tensile ultimate strength of 235 N/mm² were used. Material properties are grouped in Table 2.4.

Table 2.4. Material properties.

Material	Density [kN/m³]	Young's Modulus [N/mm²]	Poisson's Ratio	Element
Reinforced concrete (slab)	25	35'000	0.2	Shell 181
Steel (girder)	78.5	210'000	0.3	Shell 181

Mesh density was checked in longitudinal and cross-sections by comparing simulated strains for different element sizes. An optimal element size of 100 mm in the longitudinal section and 50 mm in the cross-section were found to give accurate results without time-consuming simulations.
The connection between the RC slab and the girder was assumed a total fixity.

For the boundary conditions, the span was articulated from one side and simply supported as a continuous beam from the other side. The longitudinal displacement and rotations were thus free on one side, and all the displacements and rotations were restricted on the other side. Figure 2.16 includes simulation results for a five-axle truck with a load of 640 kN at the midspan.
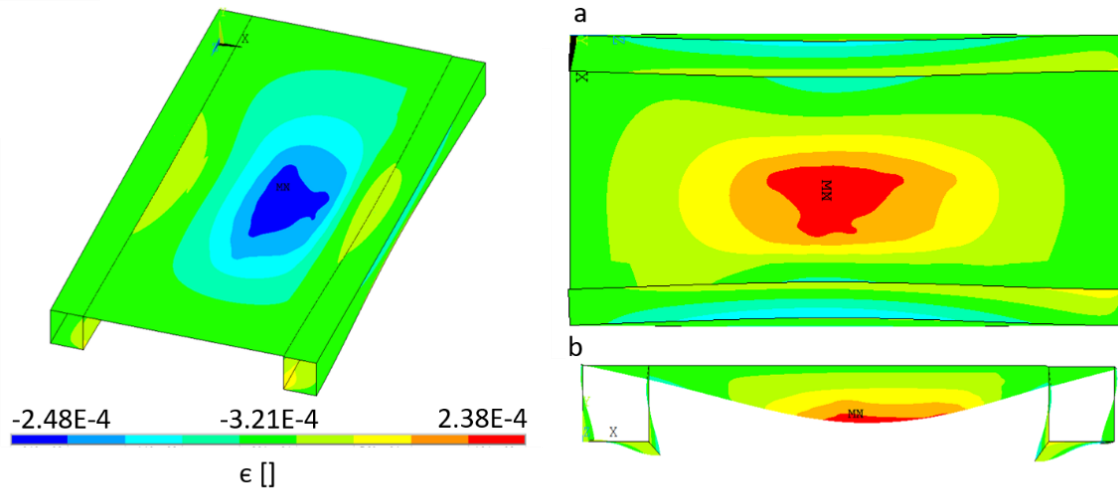
Figure 2.16. Finite element model (FEM) simulation results of the deck, bottom side (a), and cross-section side (b).

2.4.1.3   Calibration of the Finite Element Model

The FEM was calibrated using measured strains and deflections as obtained from the load test. The calibration included changes in material properties, the connections, and the boundary conditions in order to have the same measured parameters as in the load test [36].

For this case study, the calibration minimising the difference between monitoring and finite element results was performed in two steps. The first step was calibrating strains of the longitudinal section by changing the stiffness, and the second was calibrating strains and the deflection of the transverse section by introducing a calibration factor. Three models were defined: the initial theoretical model, the calibrated model with a different stiffness, and the calibrated model with the new stiffness and the calibration factor.
The passages of the 400 kN truck in the centre of the roadway were used for the calibration. The longitudinal response was calibrated by taking the elastic modulus of the concrete as a parameter. It was modified to minimise the difference between the measured and the calculated longitudinal strains.

For the cross-section, a comparison between the results of the noncalibrated FEM and the load-test model showed that the RC slab is not totally fixed in the steel girder. In fact, the simulated longitudinal strains were identical to monitoring data, but the transverse strains were different. To come closer to real-time measured strains, calibration was proceeded by the modelling of the elastic flexibility

between the girder and the RC slab. This generated some convergence issues due to the use of nonlinear behaviour. Therefore, the flexibility between the girder and the slab was introduced by a calibration factor that compensates the difference between the simulated and the measured transverse strain. The calibration factor found to provide the same results as those obtained by monitoring was 1.5.

The two-dimensional model was developed to run simulations more quickly and to lighten the calculations while providing the same response of the RC slab as obtained by load-test data.

2.4.2 Simulation and Results

Traffic loads were simulated with the toolbox ANSYS_aaS in MATLAB to provide a direct link between the programs. A MATLAB code was developed to run ANSYS commands and save the results for several simulations. Once the deck was modelled, the code generated a new vehicle with a specific load and position, calculated the loads and the positions of the axles, applied the calculated axle loads to the FEM, ran the model and took the transverse strain at the midspan.

The results of the simulation provide the distribution of the strain in the deck for the 82 possible positions and 64 possible loads.

Figure 2.17 includes the distribution of stress ranges in the transverse rebar at the midspan as a function of vehicle positions and loads. Stress ranges are calculated from the simulated strains using
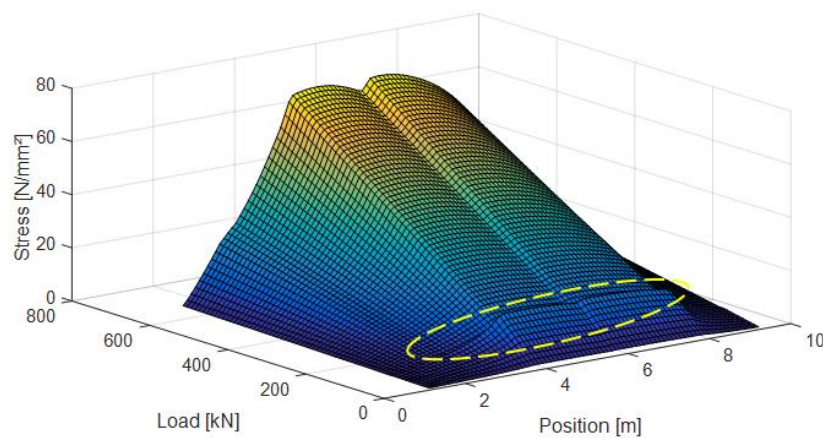
Figure 2.17. Distribution of the simulated stresses at the transverse rebar of the midspan.

the elastic modulus of steel, 210,000 N/mm², and the elastic modulus of concrete, 35'000 N/mm².

A small peak can be observed (surrounded by the dashed line in Figure 2.17), which is located for stresses under 100 kN load, where the passage from two axles to five axles is performed. The peak is present due to the local effect of the applied loads and is more pronounced for two axles. However, this local peak stress is very low at less than 1 N/mm². As highlighted in Section. 2.3.1.7, the number of axles does not induce a significant difference between the simulated stresses. The choice of two axles for loads less than 100 kN and five axles for loads greater than 100 kN is thus appropriate.

The simulated and the measured maximum stresses are alike, which proves that the FEM is well calibrated for the structural response of heavy trucks.

The heavy trucks located at the midspan cause the maximum stresses. The trucks create two peaks 1 m away from the midspan, which corresponds to the location of the axles.

To define the annual statistical distribution of stresses due to traffic, vehicle position and load were considered independent stochastic variables. The annual number of cycles is defined by the distributions of the loads and positions, with the strain range $\varepsilon_{i,j}$ generated by the vehicle with the position-load $[x_i, L_j]$ (Figure 2.8 and Figure 2.9) according to Equation (2.11).

$$n_{i,j} = P_{x_i} P_{L_j} N \tag{2.11}$$

where $n_{i,j}$ is the number of vehicles with the position x_i and the load L_j, creating the strain range $\varepsilon_{i,j}$

P_{L_j} is the probability that the vehicle has a load L_j

P_{x_i} is the probability that the vehicle is at position x_i

N is the total number of vehicles per year

Figure 2.18 provides steps for identifying the probabilistic distribution of stresses as a function of the loads and the positions of the vehicles.
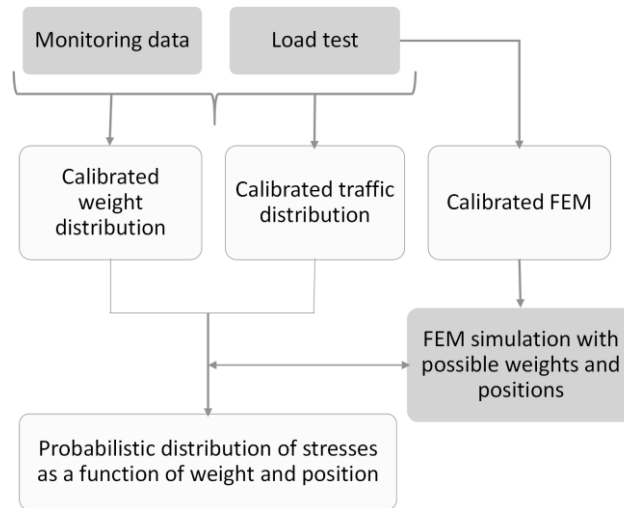
Figure 2.18. Steps to define the statistical distribution of traffic stresses.

2.5   Fatigue Examination

In this study, the fatigue safety examination of the RC slab, which is designed to predominantly resist in the transverse direction is focused on the bending failure mode, which may result either in compression failure of the concrete or tensile failure of the reinforcement.

The recorded strains in the transverse rebars were greater than the strains in the longitudinal rebars, which are mainly due to the distribution of the actual traffic loads on both the RC slab and the steel girder carrying in the longitudinal direction, while in the transverse direction, only the 17 cm-thick RC slab is acting. The mechanism of fatigue failure of reinforced-concrete slabs is complex and depends on many variables (stress ranges, reinforcement ratio, boundary conditions, etc.). Previous studies have shown that failure can be induced by the interaction of flexural-shear concrete cracks [19]–[21] or rebar fracture when there is no longer stress transfer [37], [22]. In this study, no concrete cracking was visible at the midspan of the RC slab. The reversal stresses were present in the longitudinal response, as shown in Figure 2.4, but they were smaller than transverse stresses. Even under significant shear fatigue stress, these types of slabs were reported to fail due to fatigue failure of the rebars [37]. Therefore, the cross-section of the RC slab was defined as the critical section, and the fatigue stress was investigated using the transverse strains. The investigation of stress-reversal effects is presented in Chapter 5.

2.5.1   Fatigue Examination of Steel Reinforcement

Fatigue of steel reinforcement is examined at two levels. Level 1 requires fatigue stresses to be below the endurance limit. Level 2 is performed when Level 1 is inconclusive, and it requires the calculation of the fatigue damage. In the Swiss standard SIA269/2, the fatigue resistance of straight rebars with a diameter less than 30 mm is equal to $\Delta\sigma_{sd, fat} = 150$ N/mm^2, and the endurance limit is equal to 80% of the fatigue limit (i.e., $\Delta\sigma_{sD} = 120$ N/mm^2, and the slope of the S-N curve is equal to m = 4 [38].

Level 1 is fulfilled for the rebars at the midspan since all the measured stress ranges are below 120 N/mm^2. Therefore, steel reinforcements do not present any fatigue problem based on the one-year monitoring data. The Level 2 fatigue examination therefore does not need to be performed. However, to illustrate the damage as a function of the actions relevant to fatigue, the recorded stresses were arbitrarily amplified by a factor of four to obtain stress values higher than the endurance limit. Subsequently, the Level 2 examination was conducted with fictitious stress values that relate to real loading conditions.

Fatigue damage is quantified in terms of Miner's damage summation to deal with variable amplitude loading in the S-N approach. According to this rule, all stress cycles induce proportional fatigue damage, which is linearly additive. The scatter in the stress history may be ignored, and the damage d due to n_i cycles for the stress range $\Delta\sigma_i$ is equal to:

$$d = \sum \frac{n_i}{N_i}$$

(2.12)

where

d is the cumulative damage

n_i is the number of cycles for the constant stress $\Delta\sigma_i$

N_i is the total number of cycles to failure under the constant amplitude stress $\Delta\sigma_i$

Fatigue safety is fulfilled if the accumulated damage is less than 1:

$$d < 1 \tag{2.13}$$

The damage is calculated according to Equation (2.12) using the annual statistical distribution of stresses and stress cycles defined in the previous section. Figure 2.19 illustrates the annual distribution of damage for the first year of monitoring as a function of the positions and loads of vehicles.
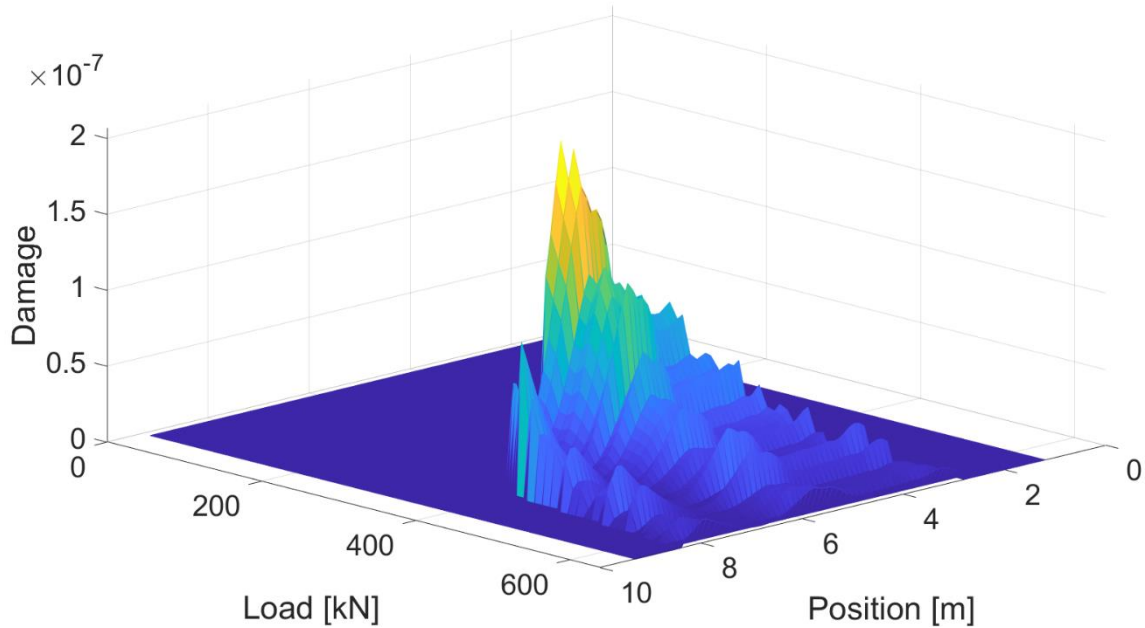
Figure 2.19. Annual fatigue damage distribution for the transverse rebar at the midspan (monitored stresses are arbitrarily amplified by a factor of four).

The fatigue damage is zero for stresses smaller than the endurance limit, which is the case for the vehicles weighing less than 300 kN, no matter their positions. Only heavy trucks are thus relevant for fatigue damage, and the light vehicles can be neglected in examining the fatigue safety of steel reinforcement. This finding justifies the threshold used in the POT approach, determining which

vehicles create a strain less than 1 µm/m. Figure 2.19 indicates that fatigue damage is more pronounced for vehicles crossing the roadway from the middle.

The trucks with loads between 350 kN and 400 kN are the most frequent, which is mainly due to the legal load limit for vehicles being fixed at 400 kN for this viaduct. The frequency of these trucks creates the highest annual fatigue damage. The trucks heavier than 400 kN create high fatigue damage. However, they are infrequent, and their annual effect is not pronounced.

To evaluate the accumulated damage during the years of service of the viaduct and to predict the total damage in the future, the four scenarios of traffic growth introduced in Section 2.3.1.6 were analysed. Accordingly, the accumulated damage was calculated for 120 years of service as shown in Table 2.5.

Table 2.5. Accumulated fatigue steel damage for 120 years of service.

Scenario	1	2	3	4
Accumulated damage	$4.80 \cdot 10^{-03}$	$4.20 \cdot 10^{-03}$	$5.90 \cdot 10^{-03}$	$5.30 \cdot 10^{-03}$

Even by amplifying the stress ranges arbitrarily by a factor of four, the fatigue damage is low and insignificant after 120 years of service, for different scenarios of traffic growth. Consequently, the fatigue service duration of the viaduct is very long when considering the actual evolution of traffic.

The scenarios of traffic growth define the evolution of the accumulated damage. There is a difference in accumulated damage of 40% between the nonconservative scenario (2) and the conservative scenario (3). Therefore, considering different scenarios of traffic growth is necessary to quantify fatigue damage when no information is available about the past and future traffic.

This inverse method allows one to evaluate the damage as a function of vehicle position and load. This information may be useful for making decisions about limiting or reducing a particular type of vehicle or imposing certain vehicle positions to restrain fatigue damage. Moreover, this information may also be useful for allowing for a controlled increase in the number of vehicles and trucks and in the legal vehicle load limit while limiting possible fatigue damage.

2.5.2   Fatigue Examination of Concrete

The fatigue of concrete is investigated based on the International Federation for Structural Concrete (FIB) Model Code [39]. The fatigue requirements under cyclic loading are met if the required lifetime (number of cycles) is less than or equal to the number of cycles to failure.

$$n \leq N \tag{2.14}$$

n is the foreseen number of cycles during the service duration

N is the number of resisting stress cycles

The recorded strains in the transverse rebars were more than twice the number of strains of the longitudinal rebars. In fact, in the longitudinal section of the viaduct, the applied traffic loads were distributed across the RC slab and the steel girder, but for the cross-section, axle loads were directly distributed along the 17 cm RC slab. Therefore, the RC was investigated for the cross-section assuming uniaxial tensile stress in the steel reinforcement bars, and uniaxial compression stress in the concrete. The fatigue damage investigation for the concrete under compression is presented as follows.

Fatigue loading of concrete is expressed in [39] by the maximum compressive stress level $S_{c,max}$ and the minimum compressive stress level $S_{c,min}$. Therefore, for $S_{c,min} > 0.8$, the S-N relations for $S_{c,min} = 0.8$ are valid, and for $0 < S_{c,min} \leq 0.8$, the following equations apply.
The number of cycles N to failure is obtained from

$$logN = logN1 \qquad \text{if} \qquad logN1 \leq 8 \tag{2.15}$$

$$logN = logN2 \qquad \text{if} \qquad logN1 > 8 \tag{2.16}$$

$$\text{where} \qquad log\,N1 = \frac{8}{Y-1}\,(S_{c,max} - 1) \tag{2.17}$$

$$log\,N2 = 8 + \frac{8\,ln(10)}{Y-1}\,(Y - S_{c,min})lo\,g\left(\frac{S_{c,max} - S_{c,min}}{Y - S_{c,min}}\right) \tag{2.18}$$

$$\text{where} \quad Y = \frac{0.45 + 1.8\,S_{c,min}}{1 + 1.8\,S_{c,min} - 0.3S_{c,min}^2} \tag{2.19}$$

$$S_{c,max} = |\sigma_{c,max}|\,/\,f_{ck,fat} \tag{2.20}$$

$$S_{c,min} = |\sigma_{c,min}|\,/\,f_{ck,fat} \tag{2.21}$$

The fatigue reference compressive strength $f_{ck,fat}$ depends on the age of concrete at the beginning of fatigue loading, and it may be estimated from [39]:

$$f_{ck,fat} = \beta_{cc}(t)\beta_{c,sus}(t, t_0)f_{ck}(1 - \frac{f_{ck}}{400}) \tag{2.22}$$

where

N \qquad is the number of cycles to failure

$S_{c,max}$ \qquad is the maximum compressive stress level

$S_{c,min}$ is the minimum compressive stress level

$\sigma_{c,max}$ is the maximum acting compressive stress in [MPa]

$\sigma_{c,min}$ is the minimum acting compressive stress in [MPa]

f_{ck} is the characteristic compressive strength

$f_{ck,fat}$ is the fatigue reference compressive strength

$\beta_{cc}(t)$ is a coefficient which depends on the age of concrete at the beginning of fatigue loading

$\beta_{c,sus}$ is a coefficient which takes into account the effect of high mean stresses during loading, for fatigue loading it may be taken as 0.85

β_{cc} represents the 'time-dependant' aspect and it is calculated according to Equation (2.23).

$$\beta_{cc}(t) = exp[s\left(1 - \sqrt{\frac{28}{t}}\right)] \tag{2.23}$$

such as s = 0.25, a coefficient which depends on the strength class of cement, and t is the concrete age in days.

The RC slab is made with a special concrete CP350, with cube strength equal to 45 N/mm² at 28 days. f_{ck} is then equal to 35 N/mm², and the elastic modulus is equal to 35'000 N/mm² [39].

The maximum compressive stress is equal to the stress due to dead loads, temperature, and traffic:

$$\sigma_{c,max} = \sigma_{traffic} + \sigma_{dd} + \sigma_{temperature} \tag{2.24}$$

The minimum compressive stress is equal to the stress due to dead loads and temperature:

$$\sigma_{c,min} = \sigma_{dd} + \sigma_{temperature} \tag{2.25}$$

where

$\sigma_{traffic}$ is the stress due to traffic loading

σ_{dd} is the stress due to dead load

$\sigma_{temperature}$ is the stress due to temperature

Strain values of the concrete are deduced from the calculated strain in the transverse rebar. These calculated strains are extracted at the midspan with respect to the neutral axis location of the cross-section. For an uncracked section, the neutral axis is located at a distance of 87.5 mm from the top. The concrete below the neutral axis is assumed to be cracked [37], and steel reinforcement bears the

tensile stress. Accordingly, the recalculation gives the new neutral-axis location at 45 mm below the top. This neutral axis is subsequently used to calculate concrete stresses due to traffic $\sigma_{traffic}$ as the highest stress at the top of the cross-section using measured strain values.

The stress due to dead loads σ_{dd} is obtained from the FEM.
The stress due to temperature $\sigma_{temperature}$ is considered as a stochastic independent variable, with a discrete distribution defined using monitoring data (Section 2.3.2.3, Figure 2.15).

Stresses are calculated from strain by multiplying them with the elastic modulus of concrete. To obtain significant fatigue stresses, an arbitrarily chosen multiplication factor of four was again used for the stress values of concrete. Each calculated stress corresponds to the passage of a vehicle with the transverse signature illustrated in Figure 2.4. Thus, for each calculated stress range there is a corresponding half cycle.

The fatigue damage of concrete was calculated as a function of temperature variations and the position and the load of the vehicles. Figure 2.20 illustrates the fatigue damage of concrete as a function of vehicle position and temperature for a load of $L = 320\ kN$, as a function of vehicle load and temperature for the position $x = 2.2\ m$, and as a function of vehicle load and vehicle position for the temperature $T = 20\ °C$.
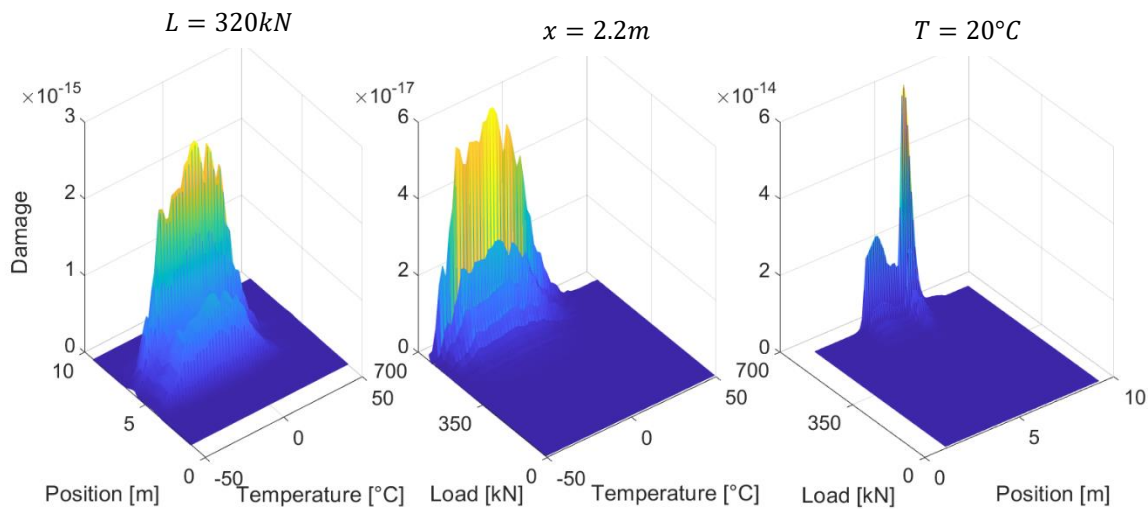
Figure 2.20. Long-term fatigue damage distribution of concrete (L = 320 kN, x = 2.2 m, T = 20 °C) (monitored stresses are arbitrarily amplified by a factor of four).

Temperature variations influence the fatigue damage of concrete, which takes the same distribution of temperature (Figure 2.15) for a fixed load or position. The fatigue damage of concrete increases significantly for loads greater than 400 kN, which means that the heavy trucks create higher fatigue damage even if they are not as frequent as the light vehicles. The damage is higher in the *Neuchâtel* direction, as the heaviest trucks in that direction are more frequent. The accumulated fatigue damage according to the four scenarios of traffic growth is presented in Table 2.6.

Table 2.6. Accumulated fatigue concrete damage for 120 years of service.

Scenario	1	2	3	4
Accumulated damage after 120 years of service	$8.90 \; 10^{-04}$	$7.74 \; 10^{-04}$	$1.10 \; 10^{-03}$	$9.81 \; 10^{-04}$

The fatigue damage of concrete due to past and future traffic is also very low, even after 120 years of service, although the values from monitoring were arbitrarily multiplied by a factor of four. Consequently, and despite highly conservative assumptions, the concrete of the RC slab currently shows no fatigue problem and will not present any notable fatigue problem in the future.

The calculated fatigue damage of concrete is 20% lower than the calculated fatigue damage of steel reinforcement. This means that, under pure compression of concrete, the steel reinforcement can be expected to fail first due to tensile cyclic loading. This result coincides with the findings of [17], [22], and [40], where steel rebars failed before concrete under fatigue loading.

2.5.3 Sensitivity Analysis

To understand the interrelation between input parameters and fatigue damage and to identify the parameters that cause significant uncertainties in the calculations, a sensitivity analysis of the fatigue damage of steel and concrete was conducted.

The sensitivity of three main parameters involved in the fatigue damage d calculations was evaluated. The compressive strength of concrete f_{ck}, the stress factor, and the annual traffic is varied such that 100% corresponds to their initial values, 35 MPa, 4, and 1'405'502 vehicles/year, respectively (Figure 2.21 and Figure 2.22).
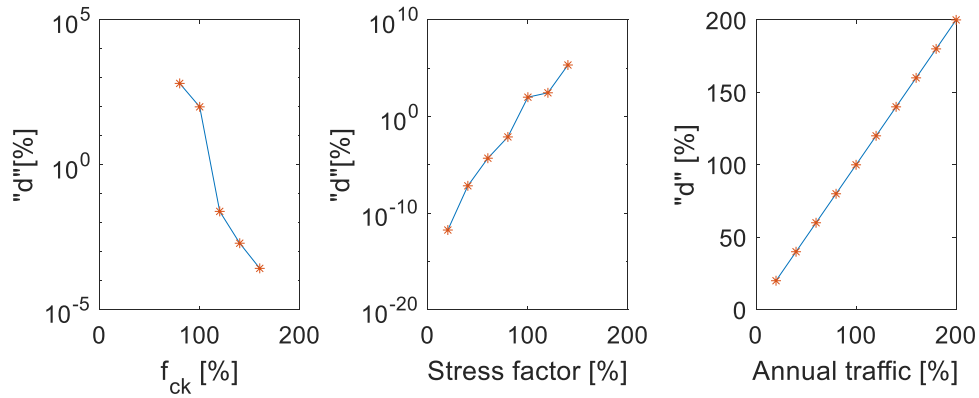
Figure 2.21. Sensitivity of the fatigue damage of concrete.
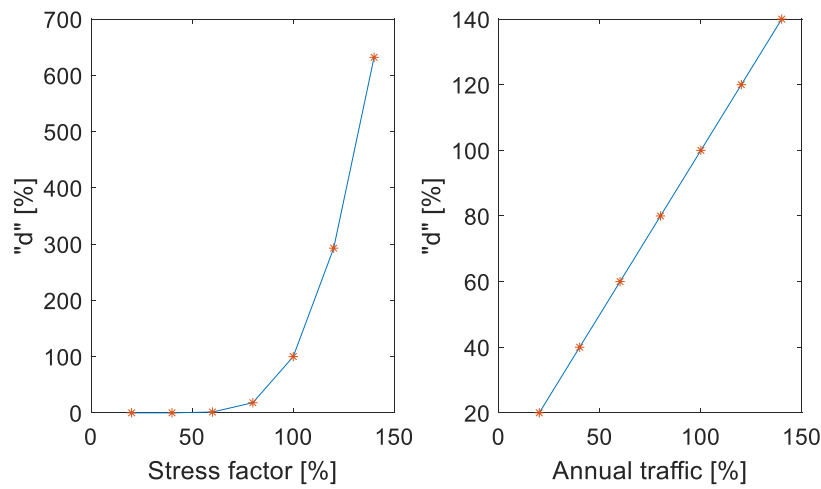
Figure 2.22. Sensitivity of the fatigue damage of steel.

The fatigue damage of steel and concrete varies linearly with annual traffic in terms of the number of vehicles. In fact, in changing the annual traffic, the positions and the loads of the vehicles remain constant. The stress ranges are thus the same for different cycles. According to Equation (2.12), the fatigue damage is linearly related to the number of stress cycles. Therefore, traffic growth under the same distribution of loads and positions will generate similar fatigue-damage growth.

The fatigue damage of steel increases exponentially with the stress factor, while the logarithm of concrete damage and the stress factor are linearly related. The stress factor presents the changes in the stress ranges due to the variation in load and position distributions. Fatigue damage is thus highly sensitive to heavy trucks and the most loaded positions.

The increase of concrete compression strength exponentially decreases the fatigue damage of concrete. It is therefore essential to adequately assess the strength of concrete when evaluating its fatigue safety because it is a critical parameter for fatigue damage.

2.6   Conclusion

The fatigue safety of an RC slab of a 60-year road viaduct was investigated based on monitoring data, where the structural response, traffic loads, temperature effect, and their combinations were considered. The main goal of this study is to develop a practical method for evaluating the fatigue safety of RC road bridges. This is particularly significant when using monitoring data that reduces the uncertainties in traffic and environmental load properties and structural responses, which is a considerable advantage of using monitoring data over design code estimates. For this purpose, the focus was on evaluating the fatigue damage of steel reinforcement and concrete and its evolution over time as a function of temperature variation and the positions and loads of vehicles.

Five main conclusions can be highlighted:

1. The inverse method precisely identifies the loads and positions of all the vehicles crossing the RC slab, using data from only four strain gauges and a load test.

2. The combination of finite-element modelling and probabilistic assessments of monitoring data provides probabilistic distributions of stresses in the RC slab as a function of the loads and the positions of the vehicles.

3. The comparative investigation of both steel reinforcement and concrete identifies the governing material in terms of fatigue safety. Steel reinforcement governs.

4. Recording ambient temperature and thermal variations of concrete over one year provides reliable data for capturing the effect of temperature on concrete fatigue.

5. The sensitivity of fatigue damage to different sources of uncertainties (associated with compressive strength, the level of stress, and the magnitude of annual traffic) can be clearly identified.

The results of the inverse method were compared to WIM data and found to be accurate. Hence, the presented methodology can be used to investigate RC slabs suspected of having fatigue problems. The accuracy of the inverse method can be further improved by installing two strain gauges for each lane and direction and performing a load test with different positions, velocities and loads.

Combining the calibrated FEM and the probabilistic assessments is demanding. However, it can be updated and used to investigate the fatigue safety of the structure for future service duration. Regarding the sensitivity analysis, in the future it can be extended to consider it from a reliability point of view, accounting for the uncertainty of fatigue load and fatigue strength and the influence of the reliability.

Chapter 3 Structural Condition Assessment of Reinforced-Concrete Bridges based on Acoustic Emission and Strain Measurements

Paper details

Chapter 3 contains a post-print version of the paper "I. Bayane, E. Brühwiler (2020). Structural condition assessment of reinforced-concrete bridges based on acoustic emission and strain measurements" published in September 2020 in the "Journal of Civil Structural Health Monitoring". Minor modifications are introduced in the text for adapting the paper to the thesis format.

Author contributions

The author of this thesis conducted the research and wrote the full paper. Professor E. Brühwiler contributed by proofreading the paper and by providing overall supervision.

Overview

This paper presents the development and implementation of continuous long-term monitoring of RC bridge-deck slab using AE measurements that are integrated with strain and temperature measurements to evaluate the internal state of concrete under operational loadings. The monitoring approach is presented in detail with the used systems, sensors, and methods of calibration. One year of AE data was evaluated using parametric analysis of AE features, cracking mode classification method, and b-value analysis. The monitoring results were used to evaluate structural characteristics, such as internal changes in concrete and conditions of support and articulation and to measure the structural response, such as strain in rebars due to traffic and temperature actions.

Link to other chapters

As this chapter contains a preliminary analysis of AE measurements, it is linked to the next chapters in which the AE data is exploited more deeply. In Chapter 4, the presented AE data was clustered and used to assess the development of an accurate set of structural analysis models. In Chapter 5, the characterised cracking activity and modes were analysed more deeply by three-dimensional location of AE events to visualise microcracks through the entire depth of the instrumented slab.

Paper II

Structural Condition Assessment of Reinforced-Concrete Bridges based on Acoustic Emission and Strain Measurements

Abstract

A reliable novel monitoring approach is developed to assess the structural condition of reinforced-concrete bridge elements. The approach is based on combining the acoustic emission technique and strain gauge measurements, and it is illustrated using the case study of a composite steel-concrete viaduct that has been in service since 1957. Monitoring was performed on its reinforced-concrete deck slab under traffic and environmental loading over one year. The monitoring setup and procedure are presented. The variation of acoustic emission signals was evaluated regarding strain and temperature measurements. A parametric study, a pencil-lead-break test, statistical analysis, crack classification and b-value analysis were performed to assess the structural condition. The acoustic emission activity of the reinforced-concrete slab was evaluated over one year under operational conditions. From the monitoring approach, it was possible to identify the nature of the cracking activity in the concrete slab as a function of traffic loading and temperature and to assess the condition of the slab-girder connection over time.

Keywords: Monitoring, road bridge, acoustic emission, strain measurement, structural condition, acoustic emission feature, parametric study, b-value analysis, cracking mode.

3.1 Introduction

The sustainable and economic use of existing reinforced-concrete (RC) bridges requires the reliable assessment of their current condition under service loading. For road bridges, RC deck slabs are the part that is most vulnerable to fatigue due to the pronounced effect of vehicle's axles [41], [42], [12], [17], [43]. RC decks often need to be assessed to meet both the safety and serviceability requirements of infrastructure, particularly because the magnitude and frequency of axle loads has increased.

The assessment of RC decks refers to the early-stage assessment of concrete and steel reinforcement conditions, and the bond between them. The effect of cyclic loading on RC structural elements was investigated in [44], [41], [45], [18], [23], and [24]. However, most of these studies were limited to laboratory testing, and only a few performed assessments on real structures. Different NDT methods were used to evaluate bridges on site such as radar, impact echo and infrared thermography [46]–[48]. Such methods allow one to detect delamination, moisture, and discontinuities in concrete, but they are limited for initial microcrack detection.

Early stage assessments are often restricted to visual inspections [49]–[51] that are subjective and not always reliable or to calculations of structural capacity [5], which are very conservative and use unrealistic assumptions and models related to loading and material properties. Assessing RC decks requires methods that can evaluate both the structural characteristics and the response of RC structural elements under traffic and environmental loading.

The acoustic emission (AE) technique has been proven efficient in assessing the condition of concrete and steel. Being drawn from the physical phenomena of elastic wave propagation, this technique was widely used for investigating internal changes in materials under loading and for detecting and classifying crack initiation and propagation at an early stage [52]–[55]. During loading, AE events are strongly dependent on irreversible deformations in a material, such as the creation or progression of new microcracks or macrocracks and the existence of friction processes [56].

The term "acoustic emission" refers to transient elastic stress waves generated by the energy released when microstructural changes occur in a material [57]. Stress waves propagate from the AE source toward the sensors, and during their propagation, they are influenced by a variety of factors such as propagation velocities, attenuations, discontinuities, and the geometry of the material. Recording stress waves can therefore provide information about the mechanical and geometrical properties of the environment in which they propagate.

The AE technique is based on recording the surface vibration of these waves by means of sensors that detect the waves and then convert them into electrical signals. The sensors are mounted on the surface of a specimen or structure using adhesives and holders. The AE sensors use different frequency ranges, such as broadband sensors, which are used when the frequency range is unknown and resonant sensors that are highly sensitive at their resonance frequency [56], [58]. The AE testing of concrete structures uses the frequency range of [20, 100] kHz. The frequency range of [100, 400] kHz is used for steel and wood structures and frequencies higher than 400 kHz are mainly considered noise [59]. More details about the basis of this technique can be found in [60]–[62].

AE evaluation of RC structural elements under cyclic loading has been studied by many researchers [63]–[68]. However, most studies were limited to laboratory testing. Pronounced noise, complex

loading, environmental conditions, as well as calibration and lack of reference present challenges to translating AE laboratory knowledge to the field. A few studies ([58], [60], and [69]–[72]) have demonstrated the feasibility of AE assessment of RC road bridges, but often for occasional testing under a load test. In fact, interpreting the AE measurements is difficult when the loading condition is unknown. Moreover, the huge amount of generated AE data under traffic presents a storage challenge. To the best of the author's knowledge, there is no work performing continuous, long-term AE monitoring of RC decks in service that relates the AE response to traffic and environmental changes.

3.2 Research Significance and Originality

Fatigue of RC is among the most studied research topics, and the AE technique has been widely used for fatigue crack detection and classification [18], [55], [63], [66], [73]. Nevertheless, many essential questions have not yet been answered. For instance, no sufficient explanation has been given about the mechanisms of degradation of RC structural elements under traffic and environmental loading. Another important point that lacks explanation is how to apply the AE technique to investigate the evolution of RC cracking activity on site at an early stage.

To address these challenges, the latest advances in the AE technique were used to perform a long-term monitoring campaign on an RC road bridge. The study is focused on the initial cracking of concrete due to fatigue under traffic and environmental loading. It is illustrated with a case study in which no other mechanism of degradation has been involved according to engineering expertise. The AE technique was associated with strain gauges and thermocouples to connect AE measurements with vehicle loading and environmental changes. The approach provides both the structural response (i.e., reinforcement strain and temperature of concrete) and the structural characteristics (i.e., material properties and the condition of structural-element connections and supports; Figure 3.1.

Structural characteristics

•Acoustic Emission technique

Structural response

•Strain gauge
•Thermocouple
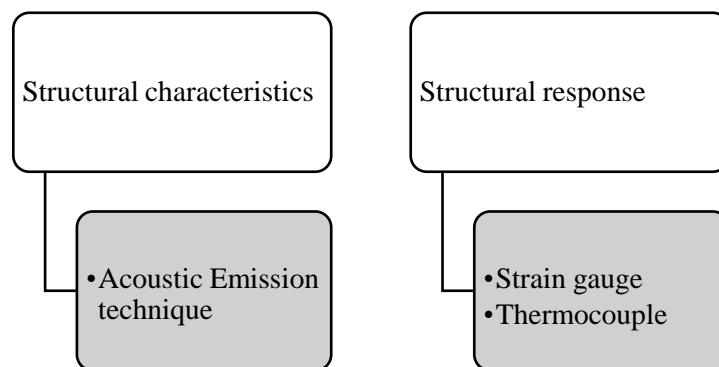
Figure 3.1. Diagram of the monitoring approach.

The originality of this work includes the following:

- the development, calibration, and synchronisation of the monitoring approach;
- the identification of the annual variation of AE features with temperature;

- the identification of the annual variation of AE features with traffic loading;
- the investigation of the initial stage of cracking phenomena in concrete with respect to traffic and thermal changes;
- the assessment of structural characteristics and structural response of an RC deck slab based on AE and strain measurements.

3.3 Monitoring of a Reinforced-Concrete Road Bridge

3.3.1 Structural Description

The presented case study concerns a composite steel-concrete viaduct that has been in service since 1957. It has two road lanes with a width of 10.5 m. The viaduct comprises seven articulated spans that are 25.6 m long and an approach span that is 15.8 m long. Each span is made from two steel-girder beams with a height of 1.3 m each fixed in an RC slab of a thickness varying from 0.17 m at the midspan to 0.24 m (Figure 3.2). The slab comprises longitudinal and transverse reinforcement bars in both the tensile and compression zones with diameters of 10 mm, 14 mm, and 18 mm.
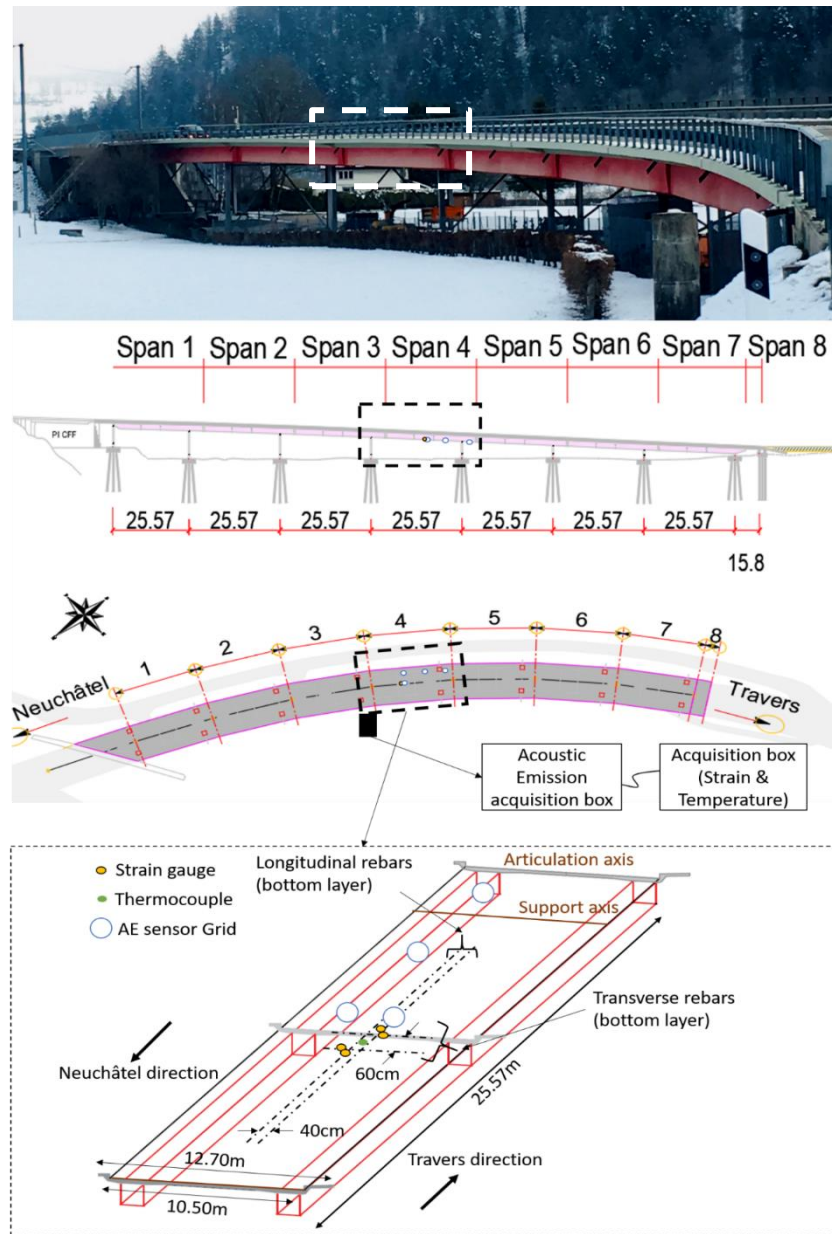
Figure 3.2. Case study of the Crêt de l'Anneau viaduct, with units in [m].

3.3.2 Monitoring System

The monitoring system comprises strain gauges, thermocouples, AE and an Ultrasonic Testing (UT) system, and is illustrated in Figure 3.3. Spans 2 and 4 were instrumented in July 2016 with strain gauges and thermocouples. Span 4 was additionally instrumented in December 2018 using the UT and AE systems. In total, three years of strain and temperature measurements, a few months of pulsing signals, and one year of AE data were recorded and processed.

Figure 3.3. Configuration of the monitoring system.

The data acquisition unit of strain is a Quantum MX1615, which acquires strain with a high frequency varying between 50 Hz and 100 Hz from eight strain gauges with half-bridge configurations and two strain gauges with quarter-bridge configurations. The data acquisition unit of temperature is a Quantum MX1609, which measures temperature with a high frequency of 1 Hz from six thermocouples. An output and input unit comprised of Quantum MX879B was used to acquire recorded data, connect the system with a 4G internet connection, and connect strain and temperature measurement units with the AE acquisition system.

The data acquisition unit of strain was equipped with a monitor to visualise the measurements on-site. The Catman program (a data acquisition software) was used to integrate all the units together and to visualise and parametrise the data analysis.

The data acquisition system of the AE technique is a sensor highway for in-situ monitoring and is comprised of a Processor Atom N2600 with a memory card of 128 Go and 32 acquisition channels of bandwidths ranging from 1 to 400 kHz at -3 dB. The system acquired data from 24 PK151 resonant sensors, resonating at 150 kHz with an integrated preamplifier of 26 dB gain. The sensors detect transient waves and convert them to an electrical signal. Resonant sensors were used because of their high sensitivity and because the emission is strongly attenuated in concrete. The integrated preamplifiers were used to avoid signal loss. The AE technique is insensitive to structural resonance since it only detects high-frequency events.

The same AE acquisition system was used to record the response of the generated waves by the UT system. This recording was made technically possible by using an ARB-1410-150 card generating arbitrary waveforms, a multiplexer with four channels on the ARB card, four PK15l sensors resonating at 75 and 150 kHz, and an industrial calculator connected to the ARB card and controlled by the AE data acquisition system. The frequency of interaction between the sensors and the card was fixed at 800 kHz to receive the last wave arrivals, while the pulse frequency was 150 kHz for concrete with the maximum aggregate diameter of 32 mm. The results of the UT system are not further discussed in this paper.

The acquisition system was equipped with a monitor to visualise the data on-site and a 4G internet connection for remote access using a remote connection program. The AEwin program (a commercial

software for real-time "simultaneous" AE-feature and waveform processing) was used to visualise the generated waves and the AE features in real time.

Data were recorded, stored, and collected every 24 hours using the file transfer protocol (FTP). AE data were stored on a DTA file, during the monitoring period of 14/03/2019 – 14/03/2020 and 400 GB of data were collected. Strain data were stored on a MATLAB file; 39 GB of data were collected during the last year of monitoring.

3.3.3 Instrumentation

Sensors were installed on the accessible critical parts that provide easy interpretation of the recoded data to understand the structural behaviour. Therefore, strain gauges were installed at the midspan, and AE sensors were mounted at the midspan and in three different longitudinal zones in the lane with the greatest number of heavy trucks (Figure 3.2). All the sensors were mounted on the underside of the RC slab since there is no access from the top side.

Spans 2 and 4 were each instrumented with four strain gauges with half-bridge configurations. Two were installed on the adjacent longitudinal rebars at the midspan, and the other two were installed on the two perpendicular transverse rebars (Figure 3.2). The rebars were detected with a rebar locator (profometer), and an area of 50 x 50 mm of the concrete cover was removed to uncover the rebars. Strain gauges were glued on each rebar and sealed with a protective layer to avoid any contact with the air.

The top and bottom flanges of one steel box girder of Span 4 were each instrumented with a strain gauge with a quarter-bridge configuration. The paint was removed, the surface was cleaned, and then the strain gauge was glued and covered with the protection layer.
Thermocouples were installed on the concrete near strain gauges at the midspan of Spans 2 and 4, and at the top and bottom flanges of the steel girder of Span 4.

To monitor the smooth functioning of the setup, one thermocouple and one humidity sensor were installed on the box of strain and temperature acquisition units.
The AE sensors (1-24) were mounted on four grids, as illustrated in Figure 3.4 The first grid comprised a circular network of six sensors (Channels 5, 6, 7, 17, 21, and 22) with a diameter of 0.34 m and was installed at the midspan. The second grid comprised nine sensors (Channels 8, 9, 10, 11, 12, 18, 19, 20 , and 24) spaced in a grid of 0.24 m and was installed at the midlane, 1.35 m away from the girder. The third grid was comprised of four sensors (Channels 13, 14, 15, and 16) spaced in a grid of 0.20 m, and was installed near the support, 1.57 m away from the girder. The fourth grid comprised a circular network of five sensors (Channels 1, 2, 3, 4, and 23) with a diameter of 0.28 m, and was installed between the support and the articulation. The UT sensors (M, R, V, and J) were distributed among the network of nine AE sensors between the midspan and the girder (Figure 3.4).

The sensors were mounted using silicone glue to provide a direct and flexible connection between the contact surfaces of the concrete and the sensors and were fixed with magnetic holders attached by metal plates screwed into the concrete to ensure strong fixity. The surface of the concrete was smoothed and cleaned before the mounting, and the rebars were detected using a profometer to avoid installing the sensors directly underneath the rebars. The electronic noise coming from the interaction

between the connection cables of the AE system and the UT system was mitigated by fixing the cables far away from each other.
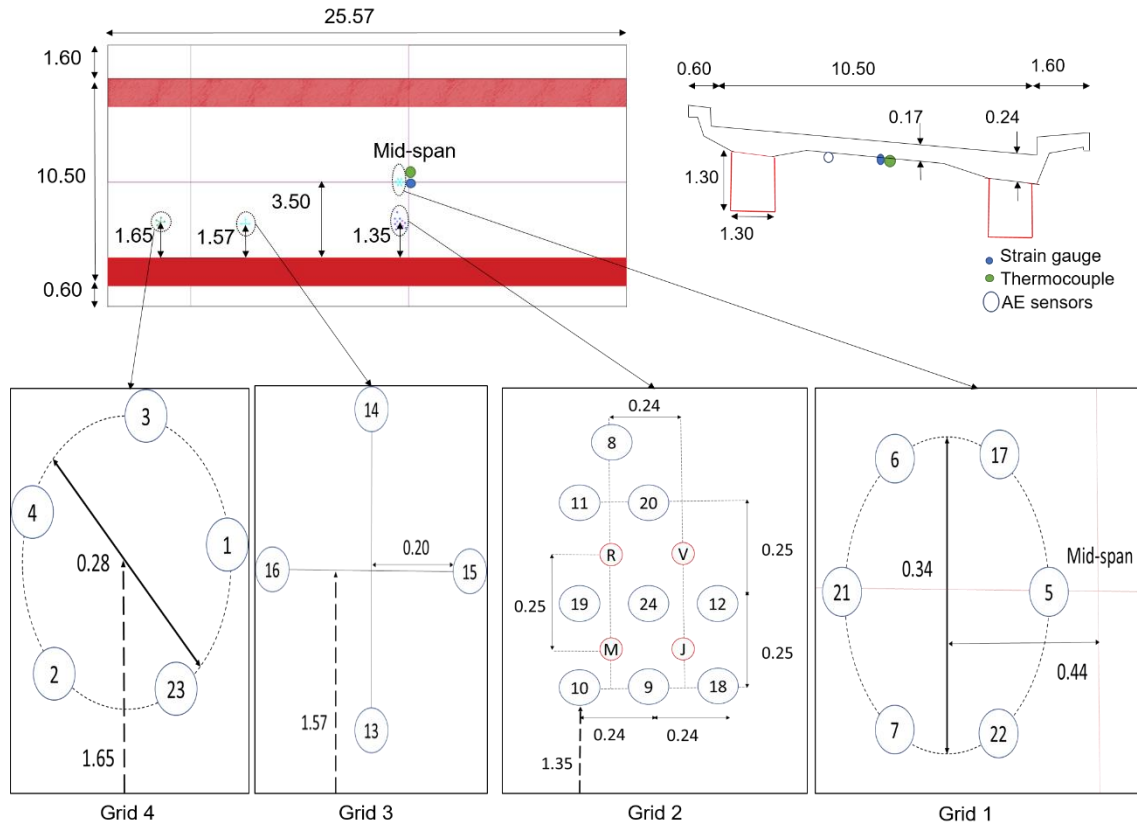
Figure 3.4. Plan view showing the instrumented Span 4 and the deployment of acoustic-emission (AE) sensors, with dimensions in [m].

3.3.4   Calibration

3.3.4.1   Strain Gauges

A load test was conducted after instrumenting Spans 2 and 4 with strain gauges. A five-axle truck with a maximum load of 400 kN was used to perform four passages per direction at four speeds. Transverse rebars were under tensile stresses during the passage of the truck. In the longitudinal direction, the girder and the rebars showed the expected stress reversal (i.e., both tensile and compressive stresses) due to vehicle passage.

The measured strains were mainly influenced by truck position and by slab slenderness, which accentuates local strains under the wheels. The axle configuration of the load-test truck has no influence on the response of the transverse reinforcement and the steel girder, which means that, during the monitoring campaign, the vehicles' s effects can be directly related to their total load [6].

3.3.4.2 Acoustic Emission

The evolution of AE activity under traffic and environmental conditions was preliminarily measured continuously over two months after instrumenting Span 4 with AE sensors. The recorded signals were analysed to define the filters for suitable noise precautions for long-term monitoring.

Real-time visualisation of AE activity was possible for a threshold above a 30 dB threshold. To remove the noise of traffic, the waveforms with counts between, 5 and 10'000, and amplitudes between 40 and 1'000 dB were recorded. A time filter was defined for peak definition time (PDT), hit definition time (HDT) and hit lockout time (HLT), as shown in Table 3.1, with channel setups and filters. Under the chosen filters, no AE activity was observed in the absence of traffic.

Table 3.1 AE setup.

PDT	HDT	HLT	Max duration
200 µs	800 µs	1'000 µs	1'000 ms

Acquisition Threshold	Pre-amplifier	Front End Filters	
		Lower	Upper
30 dB	26 Gain dB	40 dB 5 counts	1'000 dB 10'000 counts

Analogue filter		Digital filter		Waveform Setup		
Lower	Upper	Lower	Upper	Sample rate	Pre-Trigger	Length
20 kHz	400 kHz	None		2 MSPS	50	4k

Sensor-calibration and signal-attenuation tests were performed using the pencil-lead-break method according to the standard NF EN 1330-9, 2017 [74] during the installation and two months after. Five pencil breaks were completed 0.05 m away from each sensor. The three highest recorded amplitudes had to be greater than or equal to 80 dB [75], and the measured value had to have a variation of less than ± 3 dB from the mean amplitude value for all the sensors. Pencil-lead-break tests were conducted for each sensor, and the recorded amplitudes were evaluated. When the sensors gave no response according to the requirements, the coupling and fixation were repeated.

3.4   Data Processing Methods

In this paper, the recorded AE signals during one year of continuous monitoring (from 14/03/2019 to 14/03/2020) were evaluated based on parametric analysis, pencil-lead break test, *b*-value analysis, and crack-identification methods.

Three parameter inputs were used to connect the strain measurement system with the AE data acquisition system: the longitudinal strain at the midspan, the transverse strain at the midspan, and

the concrete temperature at the midspan. This connection provides the same time base and thus the synchronisation for strain-temperature measurements and recorded AE signals.

An inverse analysis was conducted on strain measurements using load-test data to calculate the position and load distributions of the vehicles crossing the viaduct. Action effects from traffic were identified along with the resulting AE signals. This identification provides a robust comparison and analysis basis with the large amount of synchronised data.

3.4.1 Parametric Analysis

AE features were extracted with the corresponding values of the input parameters of the strain (parametric 1) and temperature (parametric 2) for each detected hit. They are defined as follows [76]:

- Channel refers to a single AE sensor and the related equipment components for transmitting conditioning, detecting, and measuring the signals that come from it.
- Rise time is the time from the first threshold crossing the highest voltage point in the waveform [µs].
- Counts to peak (Pcount) represents the number of threshold crossings from the first to the highest voltage point on the waveform.
- Counts represents the number of times the signal crosses the detection threshold.
- Energy is the time integral of the absolute energy signal voltage.
- Duration is the time from the first and last threshold crossings [µs].
- Amplitude is the highest voltage in the AE waveform expressed in decibels [dB].
- Average frequency (AF) is equal to counts divided by duration [kHz] and is calculated according to Equation (3.1).

$$AF = \frac{Counts}{Duration} \tag{3.1}$$

- Reverberation frequency (RF) is equal to (Counts – Counts to Peak) divided by (Duration – Rise Time) [kHz] and is calculated according to Equation (3.2).

$$RF = \frac{Counts - Counts\ to\ Peak}{Duration - Rise\ Time} \tag{3.2}$$

- Initiation frequency (Ifrequency) is equal to counts to peak divided by rise time [kHz] and is calculated according to Equation (3.3).

$$Ifrequency = \frac{counts\ to\ peak}{rise\ time} \tag{3.3}$$

- Absolute energy (ABSenergy) is the time integral of the square of the signal voltage at the sensor before any amplification divided by a 10 kΩ impedance, expressed in attojoules [aJ] and calculated according to Equation (3.4).

$$ABSenergy = \frac{1}{10} \int V(t)^2 dt \qquad (3.4)$$

- Frequency centroid is the centre of mass of the power spectrum graph [kHz].
- Peak frequency is the point where the power spectrum if greatest [kHz].
- Event is a local material-change giving rise to AE.
- Hit is the process of detecting and measuring an AE signal on a channel.

AE features were extracted from the recorded waves using the AEwin program. The extracted features were analysed and classified using single link clustering (Figure 3.5), which is a hierarchical clustering method that combines clusters based on distance between closest elements according to Equation (3.5).

$$D(C_1, C_2) = min_{x_1 \in C_1, x_2 \in C_2} D(x_1, x_2) \qquad (3.5)$$

where D is the distance between x_1 and x_2, which are the closest elements that belong to C_1 and C_2, which are respectively clusters one and two. Clusters are formed by AE features and the distance is normalised in Figure 3.5.
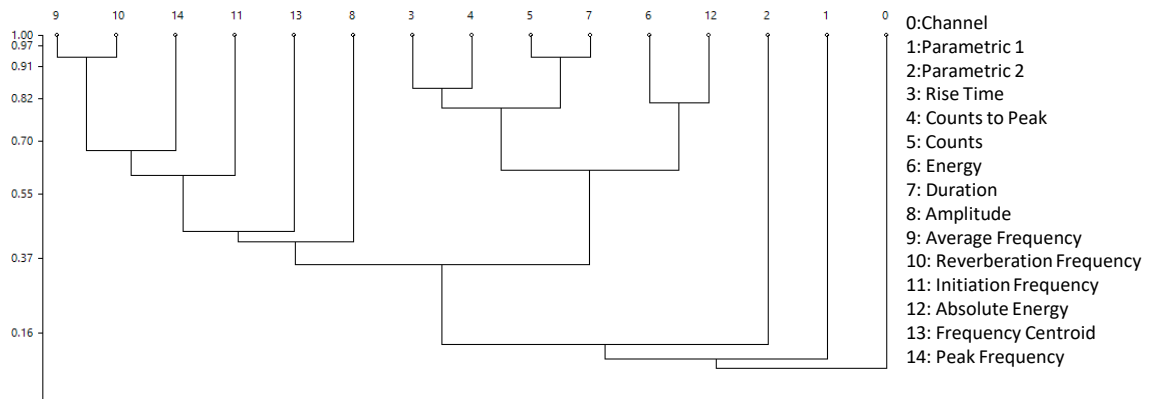
Figure 3.5. Single link clustering of acoustic emission (AE) features.

From Figure 3.5, one can observe that the AF and reverberation frequency were highly correlated. Therefore, the AF was selected to perform the analysis while the peak frequency, Ifrequency and frequency centroid were investigated in future work. Similarly, Pcount, duration, and ABSenergy were selected for data processing because of the high correlation between rise time and Pcount, counts and duration, and energy and ABSenergy.

Parametric analysis was performed using the selected AE features along with the amplitude of the signals and the input parameters (i.e., strain and temperature). The recorded waves during one year of monitoring were extracted and analysed using the AEwin program and MATLAB. The annual variation of the selected AE features was calculated for the 24 channels.

3.4.2   Pencil-Lead Break Testing

Pencil-lead break testing is a preferred method for calibrating and evaluating the precision of AE instrumentation since it presents an accurate mechanical source for identifying propagation velocity characteristics and source location [77]. It was used to investigate the AE activity during traffic loading and to measure the velocity of stress waves. In general, concrete with a P-wave velocity of higher than 3'500 or 4'500 m/s is considered good or excellent, while concrete with a velocity lower than 3'000 or 2'000 m/s is considered poor or very poor, respectively[78].

3.4.3   Cracking Process

Cracking of concrete is different than cracking of metals. It is preceded by microcracking rather than yielding. It is therefore characterised by a fracture zone rather than a crack tip, where the stresses decrease when deformation increases [79]. Figure 3.6 shows how AE features vary during concrete cracking. The friction at the level of the fracture zone and between existing cracks creates slow transverse or shear waves (Figure 3.6, b), while the creation of a new crack with two separated surfaces and the opening and closing of existing cracks generate variations in the volume, resulting in fast longitudinal or compression waves (Figure 3.6, a).
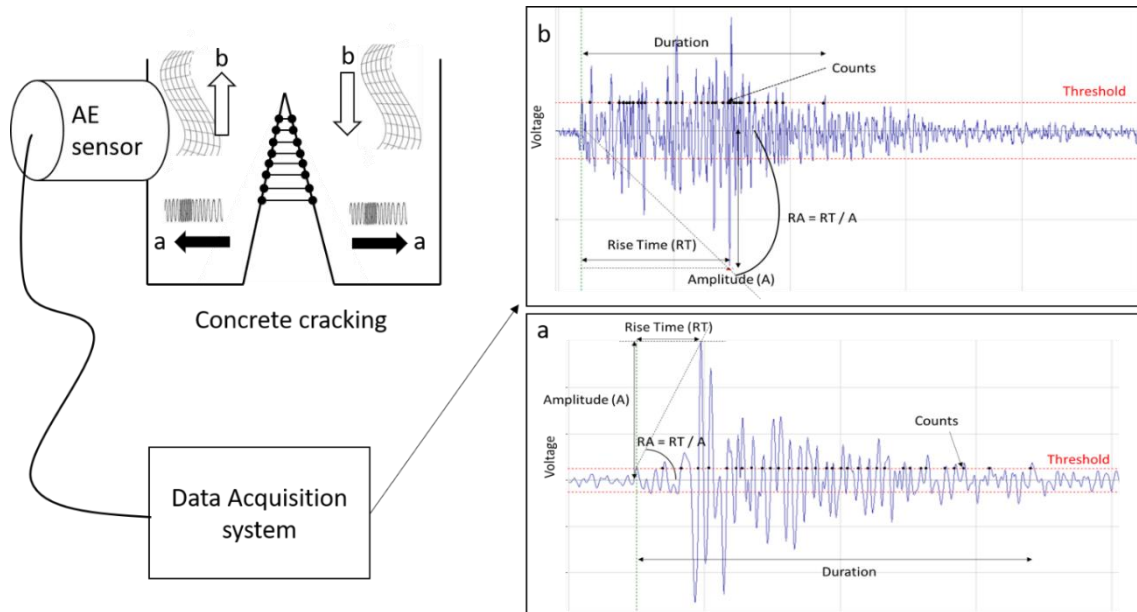
Figure 3.6. Acoustic emission (AE) features during cracking process of concrete.

Concrete under high-cycle fatigue loading goes through crack nucleation, crack propagation, and finally the appearance of long cracks until failure [80]. The concrete of the 60-year slab is estimated to be in the stage of crack propagation.

3.4.4 Cracking Modes

Wave modes exit differently with different cracking types. Tensile cracks cause a transient volumetric change inside the material, converting the released energy into mainly P-waves. The resultant AE events are longitudinal waves of high amplitude and frequency, faster than any other wave type, and the resulting rise time is short (Figure 3.6, a). For shear cracks, the majority of generated waves are S-waves. The maximum amplitude arrives later than the first arrivals creating a longer rise time (Figure 3.6, b).

Classifying crack modes as either tensile or shear was estimated using a correlation of AF variation plotted against RA values, which are equal to the rise time divided by amplitude expressed in ms/V (see Equation (3.6)).

$$RA = \frac{Rise\ Time}{Amplitude} \tag{3.6}$$

The cracking behaviour of concrete can be classified as tensile when a high AF is detected with a low RA value [81]–[85]. It occurs when cracks are nucleated and opened. Shear cracking is characterised by a high RA value and a low AF, and it is detected with the fretting or sliding of existing cracks.

3.4.5 *b*-value Analysis

The *b*-value is a statistical method used to evaluate AE amplitude-frequency distribution. The *b*-value increases with an increase in the proportion of AE events with low amplitudes and decreases when the proportion of AE events with high amplitudes increases. The emergence of microcracks generates many AE events with low amplitudes, making the *b*-value high. By contrast, the formation of macrocracks generates a large number of AE events with high amplitudes, making the *b*-value low. Therefore, changes in the *b*-value are suitable for analysing the cracking process of concrete [86].

The analysis of *b*-values was first established by Gutenberg and Richter in 1949 [87], with their law stipulating that microcracks generate many hits of low amplitude, while macrocracks generate few hits of high amplitude. The Gutenberg-Richter relation is presented in Equation (3.7) in terms of AE parameters.

$$\log_{10} N = a - b\left(\frac{A_{dB}}{20}\right) \tag{3.7}$$

where N is the number of AE hits with amplitudes greater than A_{dB}.

A_{dB} is the amplitude in dB, a is an empirical constant, and b is the *b*-value.

Table 3.2 summarises the types of cracking and cracking processes based on *b*-value variation according to studies performed on rock mechanics [88] and RC girders by [61].

Table 3.2. Quantitative result analysis [61], [88].

b-value	Description
[1, 1.2]	The channel is very near to a large crack or macrocracks are forming
[1.2, 1.7]	Cracks are uniformly distributed, and macrocracks are stable
>1.7	Microcracks are dominant, or macrocracks are opening

3.5 Results

3.5.1 Pencil-Lead-Break Results

Pencil-lead break testing was performed after setting up the monitoring system to evaluate AE activity under traffic and to calculate the velocity of stress waves. AE events were simulated using pencil-lead breaks. Simulations were repeated to record both longitudinal and shear waves.

The simulated break events were localised using the AEwin program, in which the velocity was varied with each simulation to obtain the exact location of the simulated AE event. Moreover, a time-domain

interpretation of AE events was conducted to calculate stress wave velocity based on first arrivals of longitudinal waves, which were clearly observed. Stress-wave velocity was found to be equal to 3'400 m/s ± 100 m/s based on event localisation and time-domain interpretation. Therefore, the 60-year-old concrete can be considered in "good condition" [78], [89].

Data from the pencil-lead break testing were used to identify classes of AE data. The characteristics of the generated acoustic signals in solids during the formation of cracks are similar to the generated acoustic signals due to pencil breaks [90]. AE features collected during three minutes of pencil-lead break testing under regular traffic were classified into two groups as illustrated in Figure 3.7. The ABSenergy, duration, Pcount, and AF are plotted with respect to the amplitude of the 4'301 recorded hits from the 24 channels.
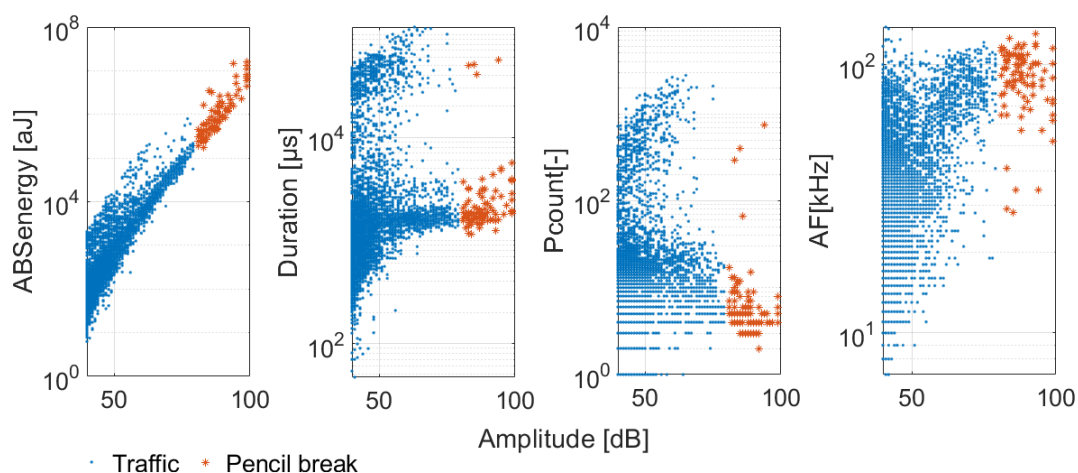
Figure 3.7. Results of the pencil-lead break test under traffic.

The AE activity due to the pencil-lead break test is characterised by high amplitudes (>80 dB), high ABSenergy levels (> 10^6 aJ), short durations (<10^4 µs), and low Pcount, which produces high AF values, while the AE activity due to traffic load presents lower ABSenergy levels and amplitudes.

The AE activity due to traffic and the activity due to pencil-lead breaks are similar to crack-like signals that form two visible clusters. It can be concluded that no cracking formation was present in the slab during the test. This result is based on data recorded for 3 min considering only surface simulations and is thus not conclusive. Therefore, a detailed investigation of the annual variations of AE features was performed.

3.5.2 Acoustic Emission Features

AE events occurred during the passage of vehicles, after the passage of heavy trucks, and rarely when there was no traffic. The 24 channels recorded a total of 47'640'543 hits during the monitoring period of 14/03/2019 – 14/03/2020. The AE activity in the concrete is caused by the principal source associated with concrete cracking and secondary sources including the friction, the opening and the

closing of existing cracks. Hits characterised by high ABSenergy levels ($>10^6$ aJ) were mostly related to AE activity caused by concrete cracking [91].

A total of 1'033 AE hits with an ABSenergy greater than 10^6 aJ and an amplitude greater than 75 dB were recorded for channels at the midspan. It can be argued that the cracking activity in concrete is active, but its evolution is very slow over time (i.e., 1.66 10^{-4}/year), which corresponds to the ratio of hits with high amplitude and energy and the number of total AE hits. The other AE events were mostly due to crack movements at the fracture-zone level and to the friction, and the opening and closing of existing cracks.

The annual variation of AE features provides qualitative indications about the condition of the concrete. In the following section, AE features are analysed along with temperature and strain variations using the input parameters to evaluate the influence of traffic and temperature on the cracking process and to investigate the source of AE activity.

3.5.3   Acoustic Emission Features and Temperature

Figure 3.8 presents the annual variation of the concrete temperature using the AE features of Channel 6 and the strain of longitudinal and transverse rebars at the midspan. To illustrate the annual effect of temperature, the moving average of the maximum values of the AE features was calculated and presented as a thick line. Similarly, the moving averages of the thermal strain of $\epsilon_{T/longitudinal}$ and $\epsilon_{T/transverse}$ were plotted for longitudinal and cross-sections.
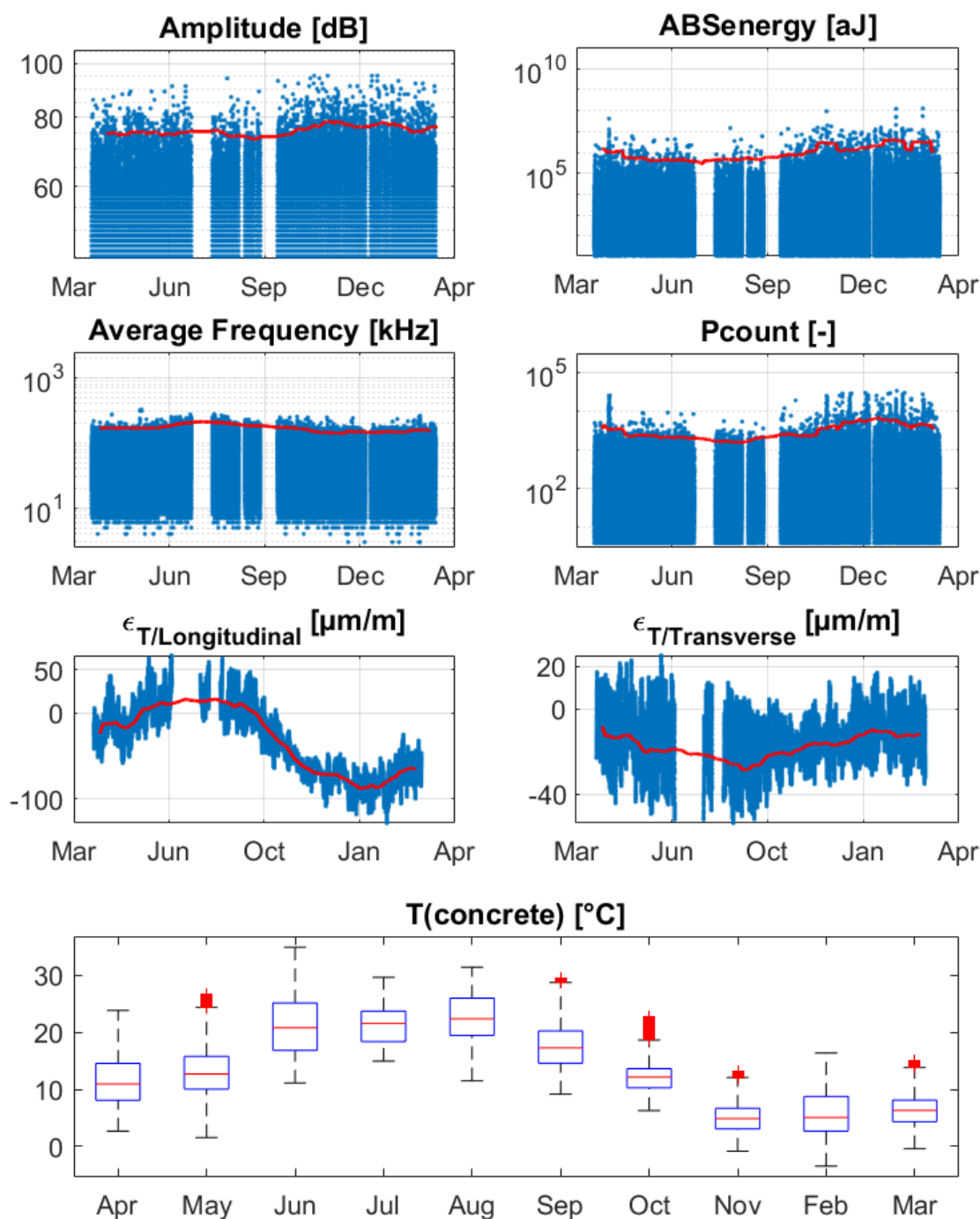
Figure 3.8. Annual variation of amplitude, absolute energy (ABSenergy), average frequency (AF), and counts to peak (Pcount) of Channel 6, longitudinal and transverse thermal strain, and the temperature of concrete.

Temperature increase causes an increase of the maximum values of amplitude, ABSenergy, and Pcount and a decrease of AF maximum values. Similar observations were found for daily cycles. Temperature increases generate an increase of longitudinal thermal strain and a decrease of transverse thermal strain due to material expansion and boundary conditions. Thermal variation is therefore inducing daily and seasonal microcrack movement and internal microcracking. Microcracks are opening and closing according to their orientation with respect to longitudinal and transverse sections.

The opening and closing of microcracks is cyclic and follows daily and seasonal temperature variations, which demonstrates the stability of the cracking activity in the RC slab.

The energy required to open the microcracks under traffic loading is less during summer if they are opening with increases in temperature, and their size is assumed constant. This fact can explain the decrease of the calculated values for ABSenergy, amplitude, duration, and Pcount with temperature increases.

The observed trends of AE features due to thermal variation were different when the temperature of the concrete was less than zero degrees Celsius. This observation can be due to the thawing and freezing of the concrete. Ice formation can be initiated in pores with interstitial solution in low-temperature conditions. The pore solution can freeze, and highly porous border zones around the aggregate might be separated from the ice front through smaller cement matrix pores, leading to high hydrostatic pressure [92]. This pressure can create the opening and closing of existing microcracks, generating more AE events under low temperatures.

3.5.4   Acoustic Emission Features and Strain

AE response was evaluated along with the strain variation of rebars on the same time scale. AE features were analysed for randomly selected vehicles with different weights and positions. The method used to calculate the weights and the positions of the vehicles is based on strain measurements and can be found in Chapter 2.

An example of an AE response and strain variation is presented in Figure 3.9, using an observation where a light vehicle and a heavy truck crossed the road viaduct separately. The light vehicle had a weight of 1.62 t, and it crossed the viaduct from the *Travers* direction. The heavy truck had a weight of 33 t and three axles, and it crossed the viaduct from the *Neuchâtel* direction. The response of Channel 6 was plotted with the variation of the longitudinal strain at the midspan.
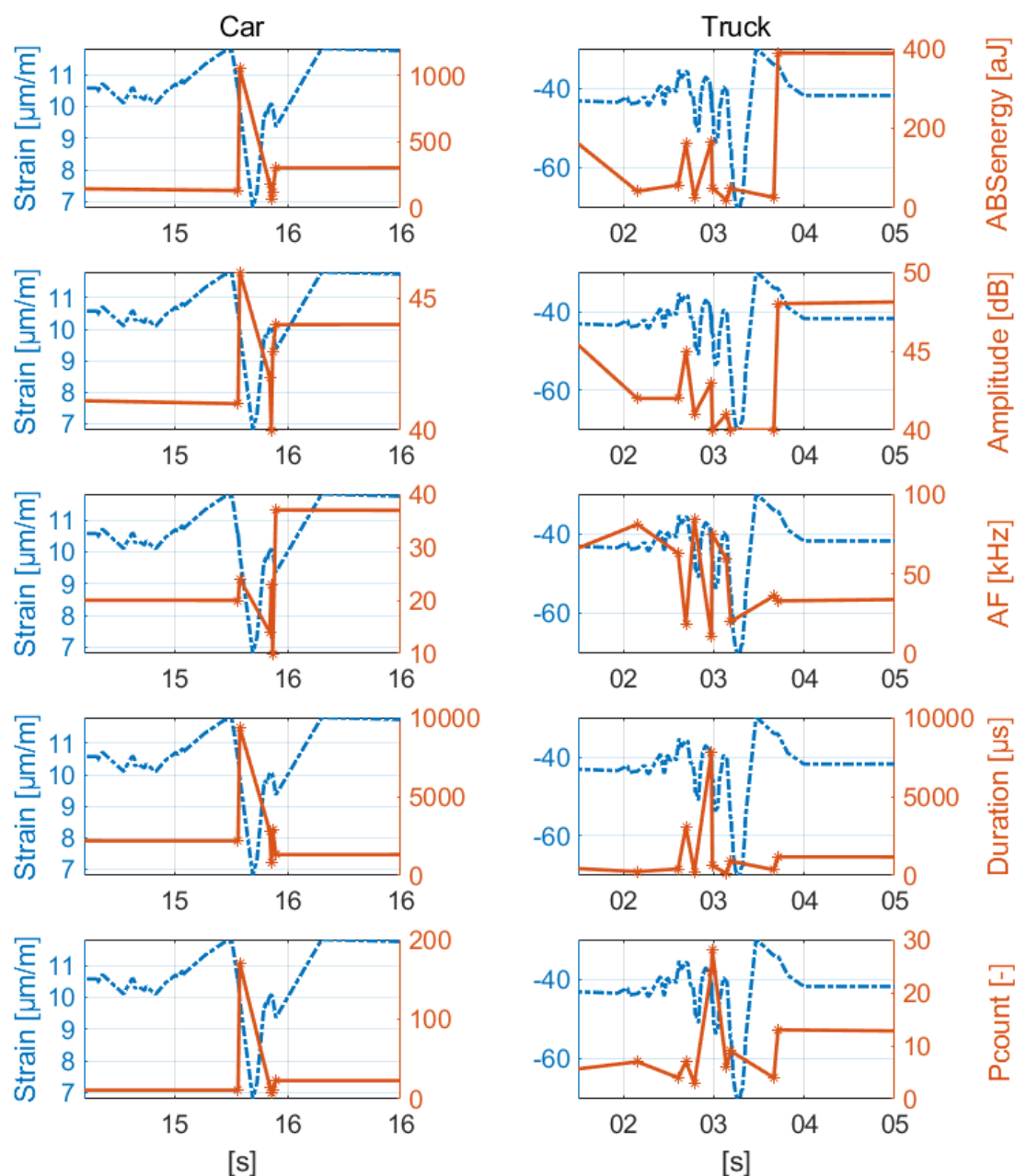
Figure 3.9. Variation of longitudinal strain and acoustic emission (AE) features of Channel 6 during the passage of a light vehicle and a heavy truck.

The hits generated by the heavy truck were characterised by lower ABSenergy and Pcount values and higher AF values, while no difference was observed in duration and amplitude.

The light-vehicle's passage lasted less than 1 s, generating eight hits in Channel 6. The released energy was concentrated at the beginning of the passage where the maximum compression of longitudinal rebar and the maximum tension of transverse rebar occur.

The truck's passage lasted 2 s, generating 12 hits in Channel 6. The released energy was distributed among the axles and reached a maximum with the passage of the last axle. The stored elastic strain energy was first steadily compiled with each axle until it reached the maximum with the last axle. This observation was also valid for many other passages.

By analysing many hits from both light vehicles (weight < 3.5 t) and trucks (weight ≥ 3.5 t), it was observed that the AE activity caused by light vehicles crossing the road viaduct was not detected by all channels, whereas AE activity caused by trucks was detected by all the channels during loading and for some heavy trucks also during unloading. This observation can be due to the opening and closing of microcracks during and after a passage. The maximum values of ABSenergy and amplitude were recorded when the maximum strain was reached in the longitudinal and transverse rebars, as shown in Figure 3.9.

The generated hits that correspond to light vehicles crossing the viaduct were characterised by higher ABSenergy, Pcount, and duration values and lower AF values compared to heavy trucks. In fact, light vehicles generated a small number of hits where the total energy was concentrated, producing high ABSenergy values per hit. Moreover, the speed of light vehicles was generally higher than the speed of trucks. This higher speed of light vehicles generates hits containing more than one AE event, which produces higher duration values.

The crossing of heavy trucks generates lower ABSenergy levels and shorter hit durations. Trucks have lower speeds and many axles that generate many sequential hits. The ABSenergy is defined as the time integral of the square of the signal voltage. The lower values of the energy calculated when trucks were crossing the road viaduct can therefore be due to low duration values. This observation was demonstrated by analysing the high ABSenergy values that correspond to light vehicles. They were found to be related to events with high durations and normal amplitudes.

The variation of ABSenergy should be evaluated along with the variation of duration. Moreover, this energy is split into local energies since each axle is generating many events. The distribution of the total energy produces lower values of energy per hit compared to the values produced by light vehicles which are concentrated in one or two hits. This observation entails that the speed of loading and the number of axles influence the detected AE energy.

AF values for trucks were higher because the generated AE signals cross the detection threshold many times compared to the AE signals generated by light vehicles. In contrast, both amplitude and Pcount variations demonstrated different trends for both light vehicles and trucks.

The presented truck in Figure 3.9 was crossing the road viaduct from the *Neuchâtel* direction, while the light vehicle was crossing from the *Travers* direction. The annual means and maximums of AE features were evaluated according to the direction of crossing. It was found that the Pcount and duration values were higher for vehicles travelling in the *Neuchâtel* direction, whereas ABSenergy, amplitude, and AF values were independent of the positions of the vehicles. It can be concluded that amplitude, ABSenergy, and AF depend more on a vehicle's weight, while duration and Pcount are related to the position and the weight of the vehicles and the position of the AE sensors.

3.5.5   Correlations and Statistics

The number of AE hits detected by every channel was different for the same loading conditions. Counting the number of hits is a simple method for evaluating the AE activity near the sensors. The presence of many hits can indicate an active cracking process near the channel, while a small number of hits indicates a stable condition. In Figure 3.10, the generated AE hits for the 24 channels are presented.
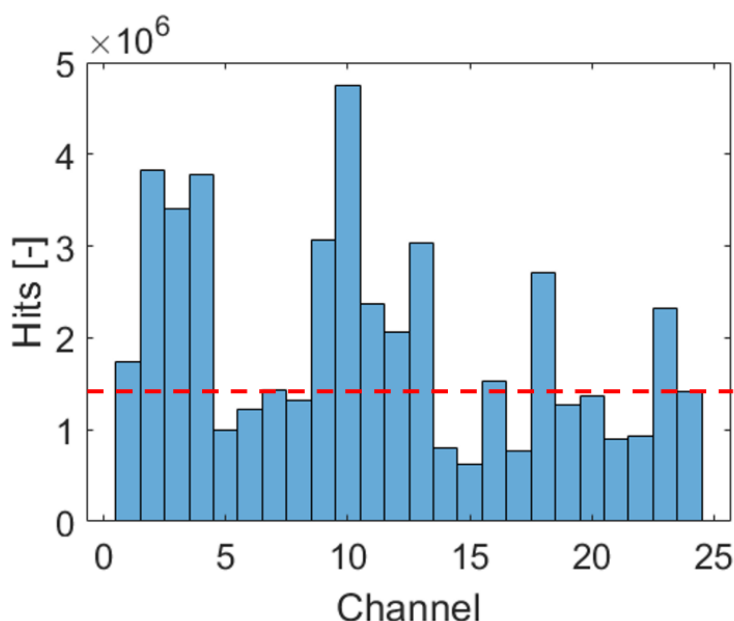
Figure 3.10. Annual acoustic emission (AE) hits for the 24 channels.

The recorded hits in Channels 2, 3, 4, 9, 10, 13, 18 and 23 were significantly higher. This observation can be attributed to the AE source originating from the minor relative displacement between the slab and the girder. Furthermore, channels near the slab-girder connection (i.e., Channels 9, 10, 18, 13, 2, and 23) detected similar number of hits and high ABSenergy ($>10^7$ aJ), duration, and Pcount values. Channels near the support (Channels 2, 3, and 4) were detecting similar number of events and a higher ABSenergy, while channels at the midspan detected a smaller number of events and a lower ABSenergy (mostly $<10^6$ aJ).

The variation of AE features presents apparent similarities and differences regarding the position of sensors, which can be due to the existence of different sources of AE. Therefore, four grids were defined to evaluate AE activity in different locations and to address the scatter of AE response.
Grid 1 comprises Channels 5, 6, 7, 17, 21, and 22 and evaluates the AE activity at the midspan. Grid 2 comprises Channels 2, 9, 10, 13, 18, and 23 and evaluates the condition of the slab-girder connection. Grid 3 comprises Channels 2, 3, and 4 near the support, and Grid 4 comprises Channels 13, 14, 15, and 16 near the articulation.
The daily mean of the AE features for the week 06/05/2019 – 12/05/2019 was calculated for each grid and illustrated in Figure 3.11 and Table 3.3 with the number of light vehicles and trucks per day.
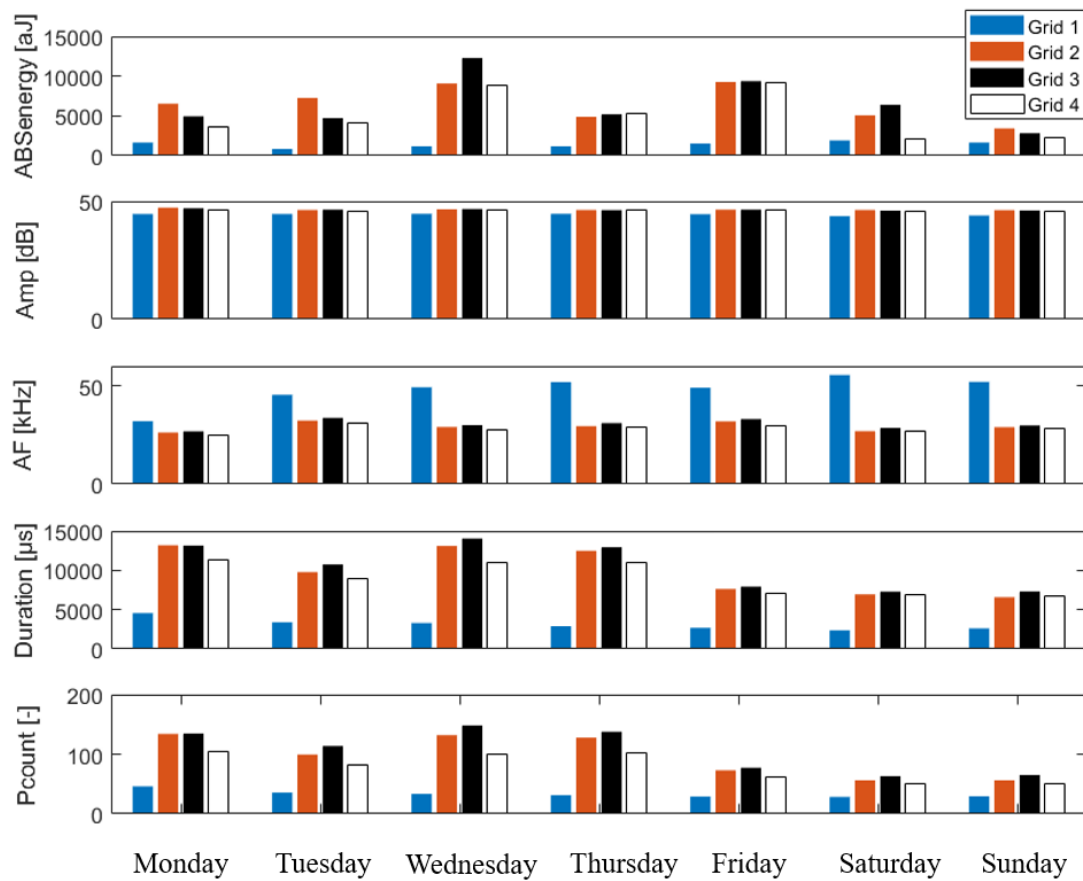
Figure 3.11. Variation of acoustic emission (AE) features per grid for one week.

Table 3.3. Number of light vehicles (<3.5t) and heavy trucks (≥3.5t).

Days	Monday	Tuesday	Wednesday	Thursday	Friday	Saturday	Sunday
Light vehicles	6'596	6'552	6'579	6'601	6'582	6'783	6'811
Heavy trucks	227	271	244	222	241	40	12

The daily mean values of amplitude varied in the range of 43 to 50 dB for all grids and did not significantly vary while the variation between grids was more apparent for ABSenergy, duration, Pcount, and AF. The highest values were recorded in Grids 2, 3, and 4 for ABSenergy, duration, Pcount, and in Grid 1 for AF. The lowest AF values recorded in Grids 2, 3, and 4 were due to long-duration events, which mainly arose from friction processes near these grids.

The daily mean values depend on the number of vehicles and their type. AF was higher during weekends, while the other AE features'values were higher during weekdays when the number of heavy trucks was more pronounced. Similar variations were observed for other weeks. On Friday, duration and Pcount showed the same tendency as the weekend. This result could be due to the number of trucks with weights between 3.5 t and 10 t, which are more frequent on Fridays. These trucks have a different speed and number of axles that influences the duration, the counts and the number of detected hits.

These weekday variations are due to the opening and closing of microcracks caused by the passage of heavy trucks. The variation between channels at the midspan and channels near the articulation, support and slab-girder connection demonstrates the existence of a second source of AE, which is mostly due to friction between different elements. In the following section, the cracking process is classified into tensile and shear modes to clarify the source of AE activity for each grid.

3.5.6   Characterisation of Cracking

AF and RA values were calculated from the moving average of 100 AE hits. The ratio of the abscissa scale to the ordinate scale was set to 50 according to the recommendations of the International Union of Laboratories and Experts in Construction Materials, Systems and Structures (RILEM) [84]. Aggelis has shown that tensile matrix cracking of concrete results in an AF that is higher than approximately 50 kHz, which corresponds to an RA value of 2'500 ms/V [81]. This AF value is assumed valid for the case study with respect to classifying cracking modes. The classification of AE events into tensile mode, shear mode and mixed mode was therefore determined based on values presented in Table 3.4, and Figure 3.12.

Table 3.4 RA and average-frequency (AF) values for cracking mode classifications.

Cracking mode	AF	RA
Tensile mode	> 50 kHz	Left side of the line
Mixed mode	≤ 50 kHz	≤ 2'500 ms/V
Shear mode	Right side of the line	> 2'500 ms/V
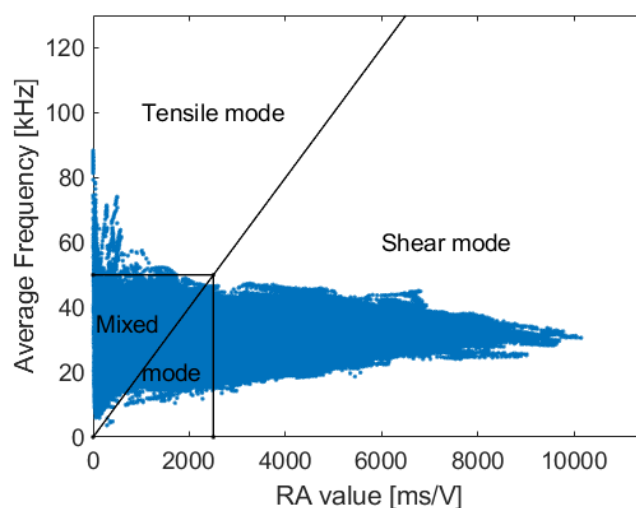
Figure 3.12. RA value analysis for Grid 1 at the midspan.

It is estimated that the pure tensile mode is caused by the expansion of the microcrack region, while the mixed mode is caused by the opening and closing of existing microcracks. The shear mode is assumed to be caused by friction between existing microcracks, friction between the slab and the girder, and friction at the level of the support and articulation. Table 3.5 presents the obtained percentages of the cracking modes for each grid.

At the midspan, 1% of AE events were classified as shear mode, 4% were classified as tensile mode, and 95% were classified as mixed mode. These modes mean that the AE activity is generated mostly by the opening and closing of existing microcracks and friction at the level of the fracture process zone, while 4% of the detected AE activity is due to the expansion of microcracks.

Table 3.5 Cracking mode classification per grid.

	Tensile mode	Mixed mode	Shear mode	N° Samples
Grid 1 (midspan)	3.55%	95.16%	1.29%	6'238'729
Grid 2 (slab-girder connection)	0.19%	81.44%	18.37%	19'727'020
Grid 3 (support)	0.19%	80.08%	19.73%	5'989'317
Grid 4 (articulation)	0.28%	85.92%	13.80%	11'004'243

The shear mode was more prominent near the support, the articulation, and the slab-girder connection, while the tensile mode less so. This observation confirms that 14% to 20% of the generated AE events for Grids 2 to 4 are caused by the friction between the slab and the girder and at the level of the articulation and the support, whereas the expansion of microcracks represents less than 3% of the total AE activity.

The opening and closing of existing microcracks is estimated to be the main source of the AE activity along the slab. To investigate the nature of the cracking process in more detail, b-value analysis was performed. This analysis is detailed in the following section.

3.5.7 b-value Analysis

The b-value analysis was performed for the AE events recorded over one year of continuous monitoring under traffic and environmental loading. A linear least square method was used to calculate the slope of the amplitude-frequency distribution. It is therefore necessary to select the appropriate number of AE hits. When the selected number is small, the oscillations are too strong, masking the general trend. If the selected number is too large, any small incidence producing a small number of events would be considered in the average of the large events. During laboratory tests, it was found that 50 is an appropriate sample size to perform b-value analysis [93]. However, there is no recommendation available for AE events generated under real traffic and environmental conditions.

To determine the proper number of AE events for b-value calculations, correlation coefficients between the logarithmic frequency $\log_{10}N$ and amplitude A_{dB} were calculated. They are presented in Figure 3.13. It was found that, in all channels, the relation between the logarithmic cumulative frequency and amplitude provides proper straight lines when the number of AE events is greater than 1'500.
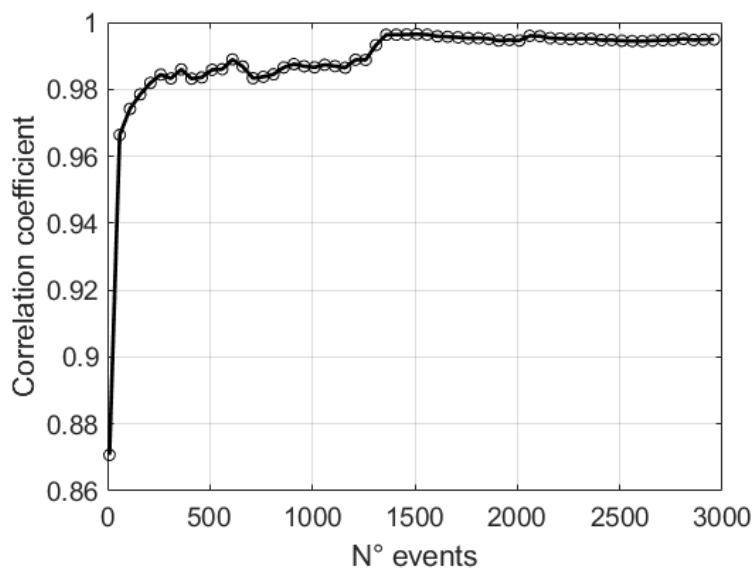
Figure 3.13. Correlation between the logarithmic frequency $log_{10}N$ and amplitude A_{dB}.

Therefore, *b*-values were calculated using two sets of amplitude frequency based on least squares curve fitting: amplitudes caused by 1'500 successive hits (Figure 3.14) and daily amplitudes (Figure 3.15). The limits of *b*-value ranges (1, 1.2, and 1.7) presented in Table 3.2 are plotted with red dashed lines.
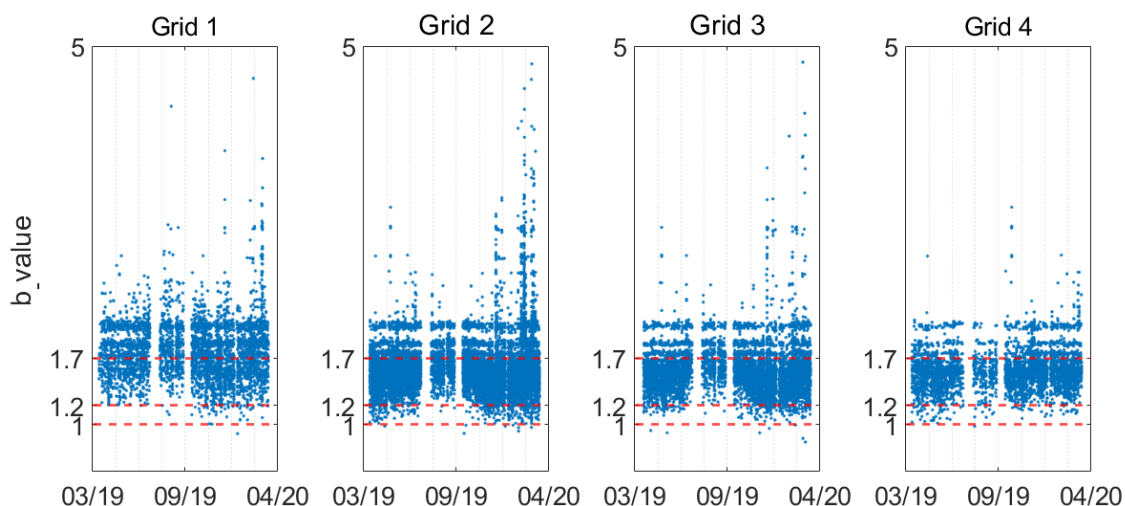
Figure 3.14. *b*-value based on 1'500 events.

Based on 1'500 events, the calculations show different trends for *b*-values and higher values for the four grids, implying changes in the range [1, 5]. Sixty-six percent of the values were in the range [1.2, 1.7], indicating uniform distribution of microcracks (39% for Grid 1, 71% for Grid 2, 75% for Grid 3, and 77% for Grid 4). The source of the AE events related to these values was therefore the

movement of the two crack surfaces of existing microcracks during traffic and environmental loading or friction at the level of the fracture process zone. By contrast, the existing macrocracks were stable.

The few values in the range [1, 1.2] comprised about 2% of the total values. They are due to AE events recorded during low traffic periods, and they are not a part of any cracking process. The values higher than 1.7 were about 60% for Grid 1, 27% for Grid 2, 23% for Grid 3, and 21% for Grid 4. The values show stable variation in the range [1.7, 2.5] for the four grids, with few values varying between 2 and 5. Values higher than 1.7 indicate the predominance of microcracks or the formation of macrocracks.

This indication is based on laboratory testing of RC girders subject to higher load magnitudes, which is different from service loading. The loading process can change the AE response and make the direct comparison between laboratory tests and in-situ tests difficult. This was reported by [66], who had performed cyclic loading tests on RC girders using a loading protocol that is representative of realistic service-level loading. They found that defining an absolute critical b-value can be unmeaning and that a parallel observation of structural performance is needed. They have suggested analysing the lowest b-values.

The lowest b-values were in the range of a uniform distribution of microcracks, and they followed temperature variation. Hits that gave low b-values (<1) or high b-values (>3) were generally associated with low traffic periods during nights or weekends. Moreover, b-values showed stable annual variation, and no visible active macrocracks were detected in the RC slab. These results show that the RC slab has uniform microcracks and stable macrocracks. For the defined grids, b-value analysis was also performed using daily values of amplitude frequency (Figure 3.15).
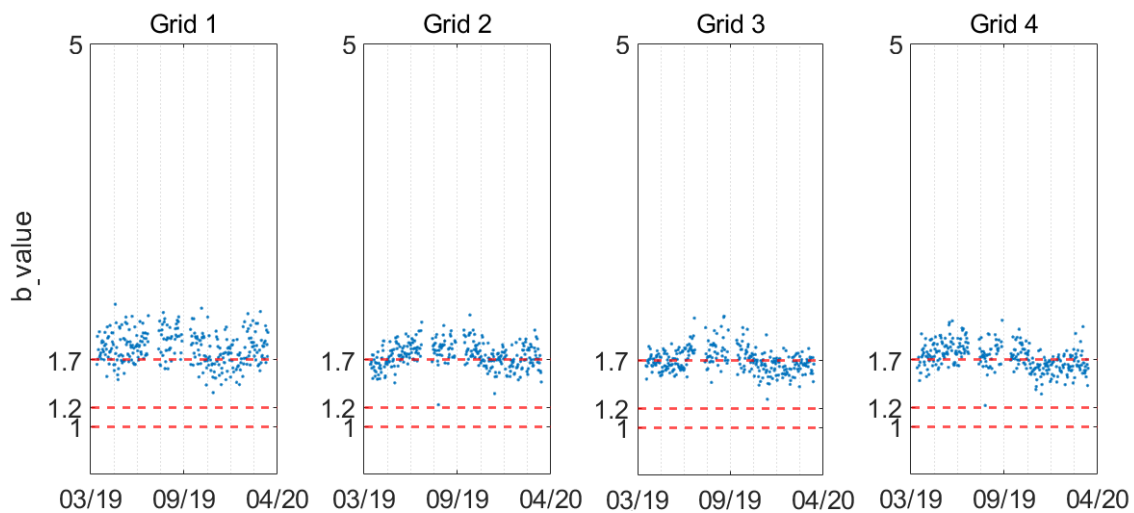
Figure 3.15. Daily b-values for the period of monitoring 14/03/2019 – 14/03/2020.

The general b-value trend is more visible with daily variations. The annual b-value varies in the range [1.5, 2], following thermal variations. Values less than 1.2 comprised about 16% of the total values for the four grids, while values between 1.2 and 1.7 comprised about 50%. Therefore, the AE activity in concrete is mainly due to the opening of microcracks during the summer and closing during the winter due to material expansion and boundary conditions, as explained in Section 2.3.2. The cyclic

annual *b*-value trend illustrated in Figure 3.15, demonstrates the stability of existing cracks. The *b*-value range implies the existence of uniformly distributed microcracks and stable macrocracks. Values higher than 1.7 comprised about 22% for Grid 1, 30% for Grid 2, 45% for Grid 3 and 38% for Grid 4. These values imply that microcracks are dominant or macrocracks are opening. These variations are present during the summer when the existing microcracks and the stable macrocracks are opening with increases in temperature.

3.6 Conclusions

This paper presents the parametric and statistical analyses conducted on AE data and strain measurements recorded during one year of continuous monitoring of an RC bridge-deck slab under traffic loading and environmental changes.

Despite the challenges of on-site bridge assessments, the presented monitoring approach demonstrated that assessing the structural response and characteristics under operational loading and environmental changes is feasible and can be done using a reasonable amount of postprocessing work. Five main conclusions are drawn:

1. The instrumentation, calibration, and synchronisation of the used techniques can be recommended for the assessment of RC road bridge-deck slabs using AE and strain measurements.
2. The presented monitoring data and applied processing methods are appropriate for quantifying the influence of environmental and operational conditions on the structural behaviour of road bridge elements.
3. Changes in AE features under traffic and environmental conditions have been determined using one year of continuous monitoring. Temperature effect should be considered when performing short-term monitoring or translating AE laboratory knowledge to the field.
4. The structural characteristics (i.e., the condition of the support, the articulation, and the slab-girder connection) affect the AE activity of the nearest sensors differently. This result reveals that different components of road bridges can be assessed over time using AE technique.
5. The use of *b*-value analysis and a cracking mode classification reveals the sources and the evolution of the cracking activity of concrete over time when operational loading and thermal variations are known.

The cyclic response of AE sensors and strain gauges demonstrates the robustness of the monitoring approach for assessing the operational conditions of road bridges. The deployment of the monitoring data using a signal-based technique, frequency analysis, and AE localisation will be presented in further work.

Chapter 4 Model-based Interpretation of Measurements for Fatigue Evaluation of Existing Reinforced-Concrete Bridges

Paper details

Chapter 4 contains a post-print version of the paper "I. Bayane, S.G.S. Pai, I.F.C. Smith, & E. Brühwiler (2021). Model-based interpretation of measurements for fatigue evaluation of existing reinforced-concrete bridges" submitted for review to the "Journal of Bridge Engineering" in August 2020. Minor modifications are introduced in the text for adapting the paper to the thesis format.

Author contributions

The author of the thesis conducted the research and wrote most of the paper. Dr. S.G.S. Pai provided structural identification codes and guidance when developing numerical models adding to the discussions offered. Professors I.F.C. Smith and E. Brühwiler contributed by proofreading the paper and by providing overall supervision.

Overview

This paper presents a model-based interpretation of measurements for which acoustic emission data, NDT measurements and load test results were used to assist the development of an accurate set of structural analysis models. Structural identification was performed afterwards using error-domain model falsification and residual minimisation. The obtained set of models was validated using strain measurements, and it was used to evaluate the fatigue safety of elements that are not accessible for monitoring.

Link to other chapters

In this chapter, uncertainty bias related to measurements and modelling are used for exploring load test results and evaluating the fatigue safety of noninstrumented parts of the RC slab. In this chapter, the load test results are extrapolated and the uncertainties are considered complementing the results of Chapter 2 where the load test results were interpolated without considering the uncertainties. The results are used in the next chapter in which the stress range in the rebars is assumed low to induce any fatigue damage. Therefore, only internal changes of concrete were evaluated under operational loading.

Paper III

Model-based Interpretation of Measurements for Fatigue Evaluation of Existing Reinforced-Concrete Bridges

Abstract

New methods are required for managing bridges sustainably and efficiently. Efficient management can be achieved with a detailed understanding of bridge behaviour obtained through monitoring and model-based data interpretation. This paper presents a methodology for evaluating the fatigue safety of existing bridges based on conducting measurements on-site and interpreting measurement data using physics-based behavioural models. The methodology combines data from different nondestructive measurements with structural models to develop a suitable set of feasible models that accurately describe structural behaviour. The methodology is illustrated with a case study of a composite steel-concrete road viaduct instrumented with acoustic emission sensors and strain gauges. Information from measurements is used to update a set of structural models and then to evaluate the fatigue safety of the viaduct. While commonly used "curve-fitting" methods are inaccurate, the new methodology can accurately use the measured behaviour of existing civil infrastructure to evaluate nonaccessible elements, to schedule inspections, and to make decisions related to actions such as strengthening and retrofit.

Keywords: Bridge, structural identification, acoustic emission, nondestructive testing, load test, numerical model, error-domain model falsification, residual minimisation.

4.1 Introduction

With increasing demand for infrastructure management, challenges exist in managing the existing stock of structures while building new ones. Bridge management is particularly challenging due to the large stock of bridges that have to be evaluated at a state level [94]. Reliable methods of evaluation are therefore necessary to allocate resources to the maintenance of bridges to ensure their utility over their lifetimes at a reasonable cost.

Monitoring and nondestructive testing (NDT) can provide valuable information about the current condition of bridges. In the last decades, many monitoring and testing techniques have been developed to improve knowledge of structural response. For example, techniques involving optic-fibre sensors, radiography, ground-penetrating radar, image correlation, tomography, and ultrasonic and acoustic emission (AE) have been proposed [95], [48], [96]. However, a close examination of previous work reveals the important challenge of transforming measurement data into knowledge that is helpful for structural identification and useful for decision-making.

The large size of civil infrastructure elements and the changing environments to which they are exposed create challenges for many techniques that otherwise fare well in laboratory settings [97], [48], and [98]. Furthermore, the monitoring and testing techniques are limited to accessible structural components, and they cannot be used for instrumenting a whole structure to obtain direct measurements. Moreover, collected data is often interpreted qualitatively, and the effect of uncertainties related to measurement error and bias are not quantified during measurement interpretation, which make measurement data unreliable for decision-making. Therefore, appropriate physics-based models and engineering expertise are required to interpret measurements and evaluate concrete bridges.

To overcome limitations related to site implementation in this research, techniques were chosen based on their usefulness for long-term monitoring with occasional on-site inspection that does not interrupt the operational use of a structure or cause damage to it. The AE technique is used to investigate structural behaviour under traffic and environmental actions. The AE technique involves the study of elastic waves generated during a stress-state change in a material to understand the physical and mechanical condition of the propagation zone [99]. This technique has been widely used to assess concrete bridges during load tests [60], [71], [72]. In addition, sound-velocity measurement and rebound-hammer testing were performed for concrete-strength assessments on-site. Finally, strain and deflection measurements were conducted to evaluate the mechanical response of the structure under a load test and normal traffic.

To consider the potential impact of uncertainties during measurement interpretation and provide quantitative information on the structure's behaviour at nonaccessible locations, information from measurements is combined with physics-based models. Interpreting measurement data using physics-based models has been referred to as structural identification, model calibration, and model updating [97]. It is an ill-posed inverse task that is sensitive to incomplete knowledge of uncertainties, systematic bias, and correlations between uncertainties at measurement locations [100].

Error-domain model falsification (EDMF) and residual minimisation (RM) are used for structural identification. RM is widely used in practice to calibrate structural models, and it is computationally inexpensive. However, it does not consider measurement and model uncertainty and bias. By contrast,

EDMF is one of the structural identification methodologies that has been successfully applied to more than 20 full-scale data-interpretation challenges [100]–[103]. EDMF has been shown to provide more accurate structural identification compared with other methodologies such as RM and traditional Bayesian model updating. Comparisons of these methodologies have been made in many full-scale case studies [101]–[103] as well as in theoretical examples where the "ground truth" was known. Finally, no work has combined AE results with advanced structural identification methods.

This paper presents an approach to interpret AE and strain measurements on-site using physics-based models calibrated using EDMF and RM with the aim to accurately evaluate the fatigue safety of nonaccessible elements. The approach is illustrated using a case study of a reinforced-concrete (RC) bridge-deck slab currently in service. The next Section 4.2 describes the measurement techniques, the structural identification methods and the requirements used for fatigue safety evaluation. Section 4.3 presents and discusses the measurements. Section 4.4 describes the development of structural models for data interpretation. Section 4.5 illustrates the use of the validated models for the fatigue evaluation of nonaccessible elements. The objectives of this work are as follows:

- Evaluate the use of AE for developing physics-based models and for structural identification of existing bridges.
- Compare and validate solutions for structural identification obtained using EDMF and RM to accurately predict responses at nonaccessible locations.
- Assess fatigue safety using validated knowledge of structural behaviour obtained by interpreting measurements with a physics-based model.

4.2 Methodology

4.2.1 Rebound-Hammer Testing

Rebound-hammer testing is an NDT that provides information related to the compressive strength of concrete. After every impact, the rebound value was saved and an average value of 10 rebound values was calculated and compared with measured values. Values greater or less than 10% of the average value were not included, and the average was recalculated. The compressive strength of concrete was obtained using the conversion curve that can be found in the rebound-hammer user manual [104] considering the rebound value and the impact direction. The median of compressive strength values was then calculated based on requirements of the standard [105]. The modulus of elasticity was then estimated from the characteristic strength according to Equation (4.1) of the International Federation for Structural Concrete's recommendations [39].

$$E_{ci} = E_{c0}\alpha_E(\frac{f_{ck} + \Delta f}{10})^{1/3}$$

(4.1)

where:

E_{ci} is the modulus of elasticity in [MPa] at concrete age of 28 day

f_{ck} is the characteristic strength in [MPa]

$\Delta f = 8 \, MPa$

$E_{c0} = 21.5 \, 10^3 MPa$

$\alpha_E = 1$ for quartzite aggregates.

4.2.2   Sound Velocity measurement

Sound velocity measurement is an NDT used to assess the compressive strength of materials. The test is carried out by passing elastic waves through materials and measuring the time of propagation to calculate wave velocity. The velocity of elastic waves propagating through a medium depends on elastic constants and the mass density of the material. Elastic waves are comprised of compressional or P-waves (first arrivals of a wave) and shear or S-waves (second arrivals of a wave).

The Young modulus is related to the compressive strength of concrete according to Equation (4.1). The velocities of P-waves v_p and S-waves v_s are related to the Young modulus E, Poisson ratio υ and density ρ of the environment according to Equations (4.2)-(4.3).

$$v_p = \sqrt{\frac{E(1 - \upsilon)}{\rho(1 + \upsilon)(1 - 2\upsilon)}} \tag{4.2}$$

$$v_s = \sqrt{\frac{E}{2\rho(1 + \upsilon)}} \tag{4.3}$$

Understanding the velocity of these waves provides information about the internal condition of the environment through which they propagate.

4.2.3   Acoustic Emission

The AE technique involves the study of elastic waves generated during a stress-state change in a material to understand the physical state of the propagation zone [99]. The stress change is assumed rapid enough to transmit the energy and dissipate it as an elastic wave. The AE technique involves the use of sensors that detect the elastic waves and convert them into electrical signals. The recorded signals are collected, preprocessed and stored in a data acquisition system, where it possible to extract, process, and visualise recorded data [58]. The AE data can be processed through many approaches, of which the most important are the parameter-based analysis [58], [82], [106], and the b-value analysis [61], [107], [108].

4.2.3.1 *Parametric Analysis*

Parametric-based analysis examines changes in AE features over time. AE feature extraction and analysis were performed using MATLAB and the AEwin program (commercial software for AE feature and waveform processing). Six features were extracted from the recorded waves, as shown in Figure 4.1, and were used to perform the analysis: amplitude, absolute energy (ABSenergy), average frequency (AF), counts to peak (Pcount), initiation frequency (Ifrequency), and duration. Amplitude and ABSenergy provide information on the intensity of internal changes, while duration and Ifrequency characterise their nature (cracking, friction, etc.). The AE features are defined according
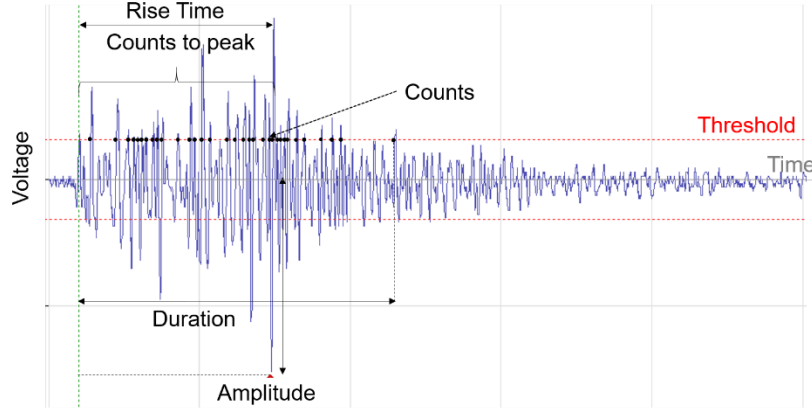
Figure 4.1. Acoustic Emission (AE) features.

to [76] as follows:

- Amplitude is the highest voltage in the AE waveform expressed in decibels [dB].
- Absolute energy is the time integral of the square of the signal voltage at the sensor before any amplification divided by a 10-kΩ impedance and expressed in attojoules [aJ].
- Duration is the time from the first to the last threshold crossing [µs].
- Counts to peak is the number of threshold crossings from the first to the highest voltage point on the waveform.
- Average frequency is equal to counts divided by duration [kHz]; see Equation (4.4).

$$Average\ frequency = \frac{Counts}{Duration} \tag{4.4}$$

- Initiation frequency is equal to counts to peak divided by rise time [kHz]; see Equation (4.5).

$$Ifrequency = \frac{Counts\ to\ peak}{Rise\ time} \tag{4.5}$$

The terms channel and hit are used as defined below.

− Channel is a single AE sensor and the related equipment components for transmitting, conditioning, detecting, and measuring the signals that come from it.
− Hit is the process of detecting and measuring an AE signal on a channel.

4.2.3.2 Ib-value Analysis

Ib-value analysis is a statistical method used to evaluate the amplitude-frequency distribution of AE hits [109]. The parameter *Ib*-value is an improvement of the *b*-value established by Gutenberg and Richter to quantify the succession of many AE hits of low amplitude generated by microcracks and the succession of a few AE high-amplitude hits generated by macrocracks [78]. The *Ib*-value includes the statistical values of amplitude and filters the low and high values, which provides selectively produced amplitude range [110]. The *Ib*-value is used to estimate cracking activity and cracking process based on AE peak amplitude distribution. The formula for *Ib*-value is given as follows:

$$Ib = \frac{logN(\mu - \alpha_1\sigma) - logN(\mu - \alpha_2\sigma)}{(\alpha_1 + \alpha_2)\sigma} \tag{4.6}$$

in which Ib value is the improved *b*-value (*Ib*-value), $logN$ is the cumulative frequency of amplitude, μ is the mean value of amplitude, σ is the standard deviation of amplitude, α_1 is a coefficient setting the lower value of amplitude, and α_2 is a coefficient setting the upper value of amplitude. The *Ib*-value is multiplied by a coefficient of 20 to compare it to *b*-value giving the quantitative analysis of [61], [88] presented in Table 4.1.

Table 4.1. Quantitative result analysis [61], [88].

b-value	Description
[1, 1.2]	The sensor is very near to a large crack or macrocracks are forming
[1.2, 1.7]	Cracks are uniformly distributed, and macrocracks are stable
>1.7	Microcracks are dominant or macrocracks are opening

4.2.4 Load Test

The structural response of the viaduct was evaluated based on the results of a load test performed using a five-axle truck with a legal limit load of 400 kN. The five axles were separately weighed, and their surface of action was identified. Two passages were performed at the midspan of Span 4 with a velocity of 10 km/h and a stop of 10 min to capture both the dynamic and static effects of vehicles, during which deflection and strain variations were measured continuously.

4.2.5 Error-Domain Model Falsification (EDMF)

Error-domain model falsification is a data-interpretation methodology based on the assertion that models should not be validated by data (weak science), but that data should be used to falsify models (strong science) [111], [100]. EDMF has been used in structural identification for different contexts such as leak detection [112], fatigue-life evaluation [101], [103], [113], damage evaluation [114], [115], and ultimate-limit state verification [116], [117].

Civil engineering structures are generally designed using conservative and simplified models. Models include significant uncertainties due to approximations and assumptions that are estimated using engineering heuristics. Examples of such approximations and assumptions are simplifications related to loading conditions, geometrical property definitions, and the modelling of boundary conditions, which contribute to modelling uncertainties.

EDMF falsifies models (instances) that provide responses (predictions) that are incompatible with measurements (observations). The criteria for compatibility are defined by considering uncertainties from different modelling and measurement sources. The quantification of many of these uncertainties for full-scale applications requires engineering knowledge.

Starting with feasible ranges of important parameters, an initial model set (IMS) is generated through sampling. Measurements and uncertainty information are then used to falsify (refute) models in the IMS to obtain a candidate model set (CMS) of models that explain measured behaviour. Several model classes can be potential candidates for describing the behaviour of a system. The model classes take system properties as arguments ($\theta_{i \in [1, n_p]}$), such as geometry, material characteristics, boundary conditions, and loading. The combination of model class (g) and input-parameter set θ give predictions at each measurement location $i \in [1, n_p]$.

The true response of a system Q_i is approximated by model predictions g_{ki} with modelling error $\varepsilon^*_{model,ki}$ at each measurement location. Similarly, the true response is observed by measurements y_i with measurement error $\varepsilon^*_{measure,i}$. These responses can be summarised as shown in Equation (4.7).

$$g_{ki}(\theta^*_k) + \varepsilon^*_{model,ki} \; = \; Q_i = y_i + \varepsilon^*_{measure,i} \tag{4.7}$$

Sources of modelling uncertainties include material properties, geometrical properties, mesh refinement, boundary conditions, the slab-girder connection, and other model simplifications. The uncertainties are estimated using engineering judgement. Sources of measurement uncertainties include the resolution of sensors, position, load, and human error. These uncertainties are estimated based on information from the sensor manufacturer and repeated testing. Uncertainties from model and measurement sources are combined to determine the combined uncertainty $U_{c,i}$.

Using this combined uncertainty $U_{c,i}$, the criteria for falsification is determined. The criteria for falsification in EDMF are thresholds computed for a target reliability of identification, Φ. This target reliability of identification for civil engineering applications is typically set to 95% ($\Phi = 0.95$).

The threshold bounds for falsification, T_{low} and T_{high}, are calculated using the target reliability of identification. Threshold bounds are obtained as follows:

$$\forall\, i \in \{1, \dots, n_m\}, \left\{ T_{low,i}, T_{high,i} : \Phi^{1/n_m} = \int_{T_{low,i}}^{T_{high,i}} f_{U_{c,i}}(U_{c,i}) dU_{c,i} \right\} \tag{4.8}$$

where $f_{U_{c,i}}$ is the probabilistic distribution function of combined uncertainties at measurement location i. Instances of model (g), are falsified when model predictions are incompatible with measurements at any sensor location. This compatibility is evaluated using Equation (4.9).

$$\forall\, i \in [1, \dots, n_m]: T_{low,i} \le g_i(\theta) - y_i \le T_{high,i} \tag{4.9}$$

Model instances that are not falsified from the CMS are model instances that demonstrate structural behaviour compatible with observations while accounting for uncertainties from modelling and measurement sources. These model instances may be utilised to predict the structural response of noninstrumented elements under conditions that are different from those during sensing to support asset management.

4.2.6   Residual Minimisation (RM)

Residual minimisation is commonly used in practice and is computationally inexpensive. It assumes that the difference between model predictions and measurements is governed by the choice of parameters [118] and that these parameters have zero-mean uncertainty distributions [102]. Calibration is therefore done by determining the model-parameter values that minimise the error between simulation results and measurement data [119]. The objective function for RM is shown in Equation (4.10).

$$\hat{\theta} = argmin_\theta \sum_{i=1}^{n_y} \left(\frac{g_i(\theta) - \hat{y}_i}{\hat{y}_i} \right)^2 \tag{4.10}$$

where $\hat{\theta}$ is the optimum model parameter set obtained using measurements, $g_i(\theta) - \hat{y}_i$ is the residual obtained between the model response $g_i(\theta)$ and measurement $\hat{y}_i$ at location i, and n_y is the number of measurement locations. The calibration is therefore done by determining the model parameter values $\hat{\theta}$ that minimise the error between the model response $g_i(\theta)$ and measurement $\hat{y}_i$ for each measurement location $i \in \{1, n_y\}$.

4.2.7 Fatigue Evaluation

Fatigue safety is evaluated according to SIA 269 (2013) following two levels. First, the endurance limit is verified. In other words, the maximum value of the measured stress range must be smaller than the endurance limit of the rebar fatigue detail. If the Level 1 evaluation is inconclusive, damage accumulation according to Palmgren-Miner's rule is calculated using the recorded histograms of stress cycles and the appropriate S-N curve for the rebar fatigue detail [38], [120]. More details can be found in Section 2.5.1.

4.2.8 Summary of Methodology

The presented methodology for the evaluation of the fatigue behaviour of RC bridges is summarised in the following principal steps:

- Estimate material properties using nondestructive measurements.
- Develop and parametrise physics-based models using AE monitoring.
- Update the models using load-test results and EDMF.
- Validate model-updating solutions by comparing updated model predictions with measurements not included for structural identification.
- Predict structural response at noninstrumented and nonaccessible locations and evaluate fatigue behaviour.

4.3 Measurements

4.3.1 Case Study

Monitoring and NDT were performed on an eight-span composite concrete-steel viaduct. It has seven articulated spans of 25.58 m and an approach span of 15.8 m. Each span comprises an RC slab of a thickness varying from 0.17 m to 0.24 m connected to two 1.3-m-height steel girder beams.

The viaduct is instrumented with AE sensors, strain gauges, and thermocouples for continuous monitoring. Linear variable differential transformers (LVDT), rebound-hammer testing, and pencil-lead-break test are used for occasional inspections. Figure 4.2 illustrates the view of the viaduct and the instrumented span.

Underside of Crêt de l'Anneau   Truck over Crêt de l'Anneau

Figure 4.2. Crêt de l'Anneau viaduct located between *Neuchâtel* and *Travers*, Switzerland.

AE channels were mounted on the RC slab at midspan, midlane, between midspan and articulation, and between articulation and the support of Span 4. Strain gauges were embedded in longitudinal and transverse rebars at the midspan and at the girder of Span 4. LVDTs were mounted on middle of Span 4 at five locations (lower flange of the girder, the midlane, and the midspan). Figure 4.3 illustrates the instrumented slab and sensor placement. Rebound-hammer testing and pencil-lead-break test were performed on the lower side of Span 4.

The load test and deflection measurements were performed in June 2016. The pencil-lead break and rebound-hammer tests were performed in February 2019. Strain and AE monitoring data used in this study were collected during one year of continuous monitoring from 14/03/2019 to 14/03/2020.
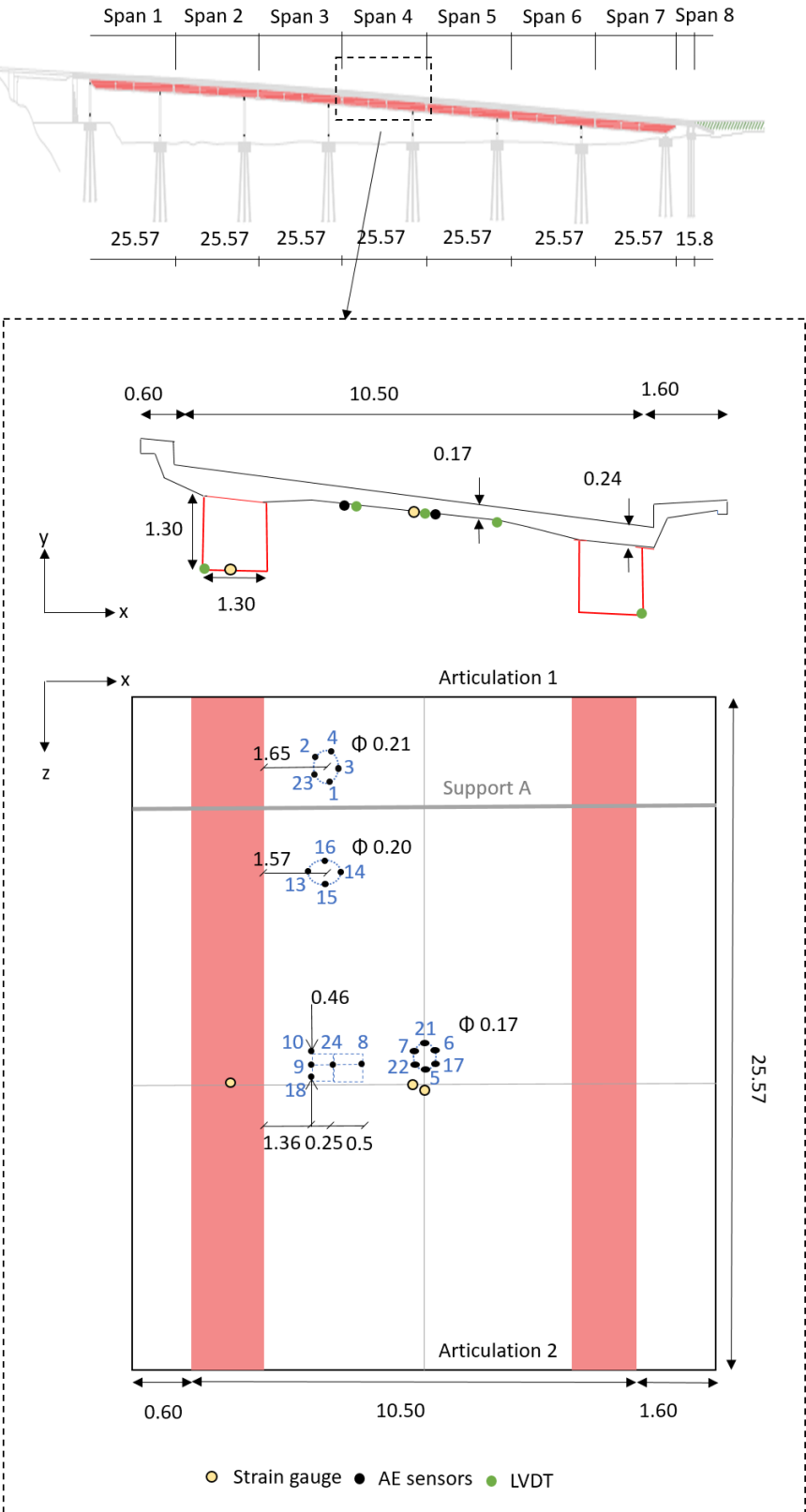
Figure 4.3. Drawings of the Crêt de l'Anneau viaduct, the cross-section, and the lower side of the instrumented span with sensor deployment; dimensions in [m].

4.3.2   Investigation of Material Properties

4.3.2.1   Concrete Strength

4.3.2.1.1 Rebound-Hammer Testing

Rebound-hammer testing and sound-velocity measurement identify material properties on-site [48]. They are used to estimate the modulus of elasticity of concrete.

Rebounds are performed in locations spaced more than 2.5 cm apart at the middle of Span 4. The 20 best readings, which are those not greater or less than 10% of the average rebound value, are used to determine the corresponding compressive strength from the conversion curve of the user manual [104]. The conversion curve was chosen based on the impact direction of the rebound hammer that forms an angle of -90 °C with the tested surface. The median of the compressive strength values was then calculated and used along with the equation of the model from the International Federation for Structural Concrete (FIB) [39] to determine the Young's modulus of concrete. The compressive strength was found to be equal to 47 N/mm², and the initial Young's modulus was taken to be approximately 35'000 N/mm². The actual Young's modulus was therefore found equal to 62'000 N/mm², which indicates a significant increase with concrete age due to the continuity of concrete hydration.

4.3.2.1.2 Sound-Velocity Measurement

Sound velocity measurement was performed to obtain a second estimation of the modulus of elasticity. Elastic wave simulation was performed using pencil-lead-break test and rebound hammer testing in the middle of Span 4. Time difference Δt_1, which is given by the acquisition system in real time for each channel was recorded. A thorough analysis of generated waves allows for the separation of P-waves from S-waves. The time difference Δt_2 between the two wave types was calculated. The two time differences were used along with the distance d between channels to estimate the velocity of P waves and S waves according to Equations (4.11)-(4.12).

$$v_s = \frac{d}{\Delta t_1 + \Delta t_2} \tag{4.11}$$

$$v_p = \frac{d}{\Delta t_1} \tag{4.12}$$

Velocity results are presented in Table 4.2.

Table 4.2. Velocity measurements.

Method	Area of interest	v_p [m/s]	v_s [m/s]
Pencil break	0.04 m	3'400	2'400
Rebound Hammer	2 m	3'500	2'000

The density of concrete was assumed 2'400 kg/m^3 with a Poisson ratio of 0.2. The Young's modulus of concrete was calculated according to Equations 1-2, and was estimated to be in the range [23'000, 33'000] N/mm².

4.3.2.1.3   Discussion

The difference between the Young's modulus of concrete obtained using rebound-hammer testing (62'000 N/mm²) and the ones obtained using sound-velocity measurement ([23'000, 33'000] N/mm²) is great and may be due to various factors. The validity of the values obtained is thus questionable. Factors such as the influence of the aggregate size, the influence of rebars, the humidity of concrete, the configuration of channels, the mode of propagation and the area of investigation can all influence the results [48]. For example, rebound measurements are highly variable on-site, and can give values up to 23% [121].

The results put into question the validity of using only these measurements to estimate Young's modulus. The variability of measurement results can be accommodated by making the Young's modulus of concrete a parameter and allowing it to vary in the range of [20'000, 60'000] N/mm², as defined by the minimum and maximum values obtained with rebound-hammer testing and sound velocity measurement.

4.3.2.2   *Homogeneity of concrete*

4.3.2.2.1   Parametric-based analysis

The homogeneity of concrete is evaluated using the AE data of five channels covering different zones of the RC slab. Five classes are defined, presenting respectively the AE data of Channel 1 near Support A, Channel 14 near Articulation 1, Channel 21 at the midspan, Channel 8 near the midlane, and Channel 24 at the midlane (see Figure 4.3 for channel placement).

The classes are visualised in Figure 4.4. Each point on the scatterplot represents the daily mean of an AE feature and the colour shows the class to which the point belongs. The two dimensions of visualisation present AE features for which the ABSenergy and amplitude provide information on the intensity of internal changes, while duration and Ifrequency characterise their nature (cracking, friction, etc.). In addition, the number of hits can indicate the presence of cracking activity.
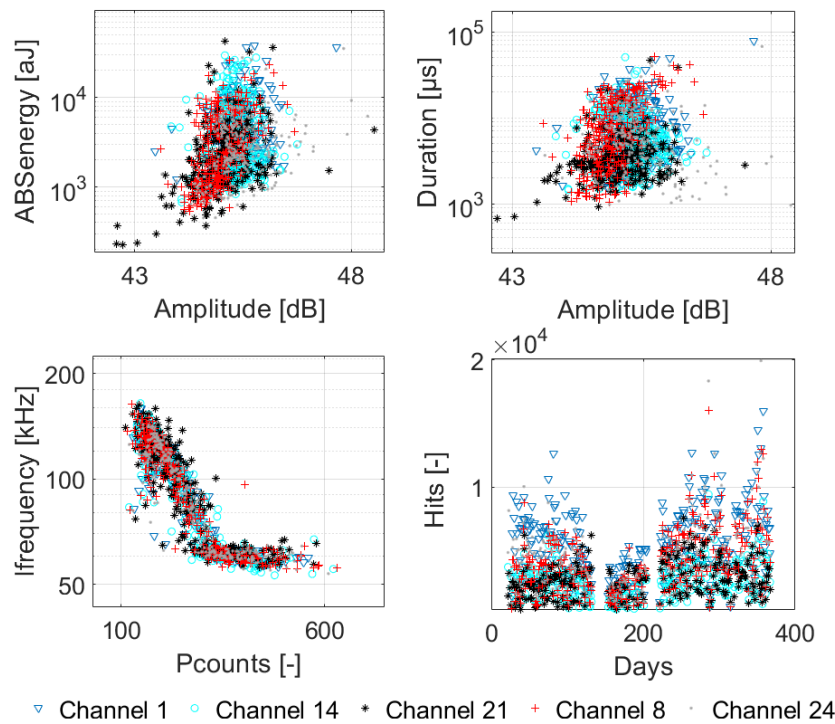
Figure 4.4. Daily mean variation of acoustic emission (AE) features for Channels 1, 14, 21, 8, and 24 covering different zones of the reinforced-concrete (RC) slab.

The AE activity of the channels distributed along the RC slab was grouped in one cluster for different combinations of AE features that present the dimensions of visualisation. First, the daily mean of ABSenergy plotted against amplitude forms one cluster for the five channels, which implies that the detected intensity of AE activity is the same for Channels 1, 14, 21, 8, and 24. Moreover, daily mean values of Ifrequency plotted against Pcounts and duration plotted against amplitude form one cluster for the five channels. The one cluster implies that the principal source of AE activity is the same for concrete around the channels in question. The number of hits over time is also similar for the five channels, which indicates similar cracking activity in the concrete.

It was concluded that the AE response of the five channels classified in one cluster implies similar internal changes in the concrete near these channels. Concrete is therefore estimated to be homogenous along the slab for the development of the structural models.

4.3.2.2.2 *Ib*-value analysis

The cracking activity in the slab due to passing vehicles and environmental influences was evaluated using *Ib*-value analysis. *Ib*-value was calculated for Channels 1, 14, 21, 8, and 24 using a step of 1'500 AE hits. Table 4.3 illustrates the variation in *Ib*-values.

Table 4.3. Percentage of *Ib*-values for channels 1, 14, 21, 8, and 24 (see Figure 4.3 for sensor placement)

	<1.2	<1.2 – 1.7>	>1.7
Channel 1	1%	48%	51%
Channel 14	1%	51%	48%
Channel 21	1%	47%	51%
Channel 8	0%	43%	57%
Channel 24	1%	48%	51%

The annual range of *Ib*-values is between 1.2 and 2.5, which indicates that 48% of AE activity is due to stable cracks and 51% is due to the opening of microcracks.

Ib-values have the same variation range for channels at different locations. The cracking process of concrete is thus considered the same along the slab. This same variation range provides further evidence for modelling the concrete of the slab as a homogeneous material with insignificant spatial variability.

4.3.2.3 *Investigation of Structural Elements*

AE features, as defined in Section 4.2.3.1, were classified into groups to better understand and compare the different sources of AE activity. The source of AE activity provides information on the condition of structural elements near the AE sensors (i.e., the condition of the support and articulation and the condition of the slab-girder connection.

4.3.2.3.1 Condition of the Support and Articulation

Three classes of AE response data were defined to evaluate the condition of the support and articulation and the condition of the slab-girder connection: the AE data of channels at the midspan (Channels 5, 6, 7, 17, 21, 22), and the AE data of channels near the slab-girder connection near Articulation 1 (Channels 2, 3, and 4) and near Support A (Channels 1, 16, and 23).

These classes are visualised in Figure 4.5. Each point on the scatterplot represents the daily mean of the number of hits plotted against AF, and the colour shows the class to which each point belongs. The AF is calculated for each grid of channels using Equation 3.
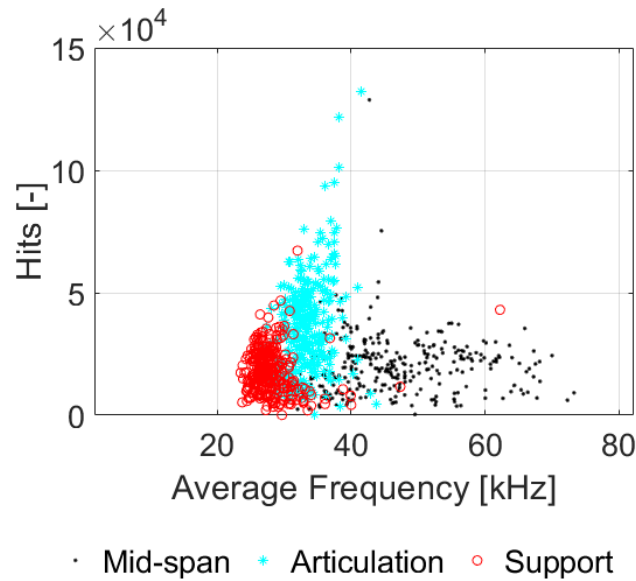
Figure 4.5. Hits versus average frequency (AF) for channels at the midspan, near the articulation, and near the support.

The daily mean of the number of hits plotted against AF forms three clusters for the three defined classes. The AE response of channels near Support A and Articulation 1 present lower values of AF and a higher number of hits compared to channels at the midspan, which is due to the existence of different AE sources.

The clusters with a high number of hits (>3'000) or low AF values (< 40 kHz) suggest the existence of many AE events with long durations that are assumed to be due to friction at the level of structural elements rather than internal changes in the concrete. More details can be found in [7].

It was concluded that the three defined clusters of the AE response imply the presence of different sources of AE near the channels in question. The sources were assumed to be due to microcracking in concrete and to friction at the level of the slab-girder connection, friction at the level of articulation, and friction at the level of support. The degrees of stiffness of the support and articulation and the slab-girder connection were therefore parametrised in the development of the structural models.

4.3.2.4   Condition of the Slab-Girder Connection

The condition of the slab-girder connection was evaluated using the AE data of three grids of channels covering different zones of the RC slab near the slab-girder connection. Three classes were defined to present the AE data of Grid 1, which includes Channels 9, 10, and 18, Grid 2, which includes Channel 13, and Grid 3, which includes Channels 2 and 23 (see Figure 4.3 for channel placement).

The classes are visualised in Figure 4.6. Each point on the scatterplot represents the daily mean of an AE feature, and the colour shows the class to which the point belongs. The two dimensions of visualisation present the ABSenergy and amplitude, which provide information on the intensity of internal changes, and the duration and Ifrequency that characterise the nature of internal changes.
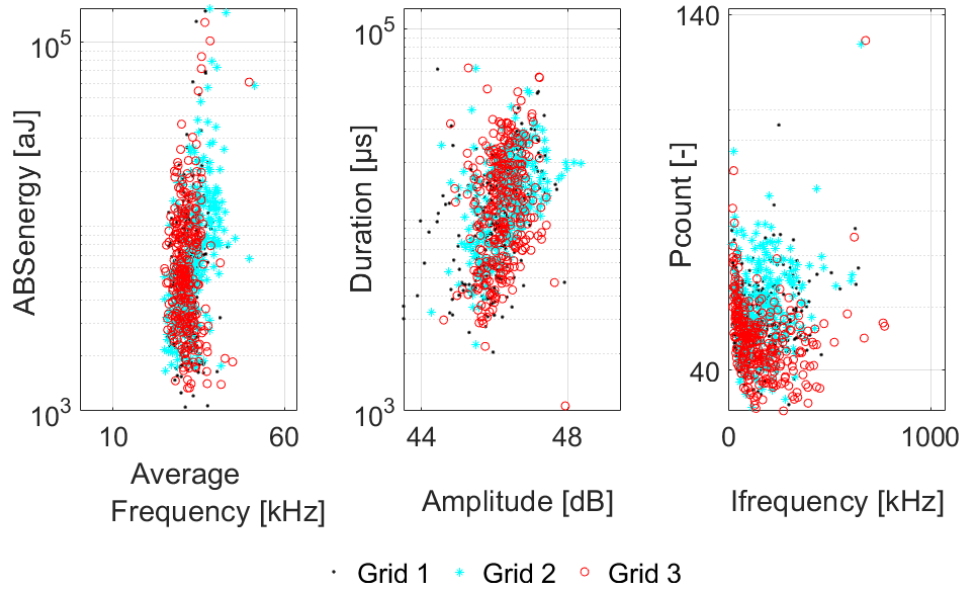
Figure 4.6. Daily mean variation of acoustic emission (AE) features for channels near the slab-girder connection.

Daily mean ABSenergy values plotted against AF, duration plotted against amplitude, and Pcount plotted against Ifrequency form one cluster for the three grids of sensors, which implies that the intensity and the source of internal changes are the same for channels near the slab-girder connection.

Classifying the AE response of three defined classes in one cluster implies that the condition of the slab-girder connection is stable along the bridge deck. The stiffness of the slab-girder connection is therefore considered constant throughout the span during the development of structural models.

4.3.3 Investigation of Structural Response

During the load test, strain responses were measured in the longitudinal and transverse rebars, and the maximum deflection of the cross-section was measured using LVDTs at the middle of Span 4. For example, strain responses are illustrated in Figure 4.7 for the passage of the load-test truck in the centre of the road with a velocity of 10 km/h and a stop of 10 s.
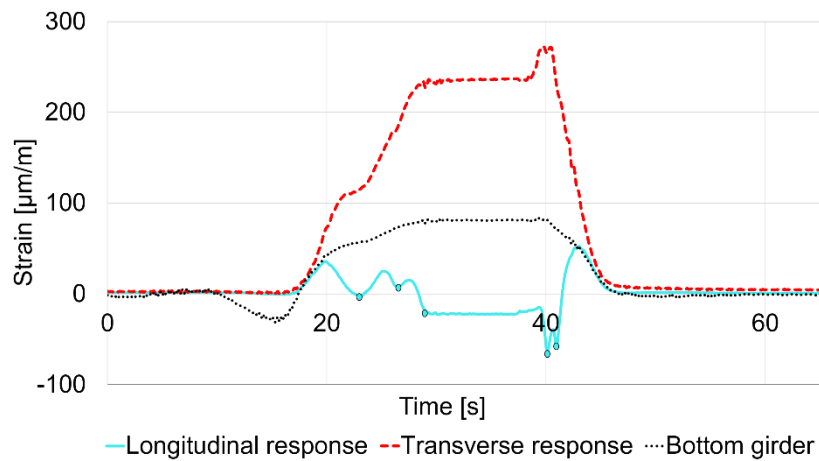
Figure 4.7. Strain variation during the load test with the maximum legal load of 400 kN in the centre of the midspan with a velocity of 10 km/h and a stop of 10 s.

Slab slenderness accentuates local strains under the wheels. The passage of truck axles was clear with the five peaks detected in the longitudinal rebar, which are illustrated with points in the longitudinal response (Figure 4.7). Transverse rebars were loaded in tensile while stress reversal was present in the longitudinal response of the span. The results of the load test were used to update the numerical model and assess the condition of the viaduct.

4.4 Model-based Data Interpretation

4.4.1 Finite Element Model

Model updating allows one to develop physics-based models of the viaduct that can accurately simulate its behaviour under conditions that are different from those present during monitoring. The model was developed based on the prior knowledge provided by AE measurements. The slab was modelled as homogenous because the variability of AE features across the slab was similar. The Young's modulus value was parametrised to be uniformly distributed in the range [20'000, 60'000] N/mm², which is defined according to the minimum and maximum values obtained with rebound-hammer testing and sound-velocity measurement. Springs were introduced between the slab and the girder to parametrise the stiffness of the slab-girder connection caused by the existence of friction between the slab and the girder, as detected by AE activity. Spring stiffness is constant across the slab since the AE features of channels near the connection present the same variation at all locations. The stiffness of supports and articulations was parametrised because friction exists at their level, as detected by AE activity.

The noninstrumented spans of the viaduct are independent and assumed to have similar structural behaviour compared to Span 4. The model therefore comprised one span, modelled from articulation to articulation. The finite element model (FEM) of the viaduct was developed using ANSYS R18 (a commercial program). Material properties and boundary condition properties are presented in Table 4.4 and Table 4.5. The RC slab and the girder were modelled using Shell Element 181. The support,

articulation, and slab-girder connection were modelled using zero-length spring elements, Combin 14, to parametrise their translational and rotational stiffness. The ranges of possible model parameters are presented in Table 4.6.

Table 4.4. Material properties

Material	Density [kN/m^3]	Young's modulus [N/mm²]	Poisson's Ratio	Element
Reinforced concrete (slab)	25	Variable in the range [20'000, 60'000]	0.2	Shell 181
Steel (girder)	78.5	210'000	0.3	Shell 181

Table 4.5. Boundary condition properties

	Stiffness (see Table 4.6 for the range of the variable)	Element
Articulation	Variable	Combin 14
Support	Variable	Combin 14
Slab-girder Connection	Variable	Combin 14

Table 4.6. Range of model parameters

Parameter	Description	Initial range
E_c	Young's modulus of concrete [GPa]	20 - 60
K_{sg_x}	Stiffness of the connection slab-girder x direction [log N/mm]	3 - 9
K_{sg_z}	Stiffness of the connection slab-girder z direction [log N/mm]	4 - 8
K_{sup_y}	Stiffness of the support y direction [log N/mm]	3 - 7
K_{sup_z}	Stiffness of the support z direction [log N/mm]	4 - 9
R_{sup_x}	Stiffness of the support x direction [log N/mm]	7 -12
K_{art1_y}	Stiffness of the articulation 1 y direction [log N/mm]	2 - 6
K_{art1_z}	Stiffness of the articulation 2 z direction [log N/mm]	4 - 8
K_{art2_y}	Stiffness of the articulation 2 y direction [log N/mm]	2 - 6
K_{art2_z}	Stiffness of the articulation 2 z direction [log N/mm]	4 - 8

Parameter range was defined based on structural response variations depending on spring stiffness. The structural response variation has an 'S' shape, in which the initial range of parameters was defined for the variable part. The first part of the constant values corresponds to a lack of stiffness, and the last part corresponds to constant values presenting full stiffness. For example, in Figure 4.8, the strain variation ε_L of the longitudinal rebar at the midspan is S-shaped when changing the stiffness of the slab-girder connection K_{sg_z}. The initial range of the parameter K_{sg_z} was therefore defined as [4, 8].
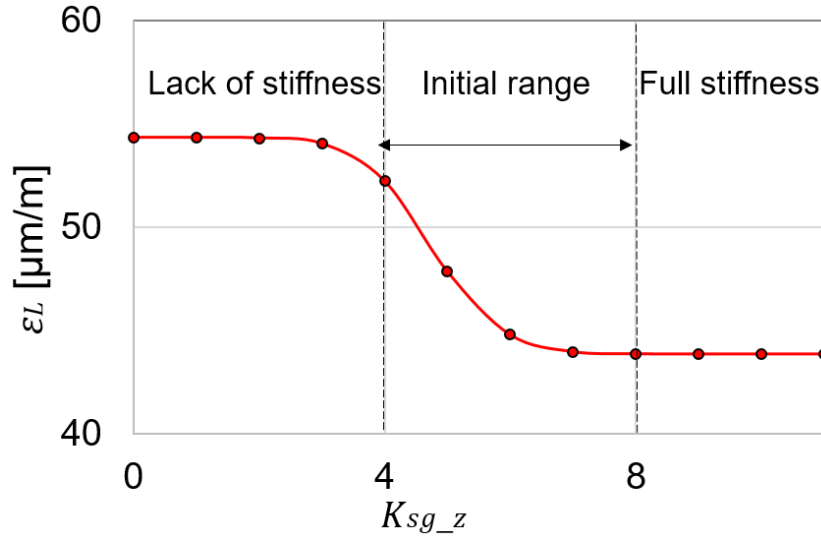
Figure 4.8. Variation of the longitudinal strain of the rebar at the midspan based on spring stiffness; the variation of the structural response to spring stiffness forms an 'S' shape.

4.4.2 Model Class Selection

The FEM of the viaduct was used to predict strain distribution and deflection at each sensor location. Strain and deflection were affected differently by the parameters that define the model. Each model parameter was quantified as a random variable with a uniform probability distribution. Bounds of the uniform probability distribution attributed to the parameters were updated using deflection measurements.

A total of 10 parameters were included in the FEM. The model class for structural identification was selected using forward-variable selection to search for a globally relevant model class (Pai et al., 2020). One thousand random samples were drawn from the initial parameter distribution (see Table 4.6) and were provided as inputs to the FEM to predict deflection at the five sensor locations. Clustering with k-means was used to characterise model predictions into classes. A support-vector machine classifier model [123] was trained using these different classes and forward-variable selection to determine parameters that govern the structural behaviour. Parameters that make significant changes to predictions at measurement locations were more important for classification than others and were therefore included in the model class for structural identification. Five of the ten

parameters were included in the model class for structural identification using this method, which are listed in Table 4.7.

Table 4.7. Ranges of prior parameter distribution

Parameter		Description	Range
1	K_{sg_z}	Stiffness of the connection slab-girder z direction [log N/mm]	4 - 8
2	K_{sup_y}	Stiffness of the support y direction [log N/mm]	3 - 7
3	K_{sup_z}	Stiffness of the support z direction [log N/mm]	4 - 9
4	K_{art1_y}	Stiffness of the articulation 1 y direction [log N/mm]	2 - 6
5	K_{art1_z}	Stiffness of the articulation 1 z direction [log N/mm]	4 - 8

4.4.3   Sources of Uncertainty

Uncertainty affecting structural identification arises from assumptions made during model development. Sources of uncertainty, such as the geometry of the RC slab and the modelling of the supports and connections between the RC slab and steel girders, are important. Additional sources of uncertainty related to sensors and loading conditions were accounted for during structural identification. Uncertainties from sources such as truck position and secondary parameters were estimated by varying these as parameters in the FEM. Uncertainties due to modelling assumptions were estimated based on engineering heuristics. Uncertainties in measurements were estimated either using the technical manual provided by sensor manufacturers or by comparing measurements recorded during multiple load tests. Table 4.8 shows the estimated distributions of uncertainties from various modelling sources. Table 4.9 shows the estimation of measurement uncertainty distributions related to strain gauges and LVDTs.

Table 4.8. Uncertainty sources and distribution (other than measurement)

Source	Min	Max	Distribution
Model	-10%	5%	Uniform
Position	>-6%	0	Uniform
Load	0	10^{-3}	Uniform
Secondary parameters	>-12%	<15%	Uniform

Table 4.9. Uncertainty sources and distribution (measurement)

	Mean	Standard deviation	Distribution
Strain gauge	0	1 µm/m	Normal
LVDT	0	1 mm	Normal

The most important uncertainty sources do not have a zero mean. Uncertainties defined in Table 4.8 and Table 4.9 were combined using Monte Carlo sampling to estimate the combined uncertainty at each sensor location. Using this combined uncertainty, threshold bounds for EDMF were calculated for each sensor location using Equation (4.7). The threshold bounds were calculated for a target reliability of identification of 0.95 (95% confidence). These bounds were used to perform EDMF using the condition defined in Equation (4.9).

4.4.4 Structural Identification Using Load-Test Data

EDMF was used to update the FEM of the steel-concrete composite viaduct with information from measurement data recorded during load test. RM assuming no model bias was also used to calculate the optimal solution using Equation (4.10). Five measurement data points were utilised for structural identification, which were midspan deflections at five locations in the cross-section. The location of LVDT sensors for measuring deflection are shown in Figure 4.3.

Grid-based sampling was used to generate the parameter space. The five identification parameters were discretised in four uniform intervals, giving 4^5 = 1'024 samples. EDMF identified 165 candidates in the CMS from an IMS of 1'024 samples (see Sections 4.1 and 4.2.7). The identified candidates in the CMS reduced the initial uncertainty related to model-parameter values in the IMS and provided predictions that are compatible with measurements. By contrast, RM identified one solution without considering measurement uncertainties, thereby assuming that either there is no uncertainty or that total uncertainty has a zero mean and that there are a statistically significant number of measurements.

In Figure 4.9, the probability of the bounds of the IMS and EDMF solutions from the CMS are shown. Furthermore, parameter values obtained using residual minimisation (RM), and design parameter values (Design) are shown.
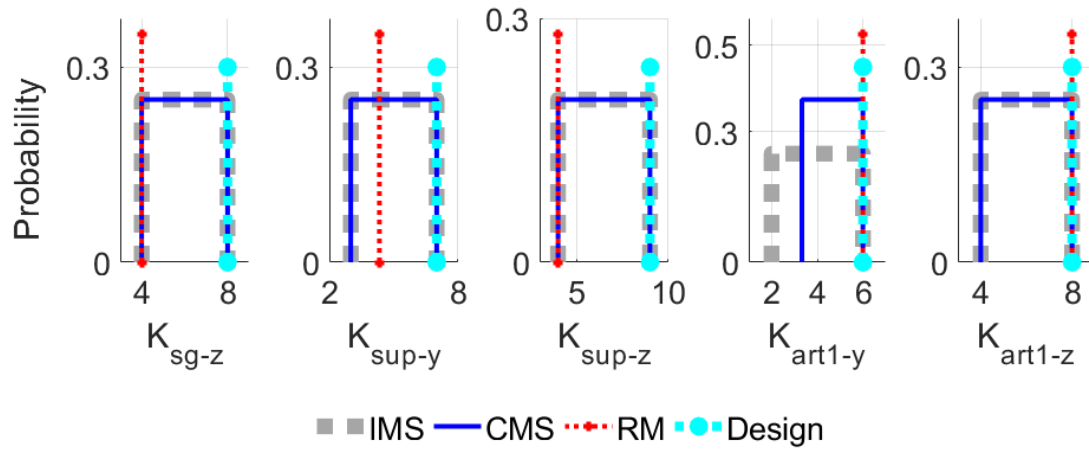
Figure 4.9. Probability of the bounds of initial model set (IMS) solutions, candidate model set (CMS) solutions, residual minimisation (RM) solutions, and initial design values (Design).

The updated model instances obtained using EDMF reduced variability related to the stiffness of Articulation 1 in the y direction, which means that the translational stiffness of the articulation in the y-direction cannot be free. While the probabilities of parameters 1, 2, 3, and 5 have similar bounds to the prior parameter ranges, the parameter variability related to the joint model-parameter probability was reduced, as demonstrated by the falsification of 84% of initial model instances. A parallel axis plot comparing the initial model population with the candidate model instances identified using EDMF is shown in Figure 4.10.
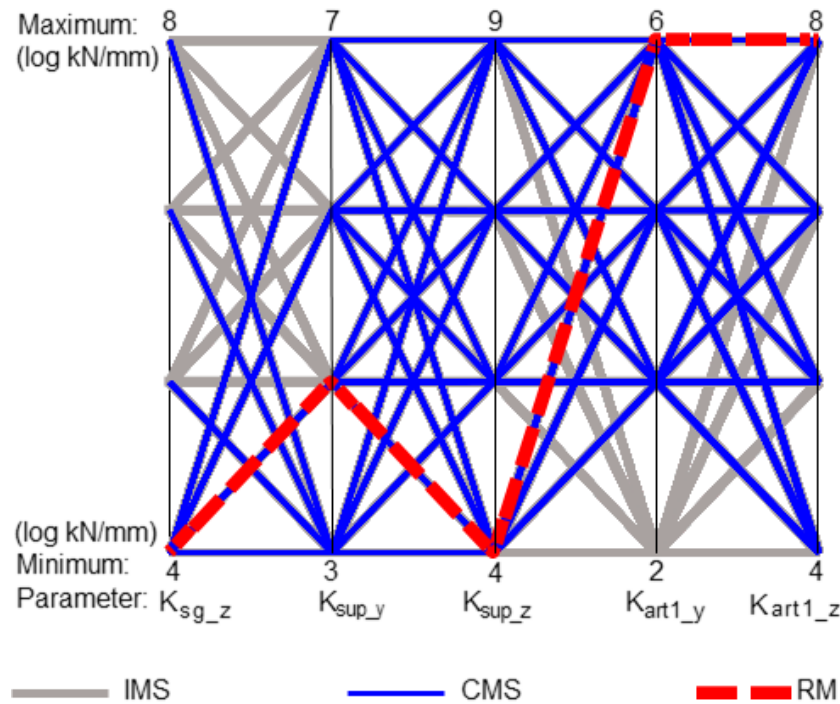
Figure 4.10. Parallel axis plot comparing initial model set (IMS) instances, candidate model set (CMS) instances and the optimal solution obtained using residual minimisation (RM).

Each point along these vertical axes corresponds to a possible value of the five chosen parameters. The bounds of the vertical axis, denoted as minimum (min) and maximum (max) correspond to the bounds of prior parameter distributions presented in Table 4.6.

Therefore, a line connecting minimum values represents a model instance with input parameters:

$$K_{sg\_z} = 4, K_{sup\_y} = 3, K_{sup\_z} = 4, K_{art1\_y} = 2, \text{ and } K_{art1\_z} = 4.$$

A line connecting maximum values represents a model instance with input parameters:

$$K_{sg\_z} = 8, K_{sup\_y} = 7, K_{sup\_z} = 9, K_{art1\_y} = 6, \text{ and } K_{art1\_z} = 8.$$

The possible combinations of model-parameter values that provide predictions compatible with measurements (as assessed by EDMF and illustrated by CMS line, Figure 4.10) form the CMS. This CMS consists of 16% of the initial model instances.

The optimal parameter values obtained using RM are also shown in Figure 4.10. The RM solution indicates stiff articulation, flexible support, and a lack of stiffness between the slab and the girder. This solution is far from the most conservative solution identified by EDMF.

While Figure 4.10 helps visualise a multi-dimensional parameter space, it does not provide information related to the accuracy of data interpretation. The next section describes data-interpretation solutions that were validated with additional data that was not utilised in model-based data interpretation.

4.4.5 Validation

Strain measurements were used to validate the solutions of structural identification that were obtained using EDMF and RM. Validation was conducted using measurements from strain gauges in the longitudinal rebar ε_{L1} and the steel girder ε_{girder} at the midspan. Updated-model parameters were used to predict the strain at these sensor locations. A comparison of the predicted and measured strains for the two sensors is shown in Figure 4.11.
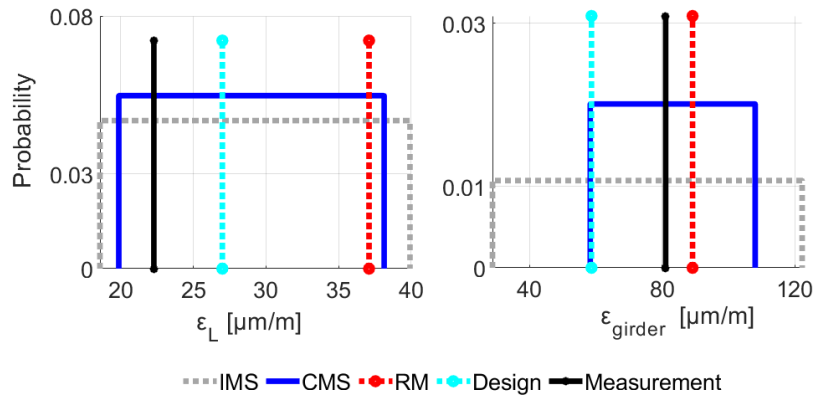
Figure 4.11. Validation results, comparison of the predicted and measured strains that have been left out of identification. Candidate-model-solution (CMS) bounds include measurements, which validate structural identification predictions, while residual minimisation (RM) fails to predict measurements that are far away from the RM solution.

The range of predicted strain was smaller than the initial prediction range due to EDMF, which reduces parameter variability.

The bounds of the updated-model prediction distributions included measurements from all sensors excluded from structural identification. The results were therefore assumed accurate, and the updated model parameters could be used to predict conservative model responses at noninstrumented locations.

RM predictions of strain were biased by measurements despite calibrating parameter values with deflection measurements. The RM solution was therefore not valid and may result in unconservative predictions.

4.5   Fatigue Examination

The cross-section of the RC slab is defined as the critical element of the viaduct due to the pronounced effect of axle loads. In fact, in the longitudinal direction, traffic loads are distributed on both the RC slab and the steel girder, while in the transverse direction, only the 17-cm-thick slab is acting. Therefore, the fatigue behaviour of steel reinforcement and concrete of the cross-section were evaluated with respect to fatigue requirements. Details of the fatigue damage calculation can be found in Chapter 2 and [124].

The RC slab was found to be safe considering the combined action of the slab and the girder under traffic loading. However, the flexural behaviour of the cross-section depends on the welded rebars' capacity to ensure the fixity between the slab and the girder. The welded rebars were used to connect the steel girder and the slab, and they were not accessible for monitoring, as illustrated in Figure 4.12.
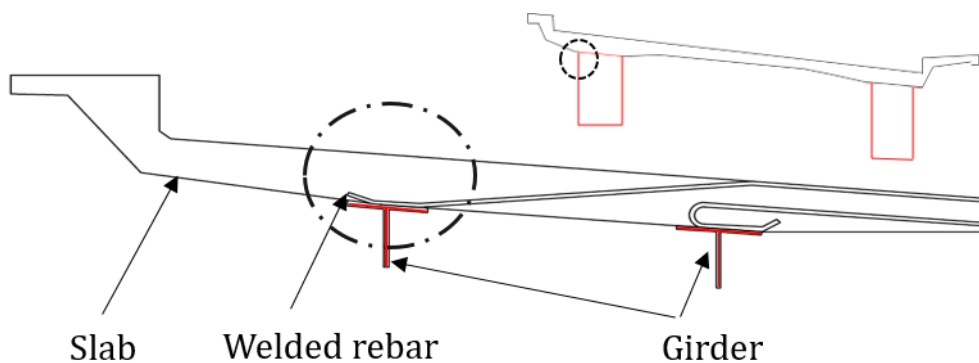
Figure 4.12. Details of welded rebars.

Welded rebars were therefore considered as a critical fatigue aspect. The fatigue resistance of the welded rebars is equal to 70 MPa, and their endurance limit is equal to 80% of the constant-amplitude fatigue limit, which is 56 MPa according to SIA 269 (2013). Influence lines of the welded rebar at the midspan were calculated using the 165 candidate model instances by applying the load model described in SIA 262 (2013) and SIA 269 (2013).

The maximum stress range was found to be equal to 12 MPa, which is four times less than the fatigue limit. The fatigue examination was therefore fulfilled, and no fatigue problem was detected for the welded rebars.

Influence lines of the welded rebar were calculated using parameter values obtained from RM by applying the same load model. The maximum stress range was found equal to 14 MPa, which is below the fatigue limit. RM solutions did not pass the validation test even though they led to the same conclusion of there being no fatigue problem. Therefore, predictions with RM were inaccurate and cannot be used for decision-making.

The welded rebars were assessed as safe using monitoring and model-based interpretations. The RC slab was therefore safe with respect to the fatigue limit even though it is not designed against fatigue. This examination adds to the growing body of evidence that most existing concrete bridges do not risk exceeding the fatigue limit under traffic loading, while they are not explicitly designed against fatigue [10]–[12]. Quantifying RC slab safety can enable better asset-management decision-making when, for example, loading increases, codes change or deterioration occurs.

4.6   Conclusions

The proposed methodology utilises monitoring data from many sources to develop accurate physics-based models for evaluating the fatigue of existing infrastructure. The following conclusions can be drawn from this study:

1. Prior to load testing, AE and NDT data estimates information related to material properties and structural behaviour and assist in the development of an accurate set of models to interpret measurements.
2. Using physics-based models and EDMF to interpret measurements enables the accurate identification of structural parameters and prognoses regarding the structural safety and performance evaluations of structural elements that cannot be directly instrumented.
3. Residual minimisation provides inaccurate structural identification and may not lead to conservative predictions due to inaccurate assumptions related to modelling uncertainty and bias.
4. For the Crêt de l'Anneau viaduct, stress ranges predicted for design loads are small, which indicates that fatigue limit is not exceeded. Hence, the bridge is safe with respect to the fatigue limit.
5. Using monitoring data, the bridge was assessed to be safe, despite potential variability between present conditions and the design condition of the structure. This assessment adds to the growing body of evidence that most civil infrastructures are safer than design requirements. Quantifying their safety can enable better asset-management decision-making.

Chapter 5 Quantification of Fatigue Microcracks in Reinforced-Concrete Bridge Deck Slabs using Acoustic Emission and Strain Measurements

Paper details

Chapter 5 contains a pre-print version of the paper "I. Bayane, E. Brühwiler (2021), Fatigue microcrack quantification in reinforced-concrete bridge deck slabs using acoustic emission and strain measurements" submitted to the journal article "Mechanical Systems and Signal Processing" in October 2020. Minor modifications are introduced in the text for adapting the paper to the thesis format.

Author contributions

The author of the thesis conducted the research and wrote the paper. Professor E. Brühwiler contributed by proofreading the paper and by providing overall supervision.

Overview

This paper presents a method to locate and visualise microcracks in concrete through the entire depth of an RC slab at an early stage of the fatigue process. 18 months of AE data was processed and localised in three-dimensions for four locations of the slab under operational loadings that are inducing compression, tensile and shear stresses. Microcrack activity in concrete volume was classified into stationary microcrack and microcrack growth and was quantified to identify existing fatigue damage and increases in fatigue damage over time.

Link to other chapters

With this chapter, the dissertation completes the analysis of different measurement methods and data interpretation approaches for fatigue evaluation of RC bridge-deck slabs. Thus, it relates largely to the conclusions and further work formulated in Chapter 6.

Paper IV

Quantification of Fatigue Microcracks in Reinforced-Concrete Bridge Deck Slabs using Acoustic Emission and Strain Measurements

Abstract

Reinforced-concrete structures subjected to cyclic fatigue loading may develop microcracks, which eventually lead to failure. A method is proposed to visualise and quantify fatigue microcracking in reinforced-concrete bridge-deck slabs using acoustic emission and strain measurements obtained from long-term monitoring. The method includes three steps: microcrack visualisation, axle number detection, and fatigue-damage quantification. Visualisation was conducted using small grids of acoustic emission sensors. Axle number detection was carried out by detecting peaks in the signal of strain measurements. New fatigue damage indices were therefore defined using localised acoustic emission events and the number of axles. The effectiveness of the method is demonstrated by a case study of an in-service reinforced-concrete bridge-deck slab. The results reveal that acoustic emission events are reliably localised in three dimensions when a small grid of sensors is used even though access is only possible from the lower slab side. The localised events indicate concrete cracking modes and microcrack distribution through the entire depth of the slab, and they are successfully used to quantify existing fatigue damage of concrete and increases in damage over time.

Keywords: Acoustic emission, bridge, monitoring, microcrack, reinforced concrete, three-dimensional location

5.1   Introduction

Fatigue cracking in concrete results from crack nucleation and propagation caused by cyclic loading, such as environmental and mechanical loadings that occur due to temperature, freeze-thaw cycles and traffic. Fatigue crack propagation results in a decrease of the rigidity and strength of concrete that can lead to a reduction in the strength and stiffness of the entire structure [125].

The fatigue process of concrete is generally defined by three stages from microcrack nucleation to failure [80], [126], [127]. The first stage is characterised by microcrack initiation and nucleation until reaching a stable state. The second stage is governed by the nucleation of new microcracks and stable microcrack extension. The third stage is governed by the accelerated growth and extension of cracks leading to failure.

Structural elements spend generally 80% of their service duration in Stage 2 [80], in which microcracks are in a stable state. Therefore, understanding microcrack growth and characteristics in this phase can provide time for implementing maintenance interventions and offering reliable information for decision-making. In Stage 2, internal changes are generally not detectable nor visible to the naked eye. Techniques are therefore required to investigate the microcracking activity of concrete at this stage.

Several types of sensors have been designed and used to examine microcracking in materials such as optical-based, magnetic-based, acoustic-based, and vibration-based sensors. Each sensor has its advantages and limitations. The main challenges arise from sensor placement and distance, and signal processing to detect and observe microcracking. One of the most used techniques for microcracking assessment is the acoustic emission (AE) technique.

The AE technique is a powerful technique for studying microcracking in concrete because the fracture process can be estimated in real-time using the three-dimensional (3D) localisations of AE sources, which was done for example by [128], who used AE technique to characterise the fracture-process zone of concrete beams under compression loading. However, this technique was not performed on-site, for fatigue microcracking, under environmental and traffic loadings, for which limitations arise from sensor placement, surrounding noise, and loading complexity.

The objective of the present work is to establish a robust method for visualising the microcracking of concrete on-site and quantifying microcrack growth under operational loadings. The method is based on combining information obtained from AE and strain measurements. It is illustrated with a case study of a reinforced-concrete (RC) deck slab of a bridge that has been in service for 60 years. Strain measurements were carried out for long-term monitoring of high-stress regions of the RC bridge-deck slab.

AE channels were used to instrument the lower side of the slab in four places. Channels were installed in grids of small areas around 40 cm² to increase the precision of the localisation. AE measurements were linked to strain measurements, which were used to calculate the number of axles and axle loads of passing vehicles. Temperature was also measured and linked to the AE system. The originality of this work includes the following:

- Overcome limitations in indirectly observing internal microcracks in concrete on-site.

- Monitor microcrack friction, nucleation, and extension in concrete under operational loading.
- Develop a data-interpretation method to differentiate between microcrack movement and microcrack growth in concrete.
- Identify and quantify existing fatigue damage in an RC bridge-deck slab.
- Identify and quantify the rate of microcrack growth on-site.

5.2 Methodology

5.2.1 Case Study and Monitoring System

The case study is on a steel-concrete composite bridge located in Switzerland. The viaduct was built in 1957 with one-lane traffic in each direction and has a legal limit load of 400 kN. The viaduct has a total length of 195 m with eight spans. Spans are supported by columns in steel and connected by Gerber articulations. Each span is comprised of an RC slab of a thickness varying from 0.17 to 0.24 m supported by two 1.3 m height steel girders. The slabs contain orthogonal grids of steel reinforcement bars in the upper and lower zones serving for the double bending behaviour in the transverse and longitudinal directions. Figure 5.1 (a, b) schematically shows the bridge along with the investigated Span 4.

The viaduct was instrumented with strain gauges, thermocouples, and the AE technique. The data acquisition system of strain gauges and thermocouples is related to the AE acquisition system as input parameters, through which strain, temperature, and AE hits can be visualised on the same time scale. In Figure 5.1 (c, d), the instrumented span is shown with the sensors. More details about the instrumentation and the monitoring system can be found in Chapter 3.

Continuous monitoring was conducted under environmental and traffic loading; thus 18 months of data were recorded and analysed for the period of monitoring: 03/2019 – 08/2020. Data obtained from strain gauges in the transverse and longitudinal rebars at the midspan were used for axle load identification, while data obtained from the 24 AE channels were used to identify and visualise concrete microcracking.

The AE channels were mounted on each grid configuration to capture the AE events inside the RC slab. The grids are comprised of four channels or more and had diameters less than 50 cm to increase the probability of detecting longitudinal waves that travel the volume of the slab, to avoid signal attenuation, and to detect enough hits for 3D location. The AE channels were installed in four grids. One grid was installed at the midspan, one at the midlane, one near the support and one between the support and articulation.

Grid 1 is a circular grid with a diameter of 0.34 m and is comprised of six channels (Channel 5, 6, 7, 17, 21, and 22) installed at the midspan (Figure 5.1 [d, G1]).

Grid 2 is comprised of nine channels (Channel 8, 9, 10, 11, 12, 18, 19, 20, and 24) in a square grid of 0.24~0.25 m installed at the midlane, 1.35 m away from the steel box girder (Figure 5.1 [d, G2]).

Grid 3 is a circular grid with a diameter of 0.2 m and is comprised of four channels (Channels 13, 14, 15, and 16) installed near the support, 1.57 m away from the girder and 2.7 m away from the support (Figure 5.1 [d, G3]).

Grid 4 is a circular grid with a diameter of 0.28 m, and is comprised of five channels (Channels 1, 2, 3, 4, and 23) installed between the support and articulation 1.65 m away from the girder and 1.5 m away from the support (Figure 5.1 [d, G4]).
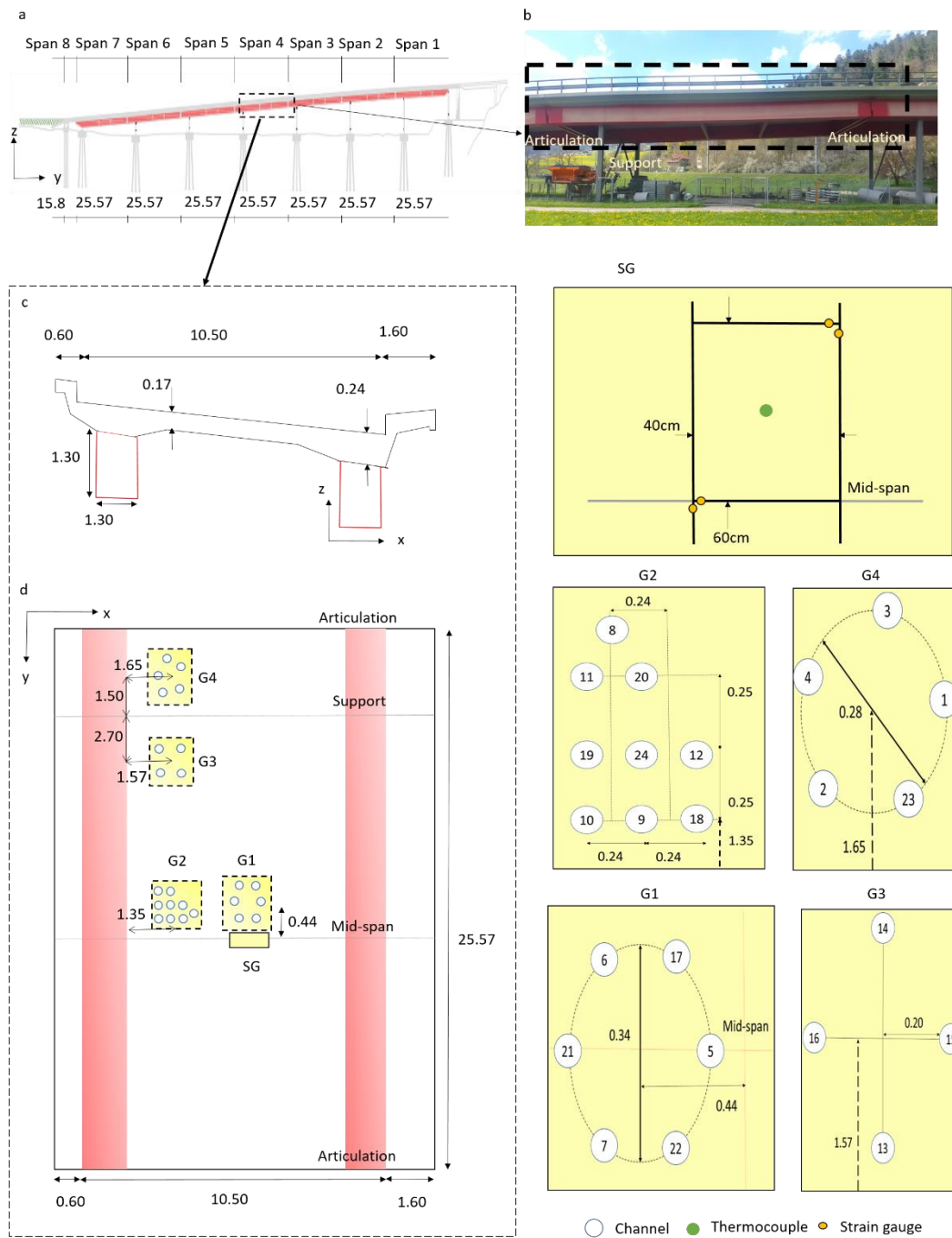
Figure 5.1. Presentation of the bridge and sensor deployment: elevation side (a); Span 4 (b); cross-section of Span 4 (c); bottom view of Span 4 (d); sensor deployment (SG, G1, G2, G3, and G4); dimensions in [m].

5.2.2 Traffic Identification

During the passage of a vehicle, transverse rebars are loaded in tensile, while longitudinal rebars are loaded in both compression and tensile with the presence of reversal stresses. Subsequently, the passage of a vehicle generates one peak in transverse rebars and as many peaks as axle number in longitudinal rebars. For example, in Figure 5.2, the passage of a truck of 400 kN with five axles generated one peak in transverse strain and five peaks in longitudinal strain, which were recorded by strain gauges glued on transverse and longitudinal rebars at the midspan, respectively (Figure 5.1 [SG]).
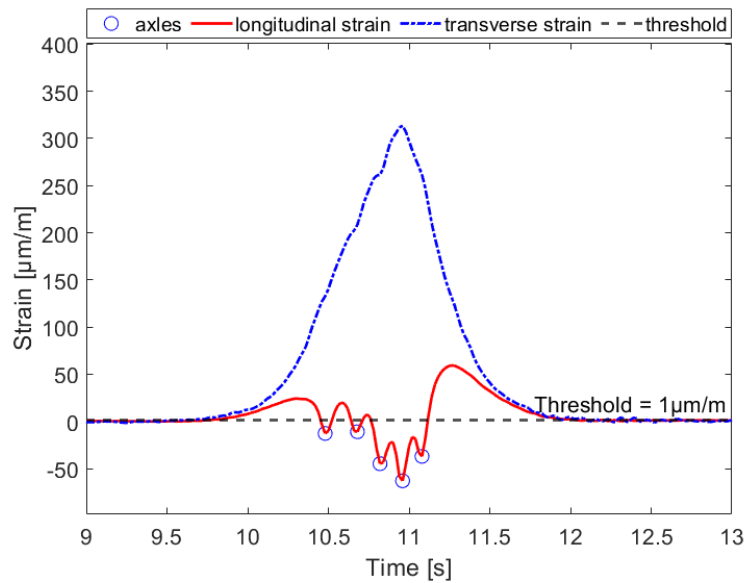
Figure 5.2. Detected axles from strain measurements during the passage of a five-axle truck with a speed of 35 km/h.

A POT approach was used to define peaks in strain measurements of transverse and longitudinal strain responses in order to detect vehicles and calculate the number of axles. The function 'findpeaks' in MATLAB was used to detect peaks. Peaks considered minimum were those above 1µm/m, which is the error of strain gauge measurements, and the minimum time between two successive peaks was set to 3 s, which is the estimated time for the passage of an axle. These defined peak filters eliminate noise and light vehicles that are not relevant for fatigue damage. Peaks were extracted accordingly from strain measurements so that the number of axles could be identified for each vehicle. Moreover, the load and the position of vehicles are calculated based on the inverse method detailed in Chapter 2.

5.2.3 Three-Dimensional Location

Usually, sensor installation on bridge-deck slabs was possible for reasons of accessibility only from the lower side of the slab where all sensors are arranged in the same plane. The detected AE events are therefore planar events in which all the detected hits were on sensors in the same plane. Consequently, it was difficult to determine the distance from the plane and to distinguish sources in

the positive direction from those in the negative direction. For example, if a 3D linear event showed a result that is +1 from the line of sensors, then -1 is an equally valid answer.

For RC slabs, the events were presumed to all be in the direction of slab thickness since no AE activity is assumed detectable in the air, and the wave velocity used for localisation was calculated with particular care. The velocity of longitudinal waves that propagate inside the volume was calculated using pencil-lead break simulations that were repeated to clearly distinguish longitudinal and shear waves in the recorded events. The velocity of longitudinal waves was found equal to 3'400 m/s. Details about velocity calculation can be found in Sections 3.5.1, 4.2.2, and 4.3.2.

AE events were located using the AEwin program, which is a commercial software for real-time "simultaneous" AE feature and waveform processing. Visualisation and interpretation of the localised events were carried out using MATLAB. The theoretical background of the 3D location basis used in AEwin is summarised below [76]. The fundamental basis is the time-distance relationship implied by distance d, time t, and stress wave velocity v expressed in Equation (5.1).

$$d = v * t \qquad (5.1)$$

The distance between two points depends on the geometry of the deployed sensors. For two points on a flat plane, point 1 (P_1) and the source (P_S) as shown in Figure 5.3, the distance equation d_1 is the Pythagorean theorem expressed in Cartesian coordinates $P_1(x_1, y_1, z_1)$ and $P_S(x_s, y_s, z_s)$:

$$d_1 = \sqrt{(x_1 - x_s)^2 + (y_1 - y_s)^2 + (z_1 - z_s)^2} \qquad (5.2)$$
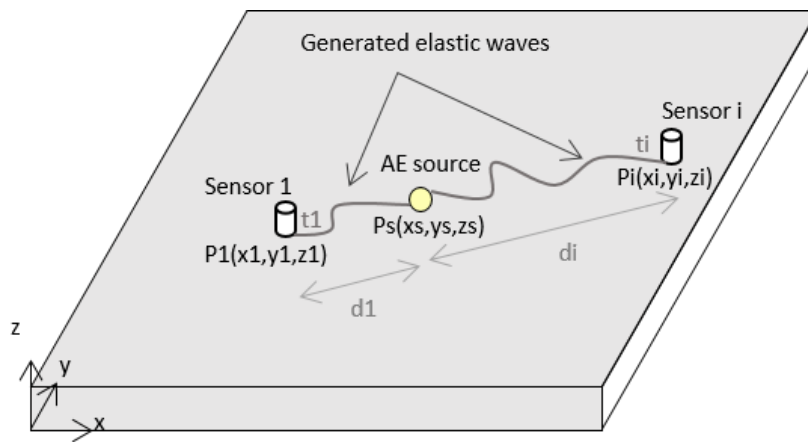
Figure 5.3. Principle of acoustic emission source localisation in a reinforced-concrete slab.

Time t is considered relative to the first hit in the event. Time difference Δt_i between the first hit sensor and the ith hit sensor is written as

$$\Delta t_i = t_i - t_1 \tag{5.3}$$

and according to Equations (5.1)-(5.2), time difference can be also written as

$$\Delta t_i = (\sqrt{(x_i - x_s)^2 + (y_i - y_s)^2 + (z_i - z_s)^2} \\ - \sqrt{(x_1 - x_s)^2 + (y_1 - y_s)^2 + (z_1 - z_s)^2})/v \tag{5.4}$$

Using the known arrival times of the hits, Equation (5.5) is used to calculate the observed time difference $\Delta t_{i,obs}$

$$\Delta t_{i,obs} = t_i - t_1 \tag{5.5}$$

For a given set of source localisation coordinates, Equation (5.6) defines the calculated time difference, $\Delta t_{i,calc}$:

$$\Delta t_{i,calc} = (\sqrt{(x_i - x_s)^2 + (y_i - y_s)^2 + (z_i - z_s)^2} - \sqrt{(x_1 - x_s)^2 + (y_1 - y_s)^2 + (z_1 - z_s)^2})/v \tag{5.6}$$

Multiple regression analysis was used to minimise the difference between the observed and calculated time differences. Therefore, a chi-square χ^2 was calculated across all channels that detect AE events according to Equation (5.7).

$$\chi^2 = \sum (\Delta t_{i,obs} - \Delta t_{i,calc})^2 \tag{5.7}$$

The quantity is dependent on the source coordinates. The sum was calculated for each potential source location. The localisation code searches for the values x_s, y_s, and z_s of the source that minimise the value of χ^2. The process is an iterative search, which was carried out using the Simplex search algorithm.

The elastic wave velocity used to perform calculations for AE event localisation was measured during system calibration and assumed constant. The variability of elastic wave velocity due to

environmental changes and uncertainties related to velocity measurements was addressed by performing 3D location using two velocities, 3'000 m/s and 3'400 m/s. The results show that the number of detected events varies slightly but that the pattern of the localised events remains the same. Calculations were therefore made using the constant wave velocity of 3'400 m/s.

5.2.4   Concrete Microcracking

Concrete cracking in structures under service loading is different from concrete cracking observed in laboratory tests in which high loads are applied. Laboratory test loadings are often higher than 50% of the compressive strength, which induces cracks in concrete in a way that is different from service loadings, which are usually significantly less than 50% of the compressive strength, resulting in a stable movement of existing microcracks. During the instrumentation of AE channels, no cracks were observed at the surface of the concrete. This research therefore focuses on concrete microcracking.

Concrete microcracks have openings smaller than 100 µm/m, and they cannot be seen by the naked eye. They are captured indirectly by AE events. Microcracks already appear during concrete hardening at a very early stage due to shrinkage and thermal contraction. In addition, tensile stresses are created depending on the restrained support conditions of the structure. These stresses may reach the tensile strength within the fracture process zone of concrete, which is the transitional regime from a continuum to a real crack (stress-free). Microcracks are finally created at the interface between the cement matrix and the aggregate and between the cement matrix and rebars under first service loadings [129].

A distinction is therefore made between 1) existing microcracks that are in Modes I, II, and III, i.e., opening and closing, and in friction under service loadings whose size remains constant, and 2) microcracks that are growing in the concrete volume. The first type is categorised as stationary microcracks, and the second one is categorised as microcrack growth, as it is illustrated in Figure 5.4.
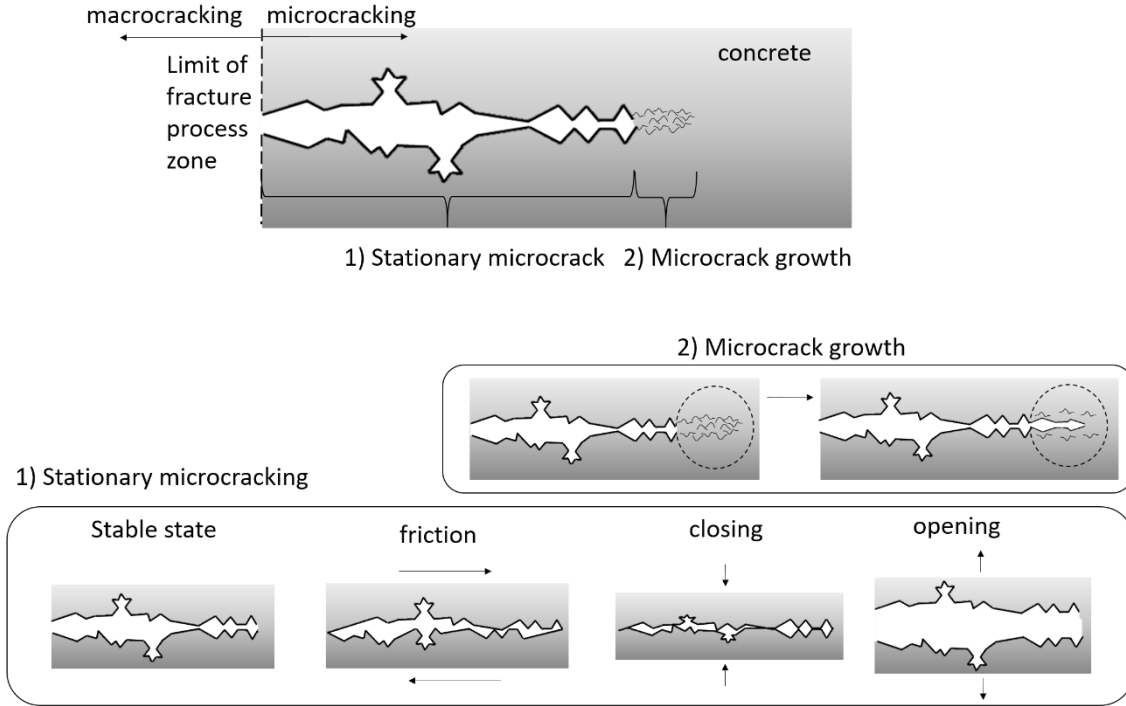
Figure 5.4. Process of concrete microcracking.

5.2.5   Energy Analysis

The absolute energy (ABSenergy) of AE events is used to differentiate between stationary microcrack and microcrack growth in the concrete of the instrumented RC slab. It is defined according to Equation (5.8).

$$ABSenergy = \frac{1}{10} \int V(t)^2 dt \qquad (5.8)$$

where

V is the signal voltage at the AE channel divided by 10 kΩ before any amplification expressed in volts [V], and t is the time. $ABSenergy$ is the absolute energy expressed in attojoules ($=10^{-18}$ J) [aJ] [76]. Absolute energy is calculated from the recorded stress waves using the AEwin program and MATLAB.

Microcracking characteristics of concrete were analysed by [128] and, [130], who have successfully identified the evolution of the fracture process zone for RC notched beams under three-point bending and for different concrete notched specimens under tensile loading through 3D location and an energy

analysis of AE events. It was found that the nucleation and friction of concrete microcracks are accompanied by an energy release in which an amount of energy is in the form of elastic waves that can be captured using the AE technique, particularly by the ABSenergy of AE events. Moreover, Bunnori et al. proposed that an ABSenergy above 10^6 aJ can be used to indicate the onset of microcrack growth in RC beams [91].

Thus, ABSenergy was used to characterise microcracking in the concrete volume through 3D location of AE events under operational loading. Events with an ABSenergy higher than 10^6 aJ were considered caused by microcrack growth, while events with lower energy were considered caused by stationary microcracks.

5.2.6   Frequency Analysis

Frequency features of AE signals provide information on concrete state, such as information on friction among existing cracks and inhomogeneities distributed in the concrete or mortar volume [131], [132]. Peak frequency is one of the most used frequency features of AE signal to characterise inhomogeneities in concrete such as microcracks. Peak frequency decreases with the progress of microcracks, and it can provide the degree of microcracking such as the difference between microcrack friction and growth.

Peak frequency refers to the point where the power spectrum of the recorded stress waves is greatest [76]. It was calculated from the recorded stress waves using the AEwin program and MATLAB. The evolution of peak frequency under operational loading was analysed using the response of the 24 AE channels. The variation of ABSenergy plotted against peak frequency is shown in Figure 5.5 for the period of monitoring 03/2019 – 08/2020.
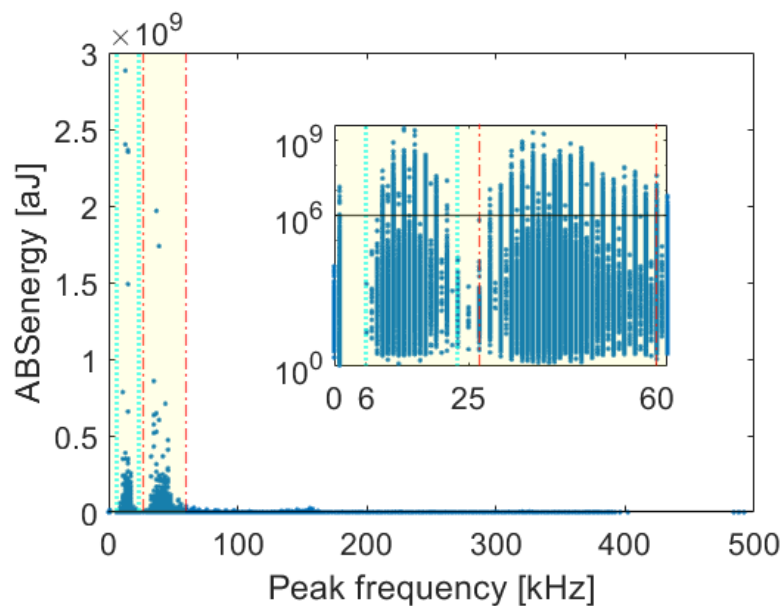
Figure 5.5. Absolute energy (ABSenergy) versus peak frequency for recorded hits of 24 acoustic emission channels during 18 months of continuous monitoring.

Peak frequency varied in the range of [0, 500] kHz for ABSenergy in the range of 1 to 3.10^9 aJ where AE hits included in the peak-frequency bands of [6, 23] kHz and [27, 60] kHz are characterised with the highest values of ABSenergy. The frequency bands are shown in Figure 5.5 with dashed vertical lines, and the energy limit of 10^6 aJ is shown with a horizontal continuous line.

The first high-energy frequency-band of [6, 23] kHz and the low-energy frequency band of [6, 60] kHz were assumed to be due to stationary microcrack, while the second high-energy frequency-band of [27, 60] kHz was assumed to indicate microcrack growth. These assumptions were made with respect to the laboratory test findings of [65] and [91]. They found that an ABSenergy higher than 10^6 aJ was caused by concrete microcrack growth, the frequency band of [45, 64] kHz was caused by microcracking in concrete, and the frequency band of [22, 32] kHz was caused by the friction and the closing of existing microcracks.

5.3 Results

AE hits recorded during 18 months of continuous monitoring from 03/2019 to 08/2020 were localised for the 24 channels. There were 59'813'676 recorded hits in which 1'773'280 events were detected and localised. The results are shown in Figure 5.6 – Figure 5.9, for Grids 1, 2, 3, and 4, respectively.

5.3.1 Grid 1

The AE events in Grid 1 were localised in three dimensions by means of six channels. Details about channel deployment and the location of Grid 1 can be found in Figure 5.1. A total of 8'147'829 hits were recorded, and 145'338 events were localised. The localised events with their ABSenergy values are presented in Figure 5.6. The cross-section, the transverse neutral axis, and the tensile rebars are also illustrated for ease of understanding.

Figure 5.6. Three-dimensional visualisation of acoustic emission (AE) events localised in Grid 1 coloured according to their absolute energy (ABSenergy) expressed in [aJ].

Ninety-nine percent of the events had an energy less than 10^6 aJ with a mean peak frequency of 48 kHz, suggesting that the microcracking activity in concrete at the midspan under traffic and temperature is dominated by stationary microcracking, as defined in Section 5.2.6.

Grid 1 is positioned at the midspan where stress is pure transverse bending so that the upper part with respect to the neutral axis is in pure compression and the lower part is in pure tensile, which explains the recurrent AE events in the tensile zone generated by existing microcracks.

Furthermore, 6% of the detected events were in the compression zone, of which six events had a high ABSenergy (i.e., they have an ABSenergy higher than 10^6 aJ), which indicates that concrete in the compression zone is not damaged under fatigue loading even with the presence of reversal stresses. In fact, in the longitudinal direction, concrete is loaded in compression with the presence of reversal

stresses (i.e., the presence of both compression and tensile) during the passage of vehicles as shown in Figure 5.3.

5.3.2   Grid 2

A total of 815'264 events were localised from 24'706'326 hits recorded by the nine AE channels of Grid 2. Details about Grid 2 position can be found in Figure 5.1. The localised events are illustrated in Figure 5.7 where events with an energy level higher than 10^6 aJ are indicated separately. Furthermore, the position of Grid 2 is illustrated with the neutral axis of the cross-section and tensile rebars.
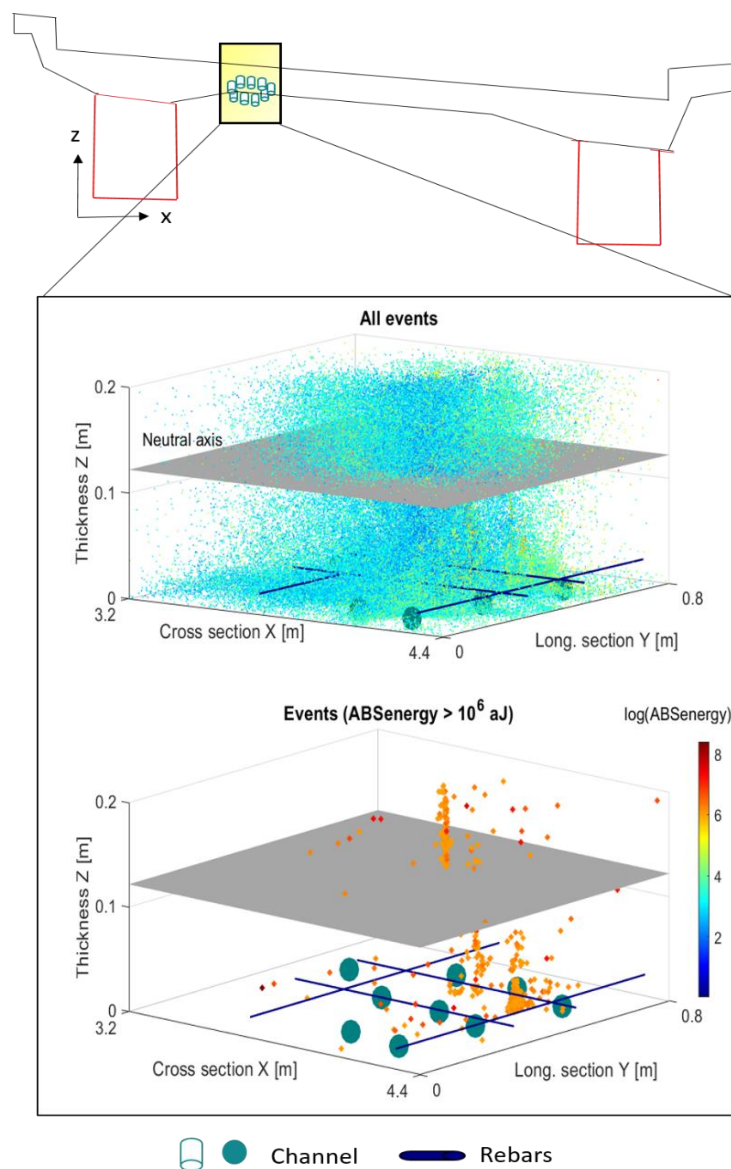
Figure 5.7. Three-dimensional visualisation of acoustic emission (AE) events localised in Grid 2, with all events and high-energy events coloured according to their absolute energy (ABSenergy).

Ninety-nine percent of the localised events had an energy less than 10^6 aJ, and their mean peak frequency was 55 kHz. Among these events, 5% were in the compression zone and 95% were in the

tensile zone. According to the assumptions made in Section 5.2.6, this indicates that microcracking activity of concrete is mostly stationary.

Grid 2 is situated in the midlane of the midspan where concrete is under both bending and shear transverse stresses. This location demonstrates the existence of the pronounced stationary microcracks in the tensile zone mainly due to both tensile and shear microcracks. Furthermore, concrete is under compression stresses in the longitudinal direction with the presence of reversal stresses during the passage of vehicles (Figure 5.3), which explains the existence of AE events in the compression zone and more particularly events with a high ABSenergy (i.e., those with an ABSenergy higher than 10^6 aJ). The high-energy events form a cluster parallel to the direction of loading (Figure 5.7, bottom), which indicates the creation of tensile and compression microcracks due to stress reversals. These events were infrequent; only 336 events were detected during the 18 months of monitoring, which represents less than 1% of all localised events. This finding suggest there is very slow increase in fatigue damage in concrete under operational loading.

5.3.3   Grid 3

Figure 5.8 includes AE events localised by the four channels of Grid 3. The cross-section, tensile rebars, and the neutral axis are also illustrated. There were 83'587 events localised from 8'095'480 detected hits, in which 96% were in the tensile zone and 4% were in the compression zone.
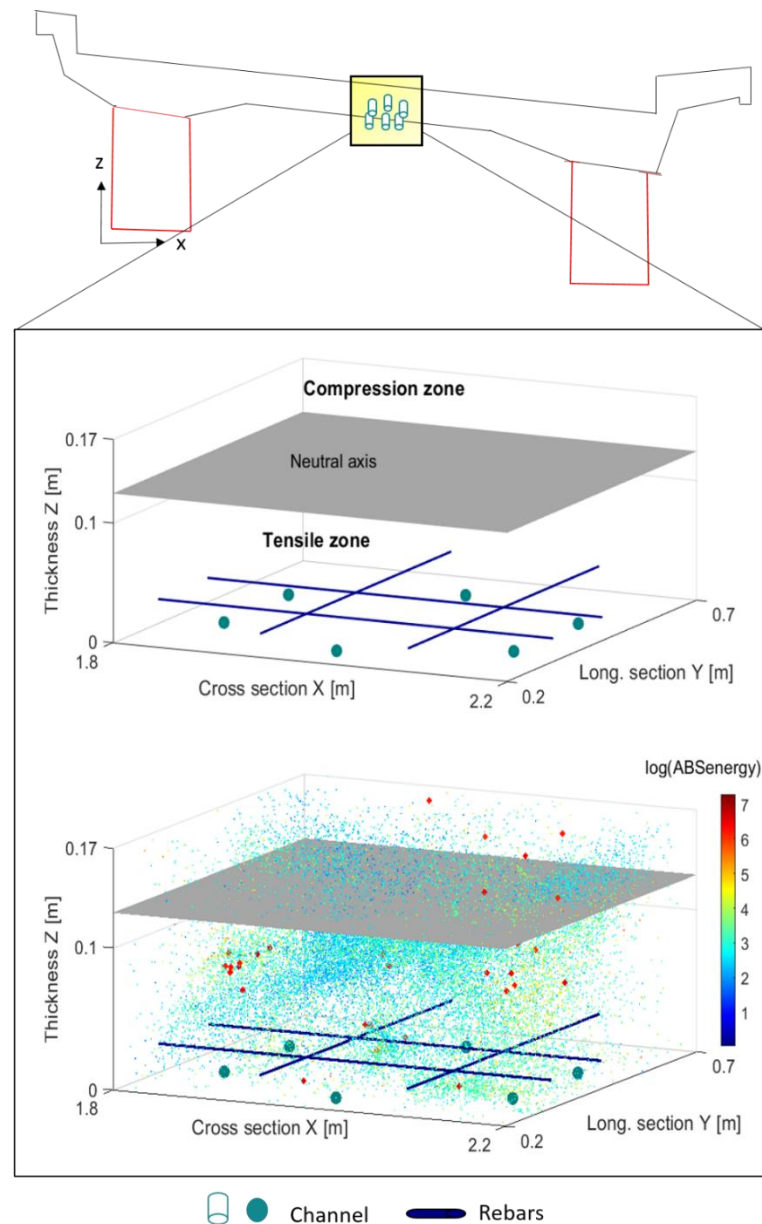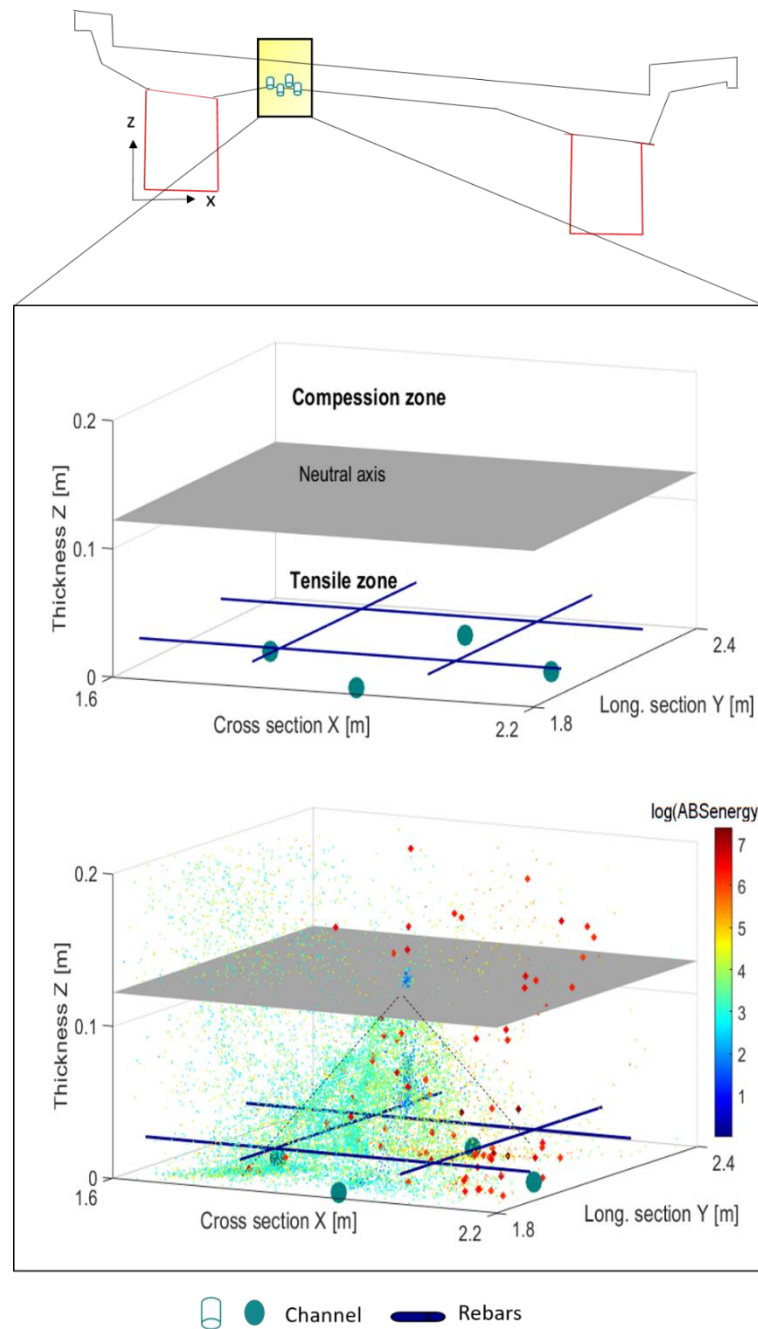
Figure 5.8. Three-dimensional visualisation of acoustic emission (AE) events localised in Grid 3 coloured according to their absolute energy (ABSenergy).

In the longitudinal direction, Grid 3 is positioned in the negative moment region, near the point where the bending moment is null, which creates low tensile and shear stresses in concrete with the presence of stress reversals during the passage of vehicles. In the transverse direction, Grid 3 is positioned near the connection between the slab and the girder, in which concrete is loaded in both shear and bending, which explains the pronounced shear mode in the tensile zone.

Ninety-nine percent of events had an energy less than 10^6 aJ, which indicates the dominance of stationary movement of existing microcracks. Furthermore, the pattern of localised events forming

an angle of 45 degrees in the tensile zone, shown with dashed lines in Figure 5.8, indicates the existence of microcracks that are opening and closing in the shear mode due to traffic loading. Events in the compression zone represent 4% of the detected events and do not form any cluster. Concrete is not damaged under longitudinal-negative moment action and with the presence of reversal stresses.

5.3.4   Grid 4

In Grid 4, a total of 408'324 AE events were localised from 18'864'041 hits. Among these events, 96% were in the tensile zone and 4% were in the compression zone, as illustrated in Figure 5.9.
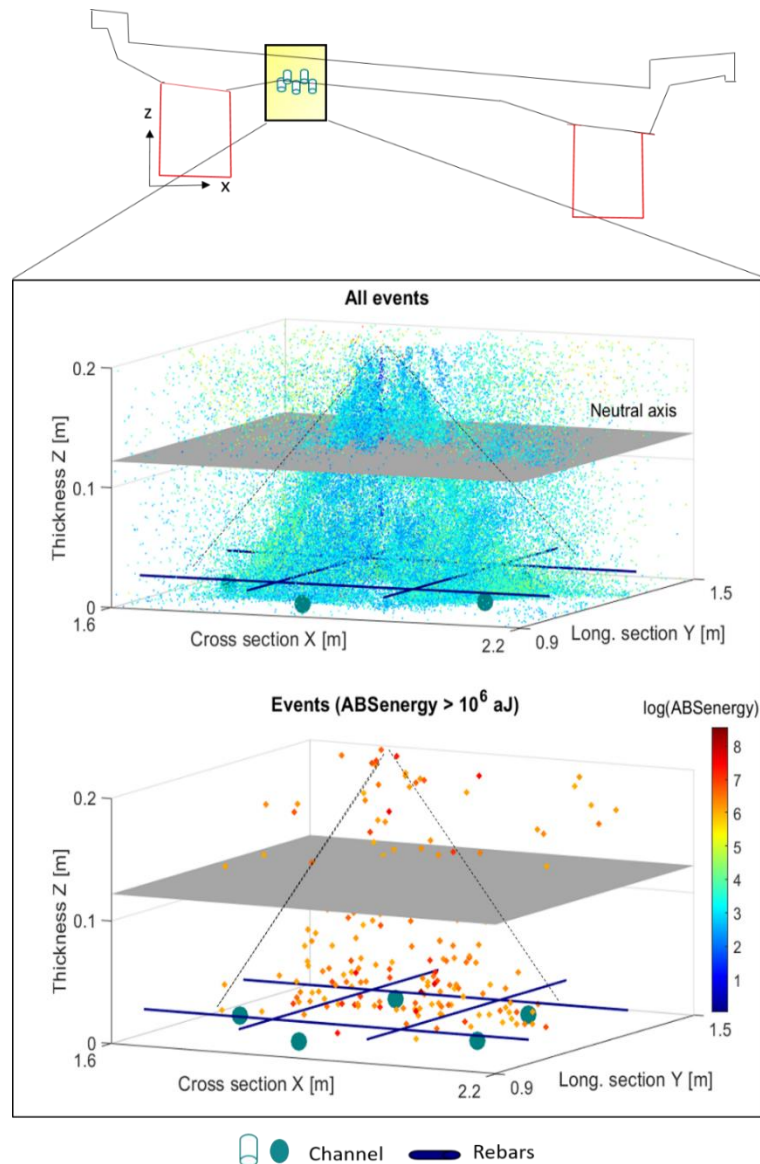

Figure 5.9. Three-dimensional visualisation of acoustic emission (AE) events localised in Grid 4, with all events and high-energy events coloured according to their absolute energy (ABSenergy).

Grid 4 is 1.5 m away from the support where the negative bending moment is acting. Concrete is subsequently under tensile and shear stresses, with the presence of both compression and tensile

during the passage of vehicles (Figure 5.3). Furthermore, Grid 4 is near the connection between the slab and the girder where significant shear stress is generated along with bending due to traffic loading. The shear mode is therefore expected to occur in both the tensile and compression zones.

A pattern of localised events forming an angle of 45 degrees through the compression and tensile zones was again identified; the angle is illustrated with dashed lines in Figure 5.9. The AE events with an energy level less than 10^6 aJ represent 99% of all events. This prevalence indicates stationary movement of existing microcracks under operational loading. Events with high energy (i.e., those with energy higher than 10^6 aJ), present only 1% of the localised events, which mainly occurred due to microcrack growth following the same shear pattern.

5.3.5   Discussion

The fact that more than 94% of all events were in the tensile zone for the four grids reveals microcracking that is produced when stress due to fatigue loading reaches fracture strength within the concrete volume. Subsequent weakening of concrete entails further stress transfer from concrete to steel rebars. Microcrack formation due to fatigue loading occurs during the first significant operational loading, and these microcracks eventually propagate under fatigue loading.

The monitoring configuration allows for the 3D visualisation of AE events, capturing changes in concrete at the microscale level. This possibility was previously limited to laboratory tests that could not create the same service-loading conditions. Visualisation of microcracking activity of concrete on-site provides information about concrete behaviour under low fatigue stress, and about stationary microcracks and microcrack growth that are detected under operational loading.

Stationary microcracking is generally confirmed to be the most frequent microcracking activity of concrete under low fatigue stress. The increase in concrete damage caused by microcrack growth is negligible, and it is thus irrelevant from the viewpoint of the fatigue safety of the bridge-deck slab. This point confirms that no fatigue problem exists in the RC bridge-deck slab, and adds evidence that there is no fatigue problem in the concrete of most RC structures.

Criteria were defined to differentiate between stationary microcracks and microcrack growth based on the ABSenergy and the peak frequency of AE events. However, several ambiguities remain regarding the assumptions made in Section 5.3.2, which are based on the results of two research studies. Additional laboratory tests that combine both the 3D-visualisation of AE events and the X-ray visualisation of internal changes of different mixes of concrete under different loading conditions are required to define energy and frequency thresholds between the stationary movement of existing microcracks and microcrack growth.

5.3.6   Fatigue Damage Quantification

Fatigue damage of the RC bridge-deck slab was evaluated by investigating both steel rebars and concrete. The fatigue of steel rebars was evaluated using recorded strains that were converted into stresses using the steel modulus of elasticity of 210'000 MPa. Rainflow counting was used to calculate stress cycles from stress variation over three years of monitoring (from 07/2016 to 08/2020).

Figure 5.10 shows the histogram of stress ranges of the transverse rebar at the midspan, which is the rebar with the highest stress range. The commonly assumed fatigue endurance limit of $\Delta\sigma_{s,D} = 120$ MPa defined by [38] is shown with a dashed line.
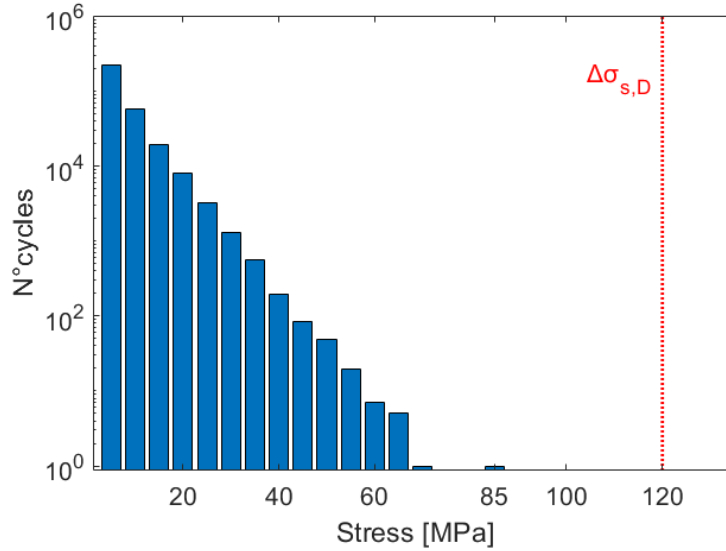
Figure 5.10. Stress range of the transverse rebar at the midspan of Span 4 during the period of monitoring 07/2016-07/2020.

The maximum stress range of 85 MPa is much lower than the endurance limit $\Delta\sigma_{s,D}$, which indicates no fatigue-damage process in the rebars. More details about the fatigue evaluation of reinforcement bars can be found in [124], and [133]. Fatigue of the RC deck slab was subsequently evaluated by investigating the condition of concrete under operational loading.

The acoustic events were analysed according to their source and nature to determine fatigue damage in concrete due to microcracking under cyclic loading. AE energy and frequency were used to distinguish between events caused by the movement of existing microcracks and those caused by microcrack growth. Moreover, events produced in the tensile zone of the concrete were differentiated from those produced in the compression zone via the position of the neutral axis.

The existing microcracks in stationary movement under fatigue loading were used to define the existing damage to the concrete, while events indicating microcrack growth were used to define increases in damage over time.

Existing fatigue damage d_1 was defined as the ratio between events in the compression zone and events in the tensile zone, as shown in Equation (5.9).

$$d_1 = \frac{N°events\ in\ compression\ zone/volume\ in\ compression}{N°events\ in\ tensile\ zone/volume\ in\ tensile} \tag{5.9}$$

Fatigue damage increase d_2 was defined as the ratio of the number of AE events indicating microcrack growth for a given volume of concrete per the number of axles that describes the number of loading cycles, as shown in Equation (5.10).

$$d_2 = \frac{N°dynamic\ cracking\ events/volume}{N°axles} \tag{5.10}$$

Damage indices d_1 and d_2 were calculated for the four grids of AE channels, and results are shown in Table 5.1.

Table 5.1. Fatigue damage of concrete for each Grid of AE channels

	d_1 Existing damage (60 years of service)	d_2 Damage increase /month
Grid 1	0.17	$9.90\ 10^{-4}$
Grid 2	0.08	$7.52\ 10^{-4}$
Grid 3	0.06	$2.60\ 10^{-4}$
Grid 4	0.06	$1.22\ 10^{-3}$

Existing damage d_1 is higher for Grid 1, doubly exceeding the existing damage for other grids. This is expected with Grid 1, as it is at the midspan where maximum bending moment occurs. Existing damage is similar for Grids 2, 3, and 4, as concrete is under similar transverse stresses. The existing amount of accumulated damage over the 60 years of the bridge's service is small, with no significant increase, which demonstrates that its concrete is still in the early phase of the second stage of the fatigue process and it is far away from a damage index d_1 equal to 1. A damage index d_1 equal to 1 means that events in compression and tensile zones are equally distributed, which may indicate fatigue damage in the third stage of the fatigue process where macrocracks are forming and propagating, leading to fatigue failure.

Damage increase d_2 is in the range of 10^{-4} to 2.10^{-3}. It is higher for Grid 4, where concrete is under negative moment action. It is lower for Grid 3 near the zone where the longitudinal bending moment is null, and it is almost the same for Grids 1 and 2, where the longitudinal bending moment is similar. Damage increase d_2 is small for all grids. It is much less than 1, which indicates that AE events with high ABSenergy are infrequent with vehicle passages. This demonstrates that increases in damage in the RC slab progress very slowly under operational loading. When AE events with high energy become more frequent with each vehicle passage in both compression and tensile zones, this indicates that a fully cracked RC section is nearly reached and stiffness of the RC element is greatly reduced. The increase in damage observed by the four grids is therefore related to the second stage of the fatigue process.

Figure 5.11 shows the existing fatigue damage and the increase in damage of the RC slab at the midspan, with theoretical fatigue failure being illustrated by the horizontal dashed line.
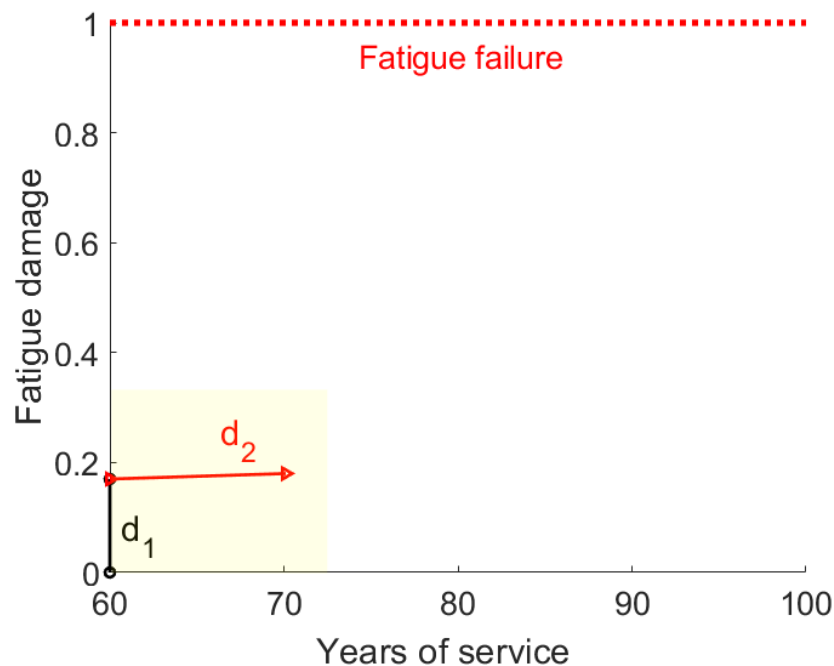
Figure 5.11. Existing fatigue damage and damage increase for concrete at the midspan.

It can be concluded that, after more than 60 years of service, the existing amount of damage of the concrete is small, and increases in damage progress slowly under the actual operational loading, which demonstrates that there is no fatigue safety issue for the concrete of the RC slab.

5.4   Conclusions

Acoustic emission events were localised and visualised to evaluate microcracking activity in the concrete of an RC bridge-deck slab subjected to fatigue loading under road traffic. Results were obtained via long-term monitoring campaign, and from them the following conclusions are derived:

1. An original monitoring approach for the investigation of microcracking activity of concrete has been presented and validated by means of a case study. This approach combines AE with strain measurements to efficiently investigate concrete microcracking under low fatigue stresses.
2. A small grid configuration for AE channel's instrumentation has been introduced and validated by means of four applications. This configuration has significantly improved the 3D location of microcracks in concrete under operational loading, enabling microcracking modes and microcrack distributions to be visualised.
3. ABSenergy and peak frequency of localised AE events have been established to determine the nature of microcracking activity in concrete. Events with an ABSenergy higher than 10^6 aJ in the frequency range of [27, 60] kHz may result from microcrack growth, and other events in the frequency range of [6, 60] kHz may be due to stationary microcracking.

4. The existing fatigue damage of RC bridge-deck slabs has been identified using secondary AE activity and validated by a case study in which concrete was found to be in the early phase of the second stage of the fatigue process. Ultimately, the highest fatigue damage was found at the midspan, where the bending moment is at its maximum.

5. An increase in the fatigue damage of the RC bridge-deck slab under low fatigue stress has been validated through a case study. This increase was found to be slow under bending and shear stresses that are due to operational loading and to be more pronounced in the region where high negative moments act.

6. The investigation of concrete microcracking under operational loading conducted through the presented case study shows that the fatigue damage in the concrete of the RC bridge-deck slab is very low, and that no significant fatigue safety issue exists.

Chapter 6 Conclusion

6.1 Overview

In this thesis, a complete strain-acoustic-emission (AE) monitoring method was developed to assess the condition of reinforced-concrete (RC) bridge-deck slabs of bridges subjected to fatigue loading. The method was implemented in a case study where an in-service 60-year-old road bridge was continuously monitored for more than one year. The method moreover allows one to formulate recommendations for instrumentation, calibration, data processing, and interpretation, which are still undeveloped in previous research. This chapter presents the main conclusions of the four main sections of the thesis and provides recommendations for future work. The conclusions answer the main objectives of the thesis formulated in Chapter 1. The key findings are synthesised using five main headings.

a) A monitoring approach involving data interpretation for fatigue safety examination.
b) Model-based data interpretation for evaluating the fatigue behaviour of noninstrumented locations.
c) A vision-based approach for investigating concrete microcracking under varying traffic and temperature conditions.
d) Newly identified data that are relevant to the fatigue of RC slabs under operational loading.
e) Recommendations for taking on-site measurements and ensuring long-term monitoring of in-service bridges with the aim to quantify their remaining fatigue life.

6.2 Synthesis of Key Findings

a) A monitoring approach involving data interpretation for fatigue safety examination.

New methods for interpreting acoustic emission and strain measurements were developed and improved upon in this dissertation regarding fatigue examination of road bridges.

- Integrating AE and strain measurement produces reliable information that was found to improve data interpretation. The recorded AE hits were associated with the generated strains in rebars, this association allows the possibility to indirectly explore internal changes in concrete due to traffic and temperature conditions.
- An inverse method was developed to estimate the load, position and number of axles of vehicles from strain and load-test measurements. This method was found to be useful for identifying the critical parameters of fatigue damage and for evaluating fatigue behaviour under different traffic scenarios.
- Clustering AE measurements obtained near structural connections helps in evaluating structural characteristics such as the condition of the support and articulation and the condition of the connection between the slab and the girder, which is useful for evaluating various components of road bridges over time.

b) Model-based data interpretation for evaluating the fatigue behaviour of noninstrumented locations.

A new approach for improving the model development of bridges based on monitoring data was proposed for evaluating the fatigue of nonaccessible parts of RC slabs.

- Implementing the results of the inverse method in structural-analysis models allows studying the extent of fatigue damage and identifying the associated uncertainties related to the compressive strength of concrete, levels of stress, and the magnitude of annual traffic.
- When AE measurements are used to assist the development of structural analysis models, critical parameter values are accurately identified. The method estimates information related to structural characteristics using measurements and considers related uncertainties, which provides accurate predictions of the fatigue behaviour of the parts that are not accessible to monitoring.
- Complementary information is obtained when using monitoring data to assist the development of structural analysis models and when interpreting monitoring data by means of accurate structural analysis models. The results demonstrate the accurate fatigue behaviour of noninstrumented parts and indicate that the bridge's structural elements are safe with respect to their fatigue limit, despite the difference between the structure's present and original design conditions.

c) A vision-based approach for investigating concrete microcracking under varying traffic and temperature conditions.

A new approach was proposed to improve the localisation of acoustic emission events and to visualise microcracks inside the concrete of an RC bridge-deck slab under in-situ fatigue loading.

- Visualisation of microcracks through the entire depth of RC slabs under traffic and temperature conditions is possible using small grids of more than four AE sensors, despite the planar configuration.
- The absolute energy and peak frequency of AE hits were found to be sensitive to the concrete microcracking process. Events with an energy higher than 10^6 aJ in the frequency range of [27, 60] kHz are considered to be caused by microcrack growth.
- Two types of microcracking were identified in the concrete volume through microcrack visualisation. Stationary microcrack occurs where the existing microcracks are opening, closing, and in friction without a change in their initial size, and microcrack growth is present with the nucleation of new microcracks and the propagation of existing microcracks.

d) Newly identified data that are relevant to the fatigue of RC slabs under operational loading.

The proposed methods provide relevant data for fatigue assessment of reinforced-concrete deck slabs for road bridges in service:

- Rather than assuming a constant value for concrete and steel-reinforcement fatigue damage, the inverse method successfully evaluates the probabilistic distribution of damage that is dependent on temperature variations and the loads and the positions of vehicles.
- The fatigue behaviour of RC under traffic and temperature conditions associated with shear and reversal stresses was found to be governed by the stationary movement of existing microcracks and slow microcrack growth in the concrete volume, while the stress intensity of reinforcing bars was found to be low.

- The quantification of stationary microcracks and microcrack growth in the concrete volume successfully supports the definition of new indices for quantifying existing fatigue damage and increases in fatigue damage over time. The maximum fatigue damage of about 17% was found at the most loaded part of the slab at the midspan and increases in fatigue damage over time were found to be more pronounced in the negative bending moment zone.

   e) Recommendations for taking on-site measurements and ensuring long-term monitoring of in-service bridges with the aim to quantify their remaining fatigue life.

From the detailed case study presented in this dissertation, the following recommendations are made:

- The configuration of two strain gauges in the longitudinal direction and two in the transverse direction allows for the incorporation of the effect of the loads, positions, and axles of vehicles passing over bridge-deck slabs. By means of load-test results, the distributions of the positions, loads and axles of the vehicles can be estimated.
- Acoustic emission measurements under operational loadings are reliable for evaluating the microcracking activity of concrete under bending and shear stresses. The most important aspects of AE measurements are to ensure solid contact between the AE sensors and the concrete surface and to delete noise without losing reliable data, for which the data calibration of the case study can be used as an initial configuration.
- Limits to continuous long-term monitoring can be prevented by choosing the best solutions for on-site monitoring. On-site acquisition systems must be protected with boxes that are resistant to humidity, ventilated, and kept away from any source of water, such as rain. Furthermore, the sensors used must be strongly fixated, using for example, magnetic holders and a silicone adhesive for AE sensors. The periodic collection of data is moreover appreciable by means of a file transfer protocol. Finally, when using various monitoring systems, one should consider connecting them through input parameters to provide same time scale and to facilitate data interpretation.
- Long-term monitoring results demonstrate the importance of measuring temperature and its daily and seasonal effects for both concrete and steel. In the case study, the variation of AE features and strain measurements due to cyclic temperature variations are identified. It was found that traffic actions are more pronounced than temperature actions.

6.3   Overall Conclusion

The main finding of this thesis is that the fatigue process of the RC slab is governed by the stationary microcracking of concrete where microcracks move without a change in their initial size. Mixed-mode microcrack behaviour was found with more than 80% of the evaluated microcracks, which demonstrates the complex movement of existing microcracks that are opening, closing, and in friction under traffic and temperature conditions. Microcrack growth over time was found to be slow. Two main patterns of microcracks were visualised in the entire depth of the slab based on the nature of the generated stress. Shear microcracks and tensile-compression microcracks were discovered mainly in the tensile zone, while a few of these microcracks were noted in the compression zone. The results demonstrate that the slab shows no detrimental fatigue behaviour even though it was not designed

with respect to fatigue and exists under different conditions compared to the original design conditions. This finding adds to the growing body of evidence that RC slabs show a high fatigue reserve capacity.

6.4 Recommendations for Future Research

Validation by means of more case studies

- In this thesis, the developed methods were produced for one case study on an RC bridge-deck slab that is relatively thin (thickness ~17 cm). Thus, the applicability of the study can be improved particularly by applying the developed monitoring approach to strengthened and massive RC bridges.
- The monitoring approach can be improved by measuring wind and evaluating its effect on the structural behaviour and the monitoring system. Thus, the approach can be applied to slender long RC spans in which the effect of wind is more pronounced.

Improve uncertainty quantification

- The quantification of uncertainties related to monitoring and data interpretation methods can be improved by performing repetitive laboratory tests in which testing is performed with known loads, material properties, and different techniques to evaluate the variability of data-interpretation results and results obtained from the monitoring approach.
- The inverse method's applicability can be improved by quantifying the related uncertainties through a second load test that uses various load and position configurations. Moreover, the distribution of traffic speed can be calculated similarly to load and position distributions to evaluate uncertainties related to the dynamic effects of vehicles.

Exploration of AE data

- The two-years of recorded AE data could be exploited more deeply to evaluate material properties and structural behaviour. For example, signal-based analysis can provide information contained in the recorded waves, such as special patterns of AE responses, to estimate microcrack characteristics. A second possible method for AE data interpretation is data clustering, which can provide the variation of the modulus of concrete elasticity and the structural boundary conditions of supports over time.
- AE activity could be simulated by means of a microscopic model of concrete, during the opening, closing, friction, and growth of microcracks under fatigue loading and temperature variations.

Improvement of codes for existing structures

- Codes for existing structures, such as Swiss code SIA269, should be introduced worldwide. These codes should include recommendations on how to monitor existing structures, and monitoring should be a main aspect of assessing existing structures. A suggestion of related aspects to introduce include the following:
    - o objectives of monitoring fatigue action effects;
    - o monitoring technique(s) and instructions for instrumenting and calibrating sensors;

- o monitoring procedures and instructions for collecting and interpreting data; and
- o instructions for evaluating fatigue-related results.

References

[1]   B. Kühn *et al.*, "Assessment of Existing Steel Structures - Recommendations for Estimation of the Remaining Fatigue Life," Office for Official Publications of the European Communities, EUR - Scientific and Technical Research Reports, 2008. Accessed: Aug. 04, 2020. [Online]. Available: https://publications.jrc.ec.europa.eu/repository/handle/111111111/13394.

[2]   ASCE, "Infrastructure report card," 2017.

[3]   P. Fehlmann, "Zur Ermüdung von Stahlbetonbrücken," *IBK Ber.*, vol. 335, 2012.

[4]   E. Brühwiler, T. Vogel, T. Lang, and P. Lüchinger, "Swiss Standards for Existing Structures," *Struct. Eng. Int.*, vol. 22, no. 2, pp. 275–280, May 2012, doi: 10.2749/101686612X13291382991209.

[5]   I. Bayane, L. Long, S. Thöns, and E. Brühwiler, "Quantification of the conditional value of SHM data for the fatigue safety evaluation of a road viaduct," presented at the ICASP13, Seoul, South Korea, 2019, Accessed: May 26, 2019. [Online]. Available: https://infoscience.epfl.ch/record/269191.

[6]   I. Bayane, A. Mankar, E. Brühwiler, and J. D. Sørensen, "Quantification of traffic and temperature effects on the fatigue safety of a reinforced-concrete bridge deck based on monitoring data," *Eng. Struct.*, vol. 196, p. 109357, Oct. 2019, doi: 10.1016/j.engstruct.2019.109357.

[7]   I. Bayane and E. Brühwiler, "Structural condition assessment of reinforced-concrete bridges based on acoustic emission and strain measurements," *J. Civ. Struct. Health Monit.*, Sep. 2020, doi: 10.1007/s13349-020-00433-0.

[8]   A. Wöhler, "Wöhler's experiments on the strength of metals," in *Engineering*, vol. 4, Lond., 1867, pp. 497–498.

[9]   J. Schijve, *Fatigue of Structures and Materials*, 2nd ed. Springer Netherlands, 2009.

[10] A. J. M. Siemes and TNO Institue for building materials and structures, "Fatigue evaluation of concrete structures preliminary studies, procedure and examples," *HERON*, vol. 33, no. 3, p. 75, 1988.

[11] S. I. A. SIA, "Ermüdung von Betonbauten. SIA Dokumentation," no. D 0133, 1997.

[12] P. Fehlmann, "Zur Ermüdung von Stahlbetonbrücken," ETH Zurich, 2012.

[13] CEB, Comité Euro-International du Béton, "Fatigue of concrete structures, state of the art," no. 188, 1988.

[14] C. A. Spathelf, "Fatigue performance of orthogonally reinforced concrete slabs," ETH Zurich, Report, 2018. doi: 10.3929/ethz-b-000253703.

[15] M. A. Treacy and E. Brühwiler, "Action effects in post-tensioned concrete box-girder bridges obtained from high-frequency monitoring," *J. Civ. Struct. Health Monit.*, vol. 5, no. 1, pp. 11–28, Feb. 2015, doi: 10.1007/s13349-014-0097-0.

[16] P. Fehlmann and T. Vogel, "Experimental investigations on the fatigue behavior of concrete bridges," in *Sustainable infrastructure : IABSE Symposium, Bangkok 2009*, 2009, vol. 96, doi: 10.3929/ethz-a-006995502.

[17] A. Herwig, "Reinforced Concrete Bridges under increased Railway Traffic Loads - Fatigue Behaviour and Safety Measures," *PhD Thesis Éc. Polytech. Fédérale Lausanne*, no. 4010, 2008.

[18] M. Schläfli and E. Brühwiler, "Fatigue of existing reinforced concrete bridge deck slabs," *Eng. Struct.*, vol. 20, no. 11, pp. 991–998, Nov. 1998, doi: 10.1016/S0141-0296(97)00194-6.

[19] E. Fathalla, Y. Tanaka, and K. Maekawa, "Remaining fatigue life assessment of in-service road bridge decks based upon artificial neural networks," *Eng. Struct.*, vol. 171, pp. 602–616, Sep. 2018, doi: 10.1016/j.engstruct.2018.05.122.

[20] E. Gebreyouhannes, N. Chijiwa, C. Fujiyama, and K. Maekawa, "Shear Fatigue Simulation of RC Beams Subjected to Fixed Pulsating and Moving Loads," *J. Adv. Concr. Technol.*, vol. 6, no. 1, pp. 215–226, 2008, doi: 10.3151/jact.6.215.

[21] K. Maekawa, E. Gebreyouhannes, T. Mishima, and X. An, "Three-Dimensional Fatigue Simulation of RC Slabs under Traveling Wheel-Type Loads," *J. Adv. Concr. Technol.*, vol. 4, no. 3, pp. 445–457, 2006, doi: 10.3151/jact.4.445.

[22] M. Schläfli and E. Brühwiler, "Fatigue considerations in the evaluation of existing reinforced concrete bridge decks," *IABSE Proc. IABSE Zurich*, no. 76, 1997.

[23] P. C. Perdikaris and S. Beim, "RC Bridge Decks Under Pulsating and Moving Load," *J. Struct. Eng.*, vol. 114, no. 3, pp. 591–607, Mar. 1988, doi: 10.1061/(ASCE)0733-9445(1988)114:3(591).

[24] K. Okada, H. Okamura, and K. Sonoda, "FATIGUE FAILURE MECHANISM OF REINFORCED CONCRETE BRIDGE DECK SLABS," presented at the Bridge Engineering Conference, 1st, 1978, St Louis, Missouri, USAFederal Highway AdministrationFederal Railroad Administration, 1978, Accessed: Apr. 22, 2019. [Online]. Available: https://trid.trb.org/view/80024.

[25] FEDRO (The Federal Roads Office), "Annual and monthly results of traffic 2002-2017." 2018, [Online]. Available: https://www.astra.admin.ch/astra/en/home/documentation/traffic-data/data-and-publication/swiss-automatic-road-traffic-counts--sartc-/annual-and-monthly-results.html.

[26] Road construction office (Service des ponts et chaussées), "Weekly traffic distribution, Road construction office. Department of territorial management, Neuchatel Canton." 2018, [Online]. Available: sitn.ne.ch.

[27] D. Stucki, M. Meystre, and J.-P. Lebet, "Updated traffic load for concrete deck slabs of existing bridges." Office fédéral des routes, 2014, [Online]. Available: http://www.mobilityplatform.ch.

[28] Barr P. J., Stanton J. F., and Eberhard M. O., "Effects of Temperature Variations on Precast, Prestressed Concrete Bridge Girders," *J. Bridge Eng.*, vol. 10, no. 2, pp. 186–194, Mar. 2005, doi: 10.1061/(ASCE)1084-0702(2005)10:2(186).

[29] F. A. Branco and P. A. Mendes, "Thermal Actions for Concrete Bridge Design," *J. Struct. Eng.*, vol. 119, no. 8, pp. 2313–2331, Aug. 1993, doi: 10.1061/(ASCE)0733-9445(1993)119:8(2313).

[30] M. Elbadry and A. Ghali, "Nonlinear Temperature Distribution and Its Effects on Bridges | Heat Transfer | Convection," *Scribd*, 1983. https://www.scribd.com/document/332503449/Nonlinear-Temperature-Distribution-and-Its-Effects-on-Bridges (accessed Aug. 07, 2018).

[31] M. J. N. Priestley, "Thermal gradients in bridges, some design considerations," *N. Z. Eng.*, vol. 27, no. 7, pp. 228–233, 1972.

[32] X. Zhu, Z. Dai, J. Ling, and L. Chen, "Thermal expansion prediction of cement concrete based on a 3D micromechanical model considering interfacial transition zone," *Constr. Build. Mater.*, vol. 171, pp. 891–900, May 2018, doi: 10.1016/j.conbuildmat.2018.03.132.

[33] E. H. El-Tayeb, S. E. El-Metwally, H. S. Askar, and A. M. Yousef, "Thermal analysis of reinforced concrete beams and frames," *HBRC J.*, vol. 13, no. 1, pp. 8–24, Apr. 2017, doi: 10.1016/j.hbrcj.2015.02.001.

[34] L. Shen, Q. Ren, L. Zhang, Y. Han, and G. Cusatis, "Experimental and numerical study of effective thermal conductivity of cracked concrete," *Constr. Build. Mater.*, vol. 153, pp. 55–68, Oct. 2017, doi: 10.1016/j.conbuildmat.2017.07.038.

[35] J. E. Mottershead and M. I. Friswell, "Model Updating In Structural Dynamics: A Survey," *J. Sound Vib.*, vol. 167, no. 2, pp. 347–375, Oct. 1993, doi: 10.1006/jsvi.1993.1340.

[36] Y. Liu, Z. Tan, and C. Yang, "Refined finite element modeling of a damaged bridge with virtual distortion method coupling solid superelement," *Mech. Syst. Signal Process.*, vol. 93, pp. 559–577, Sep. 2017, doi: 10.1016/j.ymssp.2017.02.032.

[37] M. Schläfli and E. Brühwiler, "Test Report 'Fatigue of reinforced concrete elements without shear reinforcement.'" 1999.

[38] SIA 269, "Existing structures – Concrete structures. Zurich: Swiss society of engineers and architects." 2013.

[39] CEB.FIP, "fib Model Code for Concrete Structures 2010." Paul Beverly, U. K, 2010, [Online]. Available: www.ernst-und-sohn.de/mc2010.

[40] U. Johansson, *Fatigue Tests and Analysis of Reinforced Concrete Bridge Deck Models*. 2004.

[41] C. A. Spathelf and T. Vogel, "Fatigue performance of orthogonally reinforced concrete slabs: Experimental investigation," *Eng. Struct.*, vol. 168, pp. 69–81, Aug. 2018, doi: 10.1016/j.engstruct.2018.04.058.

[42] M. A. Treacy, "The use of monitored data in the verification of structural and fatigue safety of existing post-tensioned concrete highway bridges," Éc Polytech Fédérale Lausanne, 2014.

[43] M. Schläfli, "Ermüdung von Brückenfahrbahnplatten aus Stahlbeton," *PhD Thesis Éc. Polytech. Fédérale Lausanne*, p. 128, 1999.

[44] J. Zhang, B. Bai, S. Zhao, and X. Zuo, "Fatigue characteristic and life test of reinforced concrete T girders under cyclic loading," *IOP Conf. Ser. Earth Environ. Sci.*, vol. 358, p. 052041, Dec. 2019, doi: 10.1088/1755-1315/358/5/052041.

[45] M. Rocha and E. Brühwiler, "Prediction of fatigue life of reinforced concrete bridges using Fracture Mechanics," *Proceedings Bridge Maintenance, Safety, Management, Resilience and Sustainability*, 2012. https://infoscience.epfl.ch/record/180270 (accessed Apr. 02, 2020).

[46] D. S. Prakash Rao, M. G. Tamhankar, and S. P. Sharma, "Literature survey onin situ testing of concrete bridges," *Matér. Constr.*, vol. 16, no. 6, pp. 457–466, Nov. 1983, doi: 10.1007/BF02476345.

[47] M. Scott *et al.*, "A comparison of nondestructive evaluation methods for bridge deck assessment," *NDT Amp E Int.*, vol. 36, no. 4, pp. 245–255, 2003.

[48] D. Breysse, "Nondestructive evaluation of concrete strength: An historical review and a new perspective by combining NDT methods," *Constr. Build. Mater.*, vol. 33, pp. 139–163, Aug. 2012, doi: 10.1016/j.conbuildmat.2011.12.103.

[49] Campbell Leslie E., Connor Robert J., Whitehead Julie M., and Washer Glenn A., "Benchmark for Evaluating Performance in Visual Inspection of Fatigue Cracking in Steel Bridges," *J. Bridge Eng.*, vol. 25, no. 1, p. 04019128, Jan. 2020, doi: 10.1061/(ASCE)BE.1943-5592.0001507.

[50] B. M. Phares, "9 - Visual inspection techniques for bridges and other transportation structures," in *Inspection and Monitoring Techniques for Bridges and Civil Structures*, G. Fu, Ed. Woodhead Publishing, 2005, pp. 166–182.

[51] G. Washer, M. Moore, and R. WALTHER, "FHWA APPROACH FOR RELIABILITY TESTING OF THE VISUAL INSPECTION METHOD," 1999.

[52] S. Shahidan, R. Pullin, N. M. Bunnori, and S. S. M. Zuki, "Active crack evaluation in concrete beams using statistical analysis of acoustic emission data," *Insight - Non-Destr. Test. Cond. Monit.*, vol. 59, no. 1, pp. 24–31, Jan. 2017, doi: Shahidan, S., Pullin, Rhys, Bunnori, N. M. and Zuki, S. S. M. 2017. Active crack evaluation in concrete beams using statistical analysis

of acoustic emission data. Insight - Non-Destructive Testing and Condition Monitoring 59 (1) , pp. 24-31.http://dx.doi.org/10.1784/insi.2017.59.1.24.

[53]   M. N. Noorsuhada, "An overview on fatigue damage assessment of reinforced concrete structures with the aid of acoustic emission technique," *Constr. Build. Mater.*, vol. 112, no. Supplement C, pp. 424–439, Jun. 2016, doi: 10.1016/j.conbuildmat.2016.02.206.

[54]   H. A. Elfergani, R. Pullin, and K. M. Holford, "Damage assessment of corrosion in prestressed concrete by acoustic emission," *Constr. Build. Mater.*, vol. 40, no. Supplement C, pp. 925–933, Mar. 2013, doi: 10.1016/j.conbuildmat.2012.11.071.

[55]   T. Shiotani, "Recent Advances of AE Technology for Damage Assessment of Infrastructures.," *J. Acoust. Emiss.*, vol. 30, 2012.

[56]   C. U. Grosse and M. Ohtsu, *Acoustic emission testing*. Springer Science & Business Media, 2008.

[57]   M. Wevers, "Listening to the sound of materials: Acoustic emission for the analysis of material behaviour," *NDT E Int.*, vol. 30, no. 2, pp. 99–106, Apr. 1997, doi: 10.1016/S0963-8695(96)00051-5.

[58]   A. Nair and C. S. Cai, "Acoustic emission monitoring of bridges: Review and case studies," *Eng. Struct.*, vol. 32, no. 6, pp. 1704–1714, Jun. 2010, doi: 10.1016/j.engstruct.2010.02.020.

[59]   Vallen Systeme GmbH, "Acoustic Emission Sensors," p. 50, 2017.

[60]   M. W. Felux, "Acoustic emission monitoring on bridges under regular operating conditions," ETH Zurich, Report, May 2017. doi: 10.3929/ethz-b-000169739.

[61]   Ing. S. Colombo, I. G. Main, and M. C. Forde, "Assessing Damage of Reinforced Concrete Beam Using ' b -value' Analysis of Acoustic Emission Signals," *J. Mater. Civ. Eng.*, vol. 15, no. 3, pp. 280–286, Jun. 2003, doi: 10.1061/(ASCE)0899-1561(2003)15:3(280).

[62]   T. F. Drouillard, "Acoustic emission: The first half century," EG and G Rocky Flats, Inc., Golden, CO (United States). Rocky Flats Plant, RFP-4875; CONF-9410182-1, Aug. 1994. Accessed: Apr. 01, 2019. [Online]. Available: https://www.osti.gov/biblio/10175611.

[63]   T. S. H. Asaue, T. Nishida, T. Maeshima, and Y. Tanaka, "Evolution of Fatigue Damage in Wheel-Loading Tests Evaluated by 3D Elastic-Wave Tomography," *J. Disaster Res.*, vol. 12, no. 3, pp. 487–495, Jun. 2017, doi: 10.20965/jdr.2017.p0487.

[64]   S. LI, H. SHI, G. WU, and D. WANG, "Application of Acoustic Emission Technique to Crack Detection of Concrete Hollow Slab Bridges," *Bridge Constr.*, no. 5, p. 15, 2017.

[65]   M. E. Zitto, R. Piotrkowski, A. Gallego, F. Sagasta, and A. Benavent-Climent, "Damage assessed by wavelet scale bands and b-value in dynamical tests of a reinforced concrete slab monitored with acoustic emission," *Mech. Syst. Signal Process.*, vol. 60–61, pp. 75–89, Aug. 2015, doi: 10.1016/j.ymssp.2015.02.006.

[66]   T. Schumacher, C. C. Higgins, and S. C. Lovejoy, "Estimating Operating Load Conditions on Reinforced Concrete Highway Bridges with b-value Analysis from Acoustic Emission Monitoring," *Struct. Health Monit. Int. J.*, vol. 10, no. 1, pp. 17–32, Jan. 2011, doi: 10.1177/1475921710365424.

[67]   S. D. Butt, V. Limaye, A. A. Mufti, and B. Bakht, "Acoustic Transmission Technique for Evaluating Fatigue Damage in Concrete Bridge Deck Slabs," *Struct. J.*, vol. 101, no. 1, pp. 3–10, Jan. 2004, doi: 10.14359/12992.

[68]   S. Yuyama, Z.-W. Li, M. Yoshizawa, T. Tomokiyo, and T. Uomoto, "Evaluation of fatigue damage in reinforced concrete slab by acoustic emission," *NDT E Int.*, vol. 34, no. 6, pp. 381–387, Sep. 2001, doi: 10.1016/S0963-8695(01)00004-4.

[69]   M. Ohtsu, *Acoustic Emission and Related Non-destructive Evaluation Techniques in the Fracture Mechanics of Concrete: Fundamentals and Applications*. Woodhead Publishing, 2015.

[70]   Shiotani Tomoki, Ohtsu Hiroyasu, Momoki Shohei, Chai Hwa Kian, Onishi Hiroshi, and Kamada Toshiro, "Damage Evaluation for Concrete Bridge Deck by Means of Stress Wave Techniques," *J. Bridge Eng.*, vol. 17, no. 6, pp. 847–856, Nov. 2012, doi: 10.1061/(ASCE)BE.1943-5592.0000373.

[71] R. Anay, T. M. Cortez, D. V. Jáuregui, M. K. ElBatanouny, and P. Ziehl, "On-Site Acoustic-Emission Monitoring for Assessment of a Prestressed Concrete Double-Tee-Beam Bridge without Plans," *J. Perform. Constr. Facil.*, vol. 30, no. 4, p. 04015062, Aug. 2016, doi: 10.1061/(ASCE)CF.1943-5509.0000810.

[72] L. Golaski, P. Gebski, and K. Ono, "Diagnostics of Reinforced Concrete Bridges by Acoustic Emission," p. 16, 2002.

[73] T. Shiotani, T. Nishida, H. Asaue, and Y. Kobayashi, "Interpretation of Fatigue Damage Evolution in RC Slabs by Means of Innovative 3D AE Tomography. In 9th International Conference on Fracture Mechanics of Concrete and Concrete Structures. FraMCoS-9V. Saouma, J. Bolander and E. Landis(Eds). DOI 10.21012/FC9.225," May 2016, doi: 10.21012/FC9.225.

[74] A. NF EN 1330-9, "NF EN 1330-9 Non-destructive testing - Terminology - Part 9 : terms used in acoustic emission testing," 2017. https://www.boutique.afnor.org/xml/1941133/false.

[75] AFIAP, "Guide AFIAP Emission Acoustique 2009 | Signal électrique | Contrôle non destructif," *Scribd*, 2009. https://fr.scribd.com/document/246989415/Guide-AFIAP-Emission-Acoustique-2009 (accessed Jan. 22, 2020).

[76] G. Mistras INC, "Sensor Highway III, user's manual." 2015, [Online]. Available: www.mistrasgroup.com.

[77] J. Hardy H. Reginald, *Acoustic Emission/Microseismic Activity: Volume 1: Principles, Techniques and Geotechnical Applications*. CRC Press, 2003.

[78] E. A. Whitehurst, *Evaluation of Concrete Properties from Sonic Tests*. American Concrete Institute, 1966.

[79] A. Hillerborg, *Analysis of one single crack*. Elsevier, 1983, pp. 223–249.

[80] A. K. Vasudevan, K. Sadananda, and G. Glinka, "Critical parameters for fatigue damage," *Int. J. Fatigue*, vol. 23, pp. 39–53, Jan. 2001, doi: 10.1016/S0142-1123(01)00171-2.

[81] N. Md Nor, A. Ibrahim, N. Muhamad Bunnori, and H. Mohd Saman, "Acoustic emission signal for fatigue crack classification on reinforced concrete beam," *Constr. Build. Mater.*, vol. 49, pp. 583–590, Dec. 2013, doi: 10.1016/j.conbuildmat.2013.08.057.

[82] D. G. Aggelis, "Classification of cracking mode in concrete by acoustic emission parameters," *Mech. Res. Commun.*, vol. 38, no. 3, pp. 153–157, Apr. 2011, doi: 10.1016/j.mechrescom.2011.03.007.

[83] D. G. Aggelis, D. V. Soulioti, N. Sapouridis, N. M. Barkoula, A. S. Paipetis, and T. E. Matikas, "Acoustic emission characterization of the fracture process in fibre reinforced concrete," *Constr. Build. Mater.*, vol. 25, no. 11, pp. 4126–4131, Nov. 2011, doi: 10.1016/j.conbuildmat.2011.04.049.

[84] RILEM TC 212-ACD, "Recommendation of RILEM TC 212-ACD: acoustic emission and related NDE techniques for crack detection and damage evaluation in concrete* | SpringerLink," 2010. https://link.springer.com/article/10.1617/s11527-010-9640-6 (accessed Apr. 06, 2020).

[85] K. Ohno and M. Ohtsu, "Crack classification in concrete based on acoustic emission," *Constr. Build. Mater.*, vol. 24, no. 12, pp. 2339–2346, Dec. 2010, doi: 10.1016/j.conbuildmat.2010.05.004.

[86] Z. Z. Xu, Y. Wang, S. X. Wu, and Y. Wang, "Damage Evaluation of Concrete Based on Acoustic Emission *b*-Value," *Appl. Mech. Mater.*, vol. 395–396, pp. 515–519, Sep. 2013, doi: 10.4028/www.scientific.net/AMM.395-396.515.

[87] B. Gutenberg, *Seismicity of the earth and associated phenomena*. Read Books Ltd, 2013.

[88] P. R. Sammonds, P. G. Meredith, S. a. F. Murrell, and I. G. Main, "Modelling the damage evolution in rock containing pore fluid by acoustic emission," presented at the Rock Mechanics in Petroleum Engineering, Jan. 1994, doi: 10.2118/28142-MS.

[89] T. Oh, "Defect characterization in concrete elements using vibration analysis and imaging," May 2012.

[90] M. R. Kaphle, "Analysis of acoustic emission data for accurate damage assessment for structural health monitoring applications," Queensland University of Technology, 2012.

[91] N. M. Bunnori, R. J. Lark, and K. M. Holford, "The use of acoustic emission for the early detection of cracking in concrete structures," *Mag. Concr. Res.*, vol. 63, no. 9, pp. 683–688, Sep. 2011, doi: 10.1680/macr.2011.63.9.683.

[92] S. Chatterji, "Freezing of air-entrained cement-based materials and specific actions of air-entraining agents," *Cem. Concr. Compos.*, vol. 25, no. 7, pp. 759–765, Oct. 2003, doi: 10.1016/S0958-9465(02)00099-9.

[93] D. Aggelis, T. Shiotani, S. Momoki, and A. Hirama, "Acoustic Emission and Ultrasound for Damage Characterization of Concrete Elements," *ACI Mater. J.*, vol. 106, no. 6, 2009, doi: 10.14359/51663333.

[94] P. Mauro, "World Economic Forum. Long-Term Investing, Infrastructure and Development.," *World Economic Forum*, 2017. https://www.weforum.org/agenda/2017/03/before-roads-and-bridges-we-need-checks-and-balances/ (accessed Jul. 22, 2020).

[95] C. Maierhofer, H.-W. Reinhardt, and G. Dobmann, *Non-Destructive Evaluation of Reinforced Concrete Structures: Non-Destructive Testing Methods*. Elsevier, 2010.

[96] A. Méndez and A. Csipkes, "Overview of Fiber Optic Sensors for NDT Applications," in *Nondestructive Testing of Materials and Structures*, O. Güneş and Y. Akkaya, Eds. Dordrecht: Springer Netherlands, 2013, pp. 179–184.

[97] C. R. Farrar and K. Worden, "An Introduction to Structural Health Monitoring," in *New Trends in Vibration Based Structural Health Monitoring*, A. Deraemaeker and K. Worden, Eds. Vienna: Springer, 2010, pp. 1–17.

[98] N. T. Nguyen, Z.-M. Sbartaï, J.-F. Lataste, D. Breysse, and F. Bos, "Assessing the spatial variability of concrete structures using NDT techniques – Laboratory tests and case study," *Constr. Build. Mater.*, vol. 49, pp. 240–250, Dec. 2013, doi: 10.1016/j.conbuildmat.2013.08.011.

[99] A. G. Beattie, "Acoustic emission non-destructive testing of structures using source location techniques," *Albuq. Livermore*, 2013.

[100] J.-A. Goulet and I. F. C. Smith, "Structural identification with systematic errors and unknown uncertainty dependencies," *Comput. Struct.*, vol. 128, pp. 251–258, Nov. 2013, doi: 10.1016/j.compstruc.2013.07.009.

[101] R. Pasquier, J.-A. Goulet, C. Acevedo, and I. F. C. Smith, "Improving fatigue evaluations of structures using in-service behavior measurement data," *J. Bridge Eng.*, vol. 19, no. 11, Art. no. 11, Nov. 2014.

[102] I. F. C. Smith, "Studies of Sensor Data Interpretation for Asset Management of the Built Environment," *Front. Built Environ.*, vol. 2, 2016, doi: 10.3389/fbuil.2016.00008.

[103] S. G. S. Pai, A. Nussbaumer, and I. F. C. Smith, "Comparing Structural Identification Methodologies for Fatigue Life Prediction of a Highway Bridge," *Front. Built Environ.*, vol. 3, 2018, doi: 10.3389/fbuil.2017.00073.

[104] Proceq SA, "Concrete Test Hammer." 2017.

[105] NF EN 12504-2, "NF EN 12504-2 Testing concrete in structures - Part 2: Non-destructive testing - Determination of rebound number," 2013. https://viewer.afnor.org/Pdf/Viewer/?token=D_OjExxNbyQ1 (accessed Jul. 28, 2020).

[106] M. W. Felux, "Acoustic emission monitoring on bridges under regular operating conditions," *IBK Ber.*, vol. 373, 2017.

[107] Z. Z. Xu, Y. Wang, S. X. Wu, and Y. Wang, "Damage Evaluation of Concrete Based on Acoustic Emission *b*-Value," *Appl. Mech. Mater.*, vol. 395–396, pp. 515–519, Sep. 2013, doi: 10.4028/www.scientific.net/AMM.395-396.515.

[108] A. Carpinteri, G. Lacidogna, and S. Puzzi, "From criticality to final collapse: Evolution of the 'b-value' from 1.5 to 1.0," *Chaos Solitons Fractals*, vol. 41, no. 2, pp. 843–853, Jul. 2009, doi: 10.1016/j.chaos.2008.04.010.

[109] T. Shiotani, S. Yuyama, Z.-W. Li, and M. Ohtsu, "Application of the AE improved b-value to quantitative evaluation of fracture processes in concrete materials," 2001.

[110] T. Shiotani, C. Granier, and K. Hashimoto, "Damage Quantification Using an Improved b-Value for Concrete Slabs," in *Advances in Acoustic Emission Technology*, Cham, 2019, pp. 239–247, doi: 10.1007/978-3-030-12111-2_22.

[111] K. Popper, *Popper-the Logic of Scientific Discovery*. Taylor & Francis, New York, 2005.

[112] G. Moser, S. G. Paal, and I. F. C. Smith, "Leak Detection of Water Supply Networks Using Error-Domain Model Falsification," *J. Comput. Civ. Eng.*, vol. 32, no. 2, p. 04017077, Mar. 2018, doi: 10.1061/(ASCE)CP.1943-5487.0000729.

[113] R. Pasquier, L. D'Angelo, J.-A. Goulet, C. Acevedo, A. Nussbaumer, and I. F. C. Smith, "Measurement, Data Interpretation, and Uncertainty Propagation for Fatigue Assessments of Structures," *J. Bridge Eng.*, vol. 21, no. 5, p. 04015087, May 2016, doi: 10.1061/(ASCE)BE.1943-5592.0000861.

[114] Y. Reuland, P. Lestuzzi, and I. F. C. Smith, "Measurement-based support for post-earthquake assessment of buildings," *Struct. Infrastruct. Eng.*, vol. 15, no. 5, pp. 647–662, May 2019, doi: 10.1080/15732479.2019.1569071.

[115] Y. Reuland, P. Lestuzzi, and I. F. C. Smith, "A model-based data-interpretation framework for post-earthquake building assessment with scarce measurement data," *Soil Dyn. Earthq. Eng.*, vol. 116, pp. 253–263, Jan. 2019, doi: 10.1016/j.soildyn.2018.10.008.

[116] M. Proverbio, D. G. Vernay, and I. F. C. Smith, "Population-based structural identification for reserve-capacity assessment of existing bridges," *J. Civ. Struct. Health Monit.*, vol. 8, no. 3, pp. 363–382, Jul. 2018, doi: 10.1007/s13349-018-0283-6.

[117] D. G. Vernay, F.-X. Favre, and I. F. C. Smith, "Robust model updating methodology for estimating worst-case load capacity of existing bridges," *J. Civ. Struct. Health Monit.*, vol. 8, no. 5, pp. 773–790, Nov. 2018, doi: 10.1007/s13349-018-0305-4.

[118] J. E. Mottershead, M. Link, and M. I. Friswell, "The sensitivity method in finite element model updating: A tutorial," *Mech. Syst. Signal Process.*, vol. 25, no. 7, pp. 2275–2296, Oct. 2011, doi: 10.1016/j.ymssp.2010.10.012.

[119] H. W. Sorenson, "Least-squares estimation: from Gauss to Kalman," *IEEE Spectr.*, vol. 7, no. 7, pp. 63–68, Jul. 1970, doi: 10.1109/MSPEC.1970.5213471.

[120] SIA 262, "Concrete Structures. Zurich: Swiss society of engineers and architects." 2013.

[121] A. Masi and M. Vona, "La stima della resistenza del calcestruzzo in situ: impostazione delle indagini ed elaborazione dei risultati," *Progett. Sismica*, vol. 0, no. 1, Art. no. 1, May 2009, Accessed: Jul. 29, 2020. [Online]. Available: https://www.ledijournals.com/ojs/index.php/ps/article/view/487.

[122] S. G. S. Pai, M. Sanayei, and I. F. C. Smith, "Model class selection using clustering and classification for structural identification and prediction," *Journal of Computing in Civil Engineering. 10.1061/(ASCE)CP.1943-5487.0000932*, 2020.

[123] N. Cristianini, J. Shawe-Taylor, and D. of C. S. R. H. J. Shawe-Taylor, *An Introduction to Support Vector Machines and Other Kernel-based Learning Methods*. Cambridge University Press, 2000.

[124] I. Bayane and E. Brühwiler, "'Pocket-Monitoring' for fatigue safety verification of a RC bridge deck slab," p. 8, 2018.

[125] H. Toyama, H. Kishida, and A. Yonezu, "Characterization of fatigue crack growth of concrete mortar under cyclic indentation loading," *Eng. Fail. Anal.*, vol. 83, pp. 156–166, Jan. 2018, doi: 10.1016/j.engfailanal.2017.10.004.

[126] R. Lenschow, "Long term random dynamic loading of concrete structures," *Matér. Constr.*, vol. 13, no. 3, pp. 274–278, May 1980, doi: 10.1007/BF02473567.

[127] H. Mihashi, "Stochastic approach to study fatigue of concrete," *Eng. Fract. Mech.*, vol. 28, no. 5, pp. 785–793, Jan. 1987, doi: 10.1016/0013-7944(87)90070-1.

[128] K. Ohno, "3 - Identification of the fracture process zone in concrete materials by acoustic emission," in *Acoustic Emission and Related Non-Destructive Evaluation Techniques in the*

Fracture Mechanics of Concrete, M. Ohtsu, Ed. Oxford: Woodhead Publishing, 2015, pp. 41–55.

[129] A. M. Neville and J. J. Brooks, *Concrete technology*. Longman Scientific & Technical England, 1987.

[130] K. Otsuka and H. Date, "Fracture process zone in concrete tension specimen," *Eng. Fract. Mech.*, vol. 65, no. 2, pp. 111–131, Jan. 2000, doi: 10.1016/S0013-7944(99)00111-3.

[131] T. Shiotani, "Recent advances of AE technology for damage assessment in infrastructures," p. 21, 2012.

[132] T. Shiotani and D. G. Aggelis, "Wave propagation in cementitious material containing artificial distributed damage," *Mater. Struct.*, vol. 42, no. 3, pp. 377–384, Apr. 2009, doi: 10.1617/s11527-008-9388-4.

[133] I. Bayane, S. G. S. Pai, I. F. C. Smith, and E. Brühwiler, "Model-based interpretation of measurements for fatigue evaluation of existing reinforced-concrete bridges," *J. Bridge Eng Journal of Bridge Engineering*, 2021.

Appendix

Crêt de l'Anneau viaduct, the case study.

Load test, with a truck of five axles having the legal limit load of 400 kN.

The direction, velocity and position of each passage during the load test.

| N° Passage	Direction	Velocity [km/h]	Position
1	*Neuchâtel*		
2	*Travers*	80	Midlane
3	*Neuchâtel*		
4	*Travers*		
5	*Neuchâtel*	40	Tangent to the midspan axis
6	*Travers*	35	
7	*Neuchâtel*	10	Midspan
8	*Travers*		
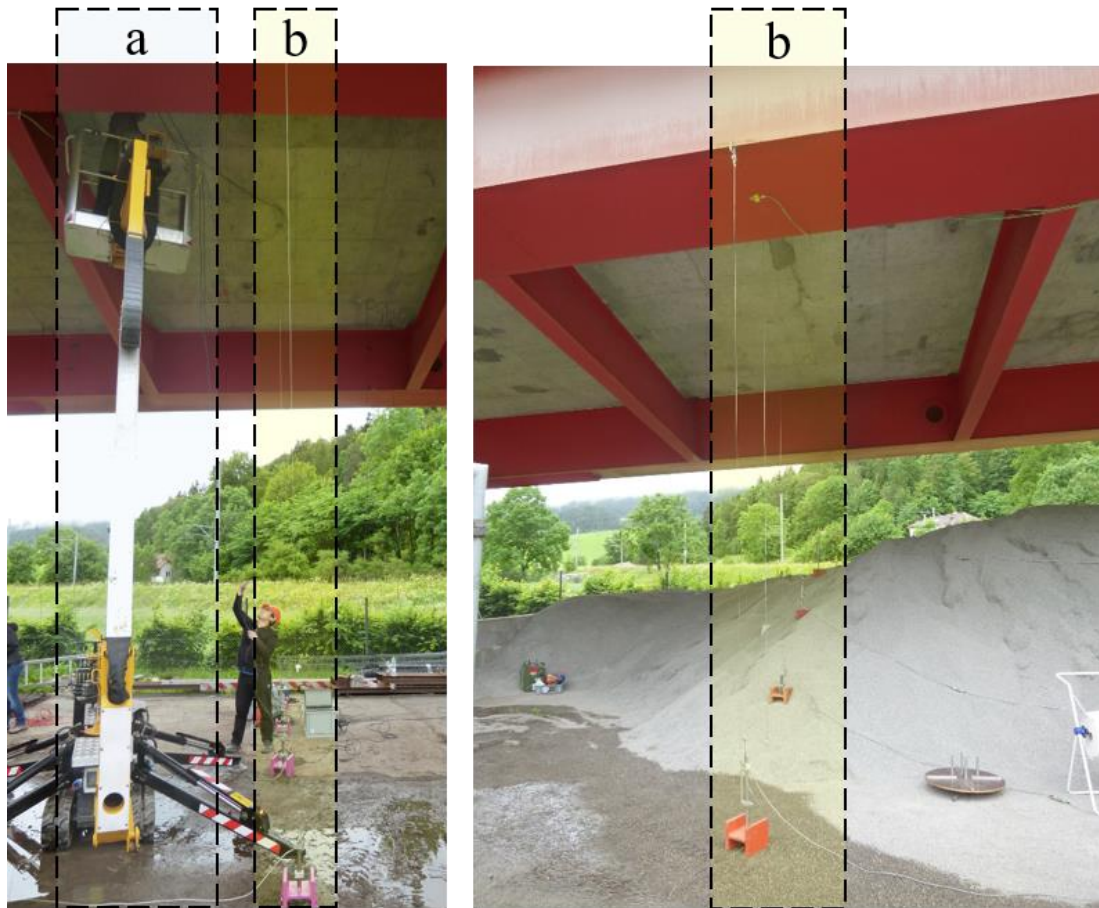
Strain gauge installation (a), deflection measurements using LVDTs (b).

The made box for protecting the acquisition systems provided with a monitor for real-time visualisation of measurements.
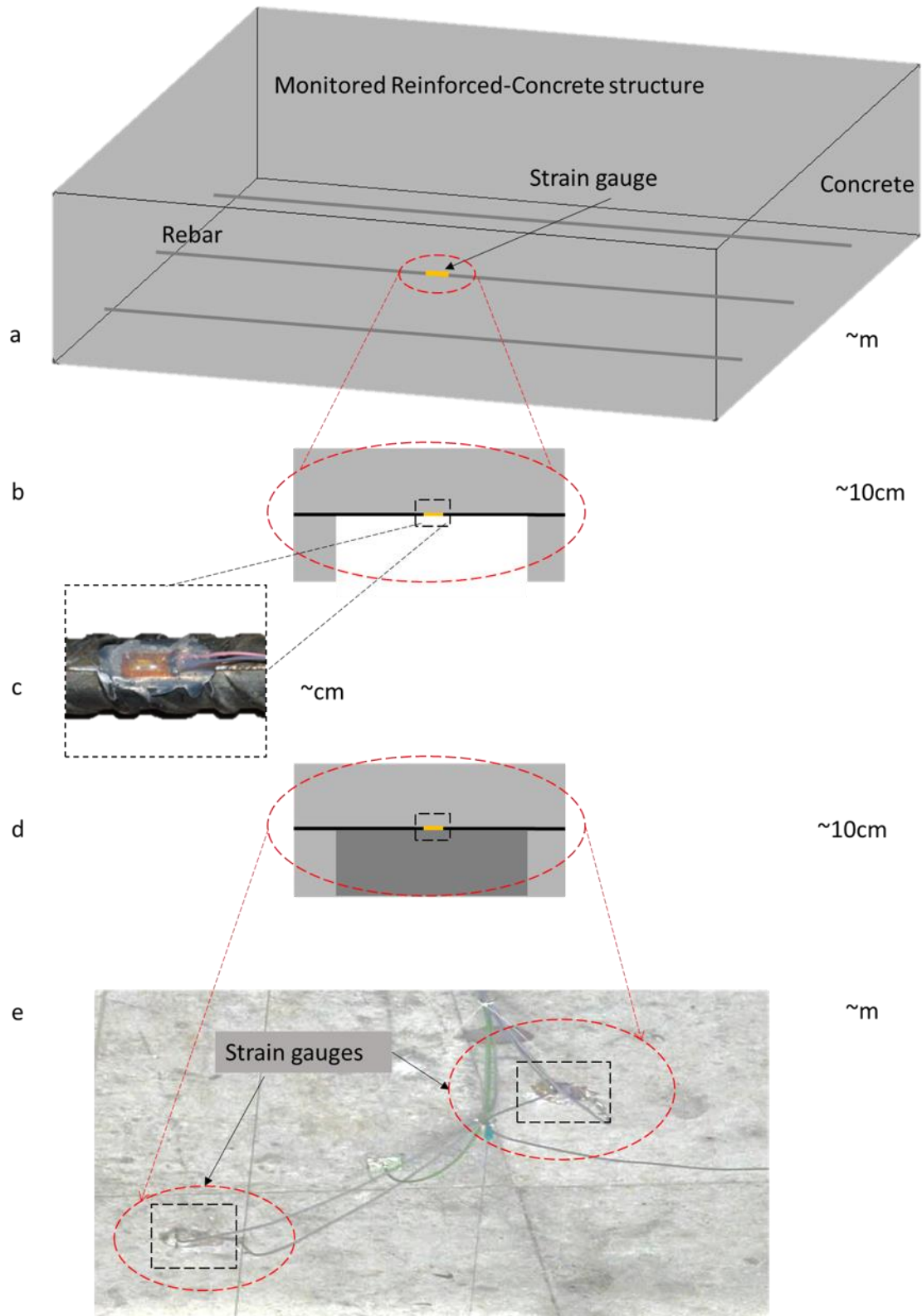
Strain gauge installation in reinforcement bars:
detecting the target rebar using a rebar locator (a);
removing few centimetres of concrete cover (b);
installation of strain gauge (c);
applying a protective layer and mortar to protect the area (d);
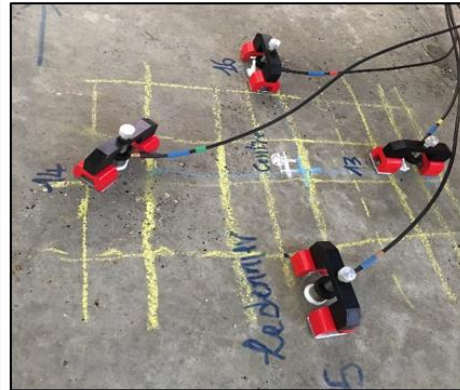strain gauge installation in the RC slab of the viaduct (e).
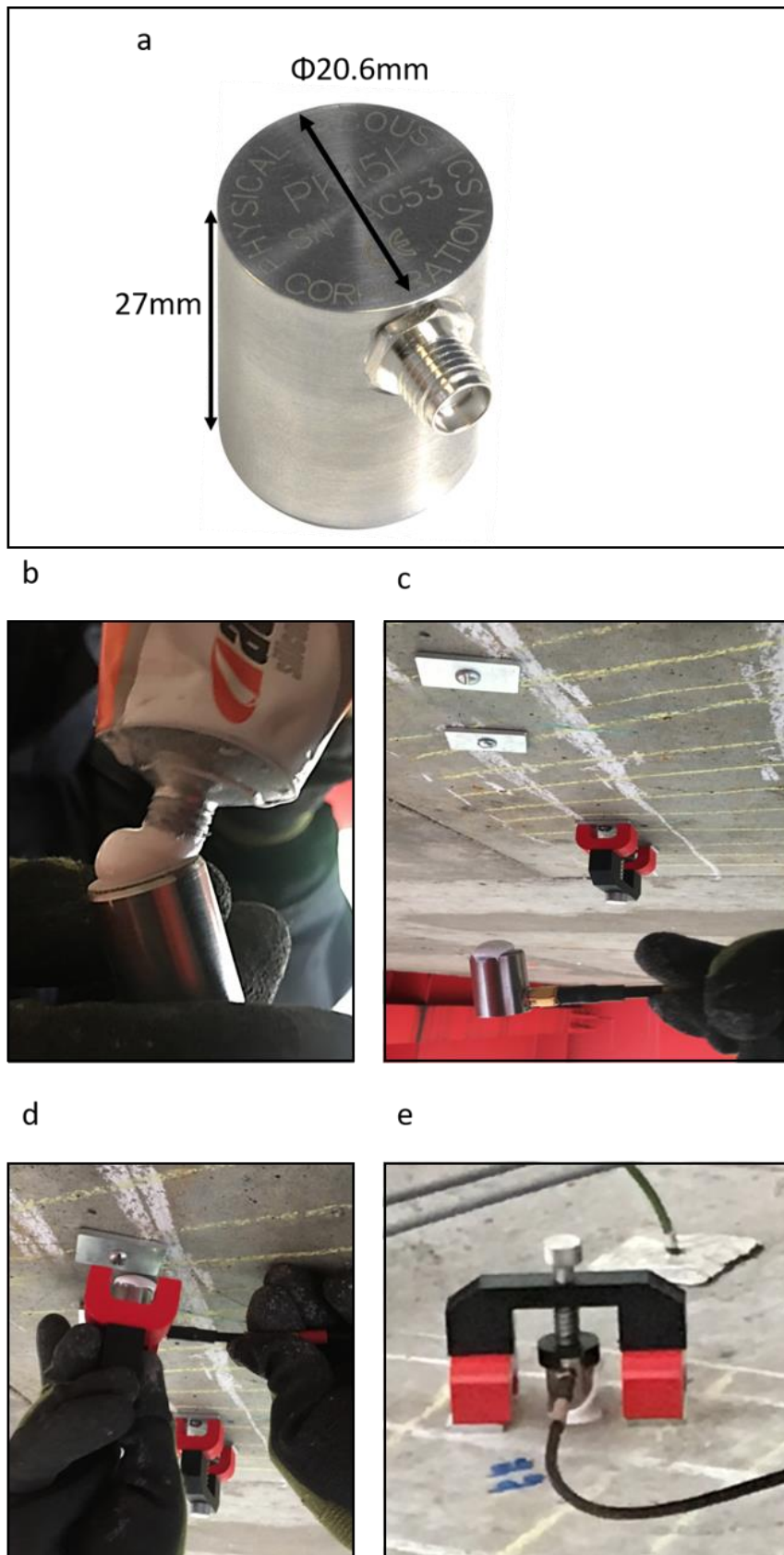
AE sensor (dimensions in [mm]) (a);
adding silicone glue for good adhesion (b);
AE sensor mounting (c); magnetic holder for AE sensor fixation (d);
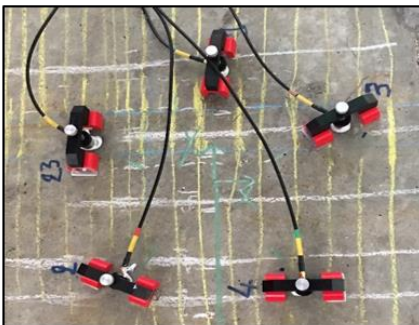AE sensor mounted on RC slab of the viaduct (e).
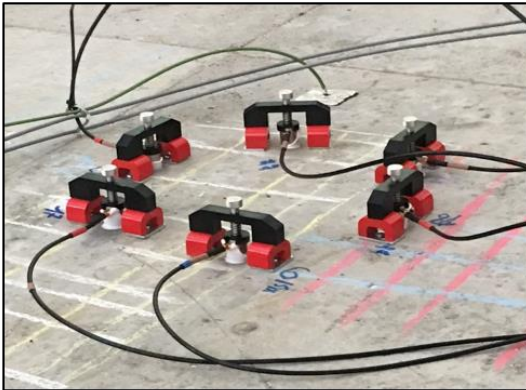
AE sensor deployment. Grid 1 with Channels (5, 6, 7, 17, 21, and 22); Grid 2 with Channels (8, 9, 10, 11, 12, 18, 19, 20, and 24); Grid 3 with Channels (13, 14, 15, and 16); Grid 4 with Channels (1, 2, 3, 4, and 23).

Curriculum Vita

IMANE BAYANE

Civil Engineer
PhD assistant

Chemin du reposoir 21, 1007, Lausanne, Suisse

+41 78 715 23 64

imane-bayane@hotmail.fr

https:/www.linkedin.com/in/imane-bayane-a312a9108

Moroccan, born on 16th of June, 1992

STRENGTH

- Enthusiastic structural engineer skilled in the field of structural monitoring to evaluate the safety of existing bridges. Experienced in the field of in-situ testing, data processing and numerical modelling.
- Willing to direct my efforts and invest my skills in the field of maintenance and design of structures.
- Creative and ambitious, flexible in the face of change, integrated in several multidisciplinary teams in Europe.

EXPERIENCE

February 2017 – November 2020	**PhD assistant | *EPFL*** ▪ **Conception of a new approach for bridge monitoring** to assess operational condition under traffic loading and temperature variation using acoustic emission and strain measurements. ▪ **Research member of INFRASTAR**, the Marie Curie European project Horizon 2020 ITN Innovation and Networking for Fatigue and Reliability Analysis of Structures - Training for Assessment of Risk.
August - September 2019	**PhD trainee | *Neostrain company, Krakow, Poland*** ▪ **Detection of microcrack initiation in reinforced-concrete bridges** by interpreting acoustic emission measurements using wavelet transform.
April - June 2018	**PhD trainee | *Aalborg University, Aalborg, Denmark*** ▪ **Comparison of the technical and economic value provided by monitoring** and design codes for bridge assessment using the value-of-information theory.
August - September 2017	**PhD trainee | *Federal Institute for Materials Research and Testing (BAM), Berlin, Germany*** ▪ **Evaluating the performance of various nondestructive testing** including ultrasonics technique, fibre optics and digital image correlation for in-situ assessment of a reinforced-concrete beam.
March - September 2016	**Trainee Engineer | *CEREMA, Ile-de-France, France*** ▪ **Development of a sustainable concrete** by replacing cement with the Seine sediment and evaluating concrete strength and hydration.
June - August 2015	**Trainee Engineer| *The Regional Directorate of Transport and Logistics*, Morocco** ▪ **Preparing public contracts** and participating in the selection of proposals for the design of roads and bridges at the regional level.

EDUCATION

2017–2020	**Ph.D. in Structural Engineering | EPFL**, *Laboratory for Maintenance and Safety of Structures (MCS)*
	• Doctoral thesis on examination of the fatigue behaviour of reinforced-concrete bridge slabs using acoustic emission and strain monitoring data.
2015–2016	**Master in Civil Engineering** / *École Centrale de Lille, Lille, France*
	• **2nd rank holder** in the master of geo-materials and structures (double Franco-Moroccan diploma).
2013–2016	**Civil Engineering Degree |** *Hassania School of Public Works, Casablanca, Morocco*
	• Engineering degree in Civil Engineering, (double Franco-Moroccan diploma).
2011–2013	**Preparatory Classes for Engineering Schools |** *Lycée Mohammed V, Morocco*
	• **104/2000 national rank holder** in mathematics, physics, and engineering science.

SKILLS

- Engineering software packages: Ansys, APDL, AutoCAD, AEwin, Noesis.
- Miscellaneous MS Office, MATLAB.
- Teamwork, multidisciplinary thinking, public speaking.
- Good professional communication skills.
- Self-motivated and goal-oriented.

LANGUAGES

- French (bilingual) ;
- English (level C1/C2) ;
- German (level A2/B1) ;
- Arabic (mother tongue, spoken and written);
- Amazigh (mother tongue, spoken);

EXTRACURRICULAR ACTIVITIES

- Organising member of TedxEcublens (2018 - 2021).
- President of the technical innovation competition Greenov (2014 - 2015).
- Developing member of the Phœnix Company of waste recycling (2014).
- Organising member of sportive and artistic events (2013).

HOBBIES

- Writing (my PhD blog: http://esr4infrastar.blogspot.com/);
- Yoga;
- Travelling;
- Climbing.

List of papers

Publications included in this thesis

Bayane, I., Mankar, A., Brühwiler, E., & Sørensen, J. D. (2019). Quantification of traffic and temperature effects on the fatigue safety of a reinforced-concrete bridge deck based on monitoring data.
Engineering Structures, 196, 109357.

Bayane, I., Brühwiler, E. (2020). Structural condition assessment of reinforced-concrete bridges based on acoustic emission and strain measurements
Journal of Civil Structural Health Monitoring, 1-19.

Bayane, I., Pai, S.G.S., Smith, I.F.C., & Brühwiler, E. (2021). Model-based interpretation of measurements for fatigue evaluation of existing RC bridges.
Journal of Bridge Engineering.

Bayane, I., Brühwiler, E. (2021). Fatigue microcrack quantification in reinforced-concrete bridge deck slabs using acoustic emission and strain measurements.
Mechanical Systems and Signal Processing.

Other publications

Bayane, I., & Brühwiler, E. (2018). Pocket-Monitoring" for fatigue safety verification of a RC bridge deck slab. *In Proceedings of the Sixth International Symposium on Life-Cycle Civil Engineering, IALCCE2018, Ghent, Belgium, October 28-31, 2018.*

Bayane, I., Long, L., Thöns, S., & Brühwiler, E. (2019). Quantification of the conditional value of SHM data for the fatigue safety evaluation of a road viaduct.
In Proceedings of the 13th International Conference on Applications of Statistics and Probability in Civil Engineering, ICASP13, Seoul, South Korea, May 26-30, 2019.

Bayane, I., & Brühwiler, E. (2019). Acoustic emission and ultrasonic testing for fatigue damage detection in a RC bridge deck slab.
In Proceedings of the 5th Conference on Smart Monitoring, Assessment and Rehabilitation of Civil Structures, SMAR 2019-5th, Potsdam, Germany, August 27-29, 2019.

Bayane, I., & Brühwiler, E. (2021). Investigation of fatigue damage in a RC deck slab due to moving loads through long-term monitoring of a road viaduct.
In Proceedings of the 10th International Conference on Bridge Maintenance, Safety and Management, IABMAS2020, Japon, April 11-18, 2021.

Mankar, A., Bayane, I., Sørensen, J. D., & Brühwiler, E. (2019). Probabilistic reliability framework for assessment of concrete fatigue of existing RC bridge deck slabs using data from monitoring.
Engineering Structures, *201*, 109788.

Lavergne, F., Fraj, A. B., Bayane, I., & Barthélémy, J. F. (2018). Estimating the mechanical properties of hydrating blended cementitious materials: An investigation based on micromechanics.
Cement and Concrete Research, *104*, 37-60.